CONTROL OF SELF-SATURATING MAGNETIC AMPLIFIERS USING RECTIFIED A-C WITH VARYING ANGLE OF TRUNCATION

by
ISAAC WEISSMAN

Report No. R-332-53, PIB-268

for
OFFICE OF NAVAL RESEARCH
Contract No. NOnr-292(00)
Project Designation No. 075-215
December 14, 1953

4/1315

MRI

POLYTECHNIC INSTITUTE OF BROOKLYN
MICROWAVE RESEARCH INSTITUTE

Microwave Research Institute
Polytechnic Institute of Brooklyn
55 Johnson Street
Brooklyn 1, New York

Report No. R-332-53, PIB-268
Project Designation 075-215

CONTROL OF SELF-SATURATING MAGNETIC AMPLIFIERS USING RECTIFIED A-C WITH VARYING ANGLE OF TRUNCATION

by

Isaac Weissman

Title Page
Acknowledgment
Abstract
Table of Contents
List of Symbols - 3 pages
41 Pages of Text
Appendix I - 2 pages
Appendix II - 3 pages
References - 2 pages
48 Pages of Figures

Contract No. NOnr-292(00)

Brooklyn 1, New York
December 14, 1953

ACKNOWLEDGMENT

The author wishes to express his appreciation to Dr. E. J. Smith and Prof. M. Liwschitz-Garik for their helpful suggestions offered during the course of this work, and to his colleagues, Messrs. W. C. Dumper and K. T. Lian for their ready cooperation.

The support of the Office of Naval Research is gratefully acknowledged.

ABSTRACT

Usually, magnetic amplifiers are excited by applying a pure d-c signal to the control circuit. The output, however, is a truncated sine wave, the angle of truncation depends on the signal strength. If several stages of magnetic amplifiers are cascaded, it is clear that the signal applied to succeeding stages is not pure d-c but usually full-wave, rectified, truncated, a-c - the average value of which varies with the angle of truncation.

This work, then, investigates the operation of self-saturating magnetic amplifiers using rectified a-c excitation as obtained from a preceding stage or from a thyratron arrangement. Only control by varying the angle of truncation with constant amplitude of signal is considered.

A theoretical analysis, in addition to an experimental study, is made for different modes of steady state operation. It is then attempted to justify the assumptions involved in the analysis and deviations from these assumptions are considered. Then results obtained from the measurement of the transient response are discussed.

Emphasis throughout is on the voltage doubler circuit since, of the basic self-saturating circuits, it is most effectively adapted to a-c control. The discussion is extended to other self-saturating circuits in a later chapter.

TABLE OF CONTENTS

TABLE OF CONTENTS (Cont.)

LIST OF SYMBOLS

B	Flux density
e	Rectifier voltage
F	Flux
F_s	Saturation flux
F_M	$V_M/\omega N$
F_o	Minimum flux during cycle
F_x	$\frac{N_c I_{cM} R^*}{N^2 \omega}$
$\bar{F}$	Average flux over a cycle
f	Line Frequency
G_{cos}	Cosine gain, $\left\lvert \frac{d(\cos \omega t_s)}{d(\cos \omega t_c)} \right\rvert$
G_I	Current gain
G_v	Voltage gain
G_p	Power gain
H	Magnetic Field Intensity
H_c	Coercive force of ideal "rectangular" material
i_1, i_2	Instantaneous mesh currents
$\bar{I}_1$, $\bar{I}_2$	Average mesh currents
i_L	Instantaneous load current
$\bar{I}_L$	Average rectified load current
i_c	Instantaneous control current
$\bar{I}_c$	Average control current
I_{cM}	Control current amplitude
I_B	D-C bias current

LIST OF SYMBOLS (Cont.)

$\bar{I}_{cMAX}$	Maximum $\bar{I}_c$, no truncation
$\bar{I}_{L\ MAX}$	Maximum $\bar{I}_L$, no truncation
L	"Average inductance" over a cycle
ℓ_m	Mean magnetic path length
M_{cos}	Cosine figure of merit
M_I	Current figure of merit
M_v	Voltage figure of merit
M_p	Power figure of merit
N	Load turns
N_c	Control turns
N_B	Bias turns
N_y	Auxiliary turns
R_L	Load resistance
R_c	Control circuit resistance
R_y	Auxiliary winding shunting resistance
R_ω	Load turns winding resistance
$R_{REC.}$	Rectifier forward resistance
R_F	Forward mesh resistance, $R_\omega + R_{REC.}$
R^*	Total mesh resistant, $R_L + R_F$
R_x	Simulated rectifier leakage resistance
R_R	Additional inserted forward mesh resistance
r	R_L/R^*
t	Time
T_1	Time constant of d-c excited stage

LIST OF SYMBOLS (Cont.)

T_2	Time constant of a-c excited stage
T	Overall time constant
v	Line voltage
V	RMS line voltage
V_M	Peak line voltage
ω	$2\pi f$
ωt	Any angle
ωt_c	Control angle
ωt_s	Firing angle
ωt_p	Angle of lag of signal with respect to load voltage

Introduction

The operation of the self-saturating magnetic amplifier is fairly well known and covered in detail in the literature (refs. 1 - 8). Not much has been written, however, regarding a-c excitation. Ramey[9] considers a special circuit using a full-wave rectified a-c signal with varying amplitude. Another paper[10] gives experimental results using a full-wave, rectified, truncated a-c signal with varying amplitude for different phase angle relations between the signal and load voltage. In multistage magnetic amplifiers, however, where the output of one stage is fed directly into the control circuit of the next stage, it is not the amplitude of the signal to the later stages that varies, but rather the angle of truncation.

The a-c excited magnetic amplifier cannot be analyzed by considering the signal to be composed of a d-c term plus a series of a-c terms because such a process is valid only for linear circuits and certainly does not apply to the highly nonlinear self-saturating circuits. One must not conclude that since the signal has a d-c level the operation is necessarily similar to the d-c excited amplifier. In general, the two types of operation will give different results.

Instead, a step-by-step analysis is required which is based on certain assuptions and which gives approximate results. For one thing, it is assumed that the B vs. H characteristics of the magnetic materials used can be represented by straight lines and that the operating point of each core over a cycle follows a minor d-c hysteresis loop as shown in Fig. MRI-13437-b.

For simplicity the angle of truncation of the signal is called the "control angle" and the angle of truncation of the load current is referred to by its popular name of "firing angle". The problem of this work is chiefly to determine how the firing angle varies as a function of control angle - both in the steady state and during a transient.

Almost all the work is concerned with the doubler circuit which is shown in Fig. MRI-13436-a. In the analysis the control current is assumed to have a waveshape as sketched in Fig. MRI-13437-a, which is obtained from the output of a previous stage. The test setup is shown schematically in Fig. MRI-13436-b. R_R is a purposely inserted resistor to simulate additional winding resistance and R_X simulates rectifier leakage. Data on the cores and rectifiers used is given in the Appendix.

The direction of the control current is such as to tend to demagnetize the cores, and is referred to as "negative" control current. If the polarity of the current were reversed, it would be called "positive" control current. It is shown later (Chapter II, Section D) that positive control is not as effective as negative control for most purposes.

All experimental transfer curves are plotted in terms of average rectified load current vs. average control current. The average control current can be read directly on a d-c ammeter, but the load current is first rectified

and then read on a d-c ammeter as indicated in Fig. MRI-13436-b.

The control angle is varies by controlling the d-c signal applied to the first stage.

I. Steady State Operation of Doubler Circuit with A-C Excitation

A. Basic Assumption

To simplify the analysis of the circuit of Fig. MRI-13436-a with a-c excitation a few idealizations are first made.

(a) It is assumed that the B vs. H characteristics of the cores are such as seen in Fig. MRI-13437-b, with infinite unsaturated inductance, zero post-saturation inductance, and a sudden transition (sharp knee) between these two regions. The operating path is assumed to follow a minor d-c hysteresis loop as indicated. As for the geometry of the cores, it is considered to be such that the flux density is the same throughout the cross-section, so that the core saturates everywhere simultaneously (this is not true for cores with large ratio of outside to inside dimension). Further, the effect of eddy-currents contributing to the total MMF is neglected.

(b) Concerning the rectifiers in Fig. MRI-13436-a, they are thought of as having a linear forward resistance, and the ability to block any reverse current flow; that is, the back (leakage) resistance is assumed to be infinite.

(c) The control current is assumed to have a perfectly truncated wave shape as shown in Fig. MRI-13437-a. The presence of the control windings in no way affects the wave shape of the control current; that is, the current is forced in the control circuit, or operates from a current source. This condition can always be achieved by using a large enough resistance in the control circuit. Also, the jump at the control angle is to be large enough to meet the minimum requirement as specified later by Eq. (16).

B. Basic Equations and Regions of Operation

For the doubler circuit of Fig. MRI-13436-a, the basic equations are written as:

$$v = V_m \sin \omega t = (R_L + R_\omega)\, i_1 + e_1 + N \frac{dF_1}{dt} - R_L i_2 \qquad (1)$$

$$-v = -V_M \sin \omega t = (R_L + R_\omega)\, i_2 + e_2 + N \frac{dF_2}{dt} - R_L i_1 \qquad (2)$$

$$i_L = i_1 - i_2 \tag{3}$$

$$\begin{aligned} i_c &= 0 && \text{for} \quad 0 < \omega t < \omega t_c \\ i_c &= -I_{cM} \sin \omega t && \text{for} \quad \omega t_c < \omega t < \end{aligned} \tag{4}$$

$$H_1 \ell_m = N i_1 + N_c i_c \tag{5}$$

$$H_2 \ell_m = N i_2 + N_c i_c \tag{6}$$

e_1 is the voltage across rectifier No. 1. When it is negative, $i_1 = 0$. When e_1 is positive, the rectifier conducts and $e_1 = i_1 R_{rec}$. Then Eq. (1) can be written as

$$V_M \sin \omega t = R^* i_1 - R_L i_2 + N \frac{dF_1}{dt}$$

where

$$R^* = R_L + R_\omega + R_{rec}$$

and is termed the "total mesh resistance". By definition,

$$R_F = R_\omega + R_{rec} \tag{7}$$

and is termed the "forward mesh resistance".

Roughly, the steady state analysis is divided into two distinct regions of operation. The theoretical relationship between the cosines of the control and firing angles is shown in Fig. MRI-13437-c. The useful region is obtained when the control angle, ωt_c, precedes the firing angle, ωt_s, and is indicated by line AB. The transition between the two regions occurs when $\omega t_c = \omega t_s$ (pt. B). As the control angle increases, the firing angle decreases from π. This characteristic relating the cosines is later translated into transfer curves relating average currents.

C. Basic Mode of Operation

Consider the region AB (Fig. MRI-13437-c) where the control angle precedes the firing angle. Impose the condition that the line voltage alone is not sufficient to cause the cores in Fig. MRI-13436-a to saturate both positive and negative simultaneously; that is

$$F_M \leqq F_S$$

(The case where $F_M > F_S$ is discussed in section G of chapter I.)

Fig. MRI-13438 shows the various wave forms that are derived in the analysis and can be used as a guide.

As a starting point consider conditions at an angle shortly after the firing angle, ωt_s. By definition one core is now saturated. Assume the other core is unsaturated and its flux decaying. Then referring to Fig. MRI-13437-d, $F_1 = F_S$ and $H_2 = -H_c$. Core No. 1 is at pt. E and moving to the right (since a positive voltage is now being applied to it tending to increase its flux, F_1) and core No. 2 is at pt. G and moving downward. Now from Eq. (4),

$$i_c = -I_{cM} \sin \omega t$$

and from Eq. (6)

$$Ni_2 = N_c I_{cM} \sin \omega t - H_c \ell_M$$

and as long as $|N_c I_{cM} \sin \omega t| > |H_c \ell_M|$, i_2 is positive. If, however, $|H_c \ell_M| > |N_c I_{cM} \sin \omega t|$, then i_2 would be computed from Eq. (6) to be negative. But this is impossible because of the rectifier in mesh No. 2. Therefore, it is concluded that at the angle where $|N_c I_{cM} \sin \omega t|$ just becomes less than $|H_c \ell_M|$, H_2 is no longer equal to the coercive force H_c as assumed but follows the control current in accordance with Eq. (6) for $i_2 = 0$. Defining this angle as ωt_o

$$\sin \omega t_o = \frac{H_c \ell_M}{N_c I_{cM}} . \qquad (8)$$

Normally ωt_o is very late in the half cycle and if the coercive force is small

$$\omega t_o = \pi \quad \text{approximately}$$

and F_2 at this angle is defined as F_o.

Then in the interval from ωt_s to ωt_o, core No. 2 decays from pt. G to pt. D (Fig. MRI-13437-d). Solving for i_2 during this interval

$$i_2 = \frac{N_c}{N} I_{cM} \sin \omega t - \frac{H_c \ell_M}{N} .$$

The term $(N_c/N)\, I_{cM} \sin \omega t$ is termed the "circulating" component and is due to the current transformer behavior of the unsaturated core. $H_c \ell_m/N$ is called the "magnetizing" component and is due to a finite coercive force. Since $F_1 = F_S$, $dF_1/dt = 0$, and tracing around mesh No. 1, shows e_1 to be positive. Substituting i_2 in Eq. (1),

$$i_1 = \left[\frac{V_M}{R^*} + \frac{R_L N_c}{R^* N} I_{cM} \right] \sin \omega t - \frac{R_L H_c \ell_M}{R^* N}$$

Solving for the load current in Eq. (3) gives

$$i_L = \left[\frac{V_M}{R^*} - (1-r) \frac{N_c}{N} I_{cM} \right] \sin \omega t + (1-r) \frac{H_c \ell_M}{N} \qquad (9)$$

where r is defined by

$$r = \frac{R_L}{R^*} \qquad (10)$$

Since i_2 is positive, e_2 is positive. Substituting i_1 and i_2 in Eq. (2) and neglecting the magnetizing component

$$N \frac{dF_2}{dt} = \left[-V_m + R^* \frac{N_c}{N} I_{cM} + \frac{R_L}{R^*} V_m + \frac{R_L^2}{R^*} \frac{N_c}{N} I_{cM} \right] \sin \omega t$$

Dividing by ωN

$$\frac{1}{\omega} \frac{dF_2}{dt} = - \left[F_m(1-r) + F_x(1-r^2) \right] \sin \omega t \qquad (11)$$

where

$$F_m = \frac{V_m}{\omega N}$$

and

$$F_x = \frac{N_c}{N^2} \frac{I_{cM} R^*}{\omega}$$

It is seen from Eq. (11) that F_2 is decreasing which was assumed as a starting point. Referring to Fig. MRI-13437-d, the flux in core No. 2, F_2, at ωt_o is called F_o and the core is at pt. D. In the very short interval from ωt_o to π, i_c is not large enough to overcome the coercive force and from Eq. (6) it is seen that i_2 cuts off. Tracing around mesh No. 2 shows the rectifier to block. H_2 must now follow i_c and the operating point moves to the right with constant flux, F_o. Thus at π the flux F_2 is F_o. But $\omega t_o = \pi$ approximately and Eq. (11) can be integrated from ωt_s to π.

Integrating and substituting the limits F_G at ωt_s and F_o at π.

$$F_G - F_o = \left[F_M(1-r) + F_x(1-r^2) \right] (1 + \cos \omega t_s) \qquad (12)$$

At the close of the half-cycle $H_1 = H_2 = 0$ from Eqs. (5) and (6). Thus at π core No. 1 is still saturated and operating at pt. A (Fig. MRI-13437-d and core No. 2 is at pt. L.

Now, in the steady state, by virtue of the symmetry of the circuit, conditions at the start of the half-cycle in one mesh are the same as the conditions at the end of the half cycle in the other mesh. Therefore, at $\omega t = 0$

$$F_2 = F_s, \quad F_1 = F_o, \quad H_1 = H_2 = 0$$

Shortly after the start of the half-cycle, no control current flows and since i_2 cannot go negative, H_2 also cannot go negative - by Eq. (6). Tracing around mesh No. 2 shows the rectifier to block since $(dF_2/dt) = 0$. Therefore, i_2 is truly zero and H_2 must remain zero as long as no control current flows. Core No. 2, which tends to come out of saturation, is prevented from doing so and stays put at pt. A (Fig. MRI-13437-d) with $F_2 = F_s$ until ωt_c, the control angle.

In the meantime core No. 1, which at the start of the half-cycle was at pt. L, has a positive voltage applied to it which tends to cause F_1 to rise. Therefore, it moves to the right with $F_1 = F_o$ until $H_1 = H_c$. Defining ωt_n as the angle when $H_1 = H_c$, and since up to ωt_n $(dF_1/dt) = 0$, Eq. (1) gives

$$i_1 = \frac{V_M}{R^*} \sin \omega t \qquad \text{from 0 to } \omega t_n$$

since $i_2 = 0$. From Eq. (5)

$$H_1 = \frac{N}{\ell_m} \frac{V_m}{R^*} \sin \omega t$$

and at ωt_n, $H_1 = H_c$. Thus

$$\sin \omega t_n = \frac{H_c \ell_m R^*}{N V_m} \tag{13}$$

Normally ωt_n is very early in the half-cycle and for small coercive force,

$$\omega t_n = 0 \qquad \text{approximately.}$$

After ωt_n core No. 1 moves up from pt. K (Fig. MRI-13437-d) with $H_1 = H_c$. The control current is zero and from Eq. (5)

$$i_1 = \frac{H_c \ell_m}{N}$$

This is only magnetizing current which is neglected. Then dividing Eq. (1) by ωN

$$\frac{1}{\omega} \frac{dF_1}{dt} = F_M \sin \omega t \tag{14}$$

Defining F_1 at ωt_c by F_c and integrating between 0 and ωt_c gives

$$F_c - F_o = F_M (1 - \cos \omega t_c) \tag{15}$$

At the control angle, ωt_c, the control current jumps on. The jump must be great enough to cause H_2 to jump to $-H_c$ in accordance with Eq. (6) for $i_2 = 0$; that is, impose the condition that

$$|i_c| \geqq \left|\frac{H_c \ell_m}{N_c}\right| \qquad \text{at the control angle} \tag{16}$$

or

$$\text{Minimum } N_c I_{cM} = \frac{H_c \ell_m}{\sin \omega t_c} .$$

At ωt_c the operating point of core No. 2 jumps from pt. A to pt. B (Fig. MRI-13437-d) with constant flux.

After ωt_c, $H_2 = -H_c$, $H_1 = H_c$, and from Eq. (6)

$$i_2 = \frac{N_c}{N} I_{cM} \sin \omega t - \frac{H_c \ell_m}{N}$$

which means that the rectifier in mesh No. 2 is forced to conduct by the presence of the control current. Now F_2 is free to decay and a negative voltage appears across core No. 2. Solving Eq. (5) for i, with $H_1 = H_c$

$$i_1 = \frac{N_c}{N} I_{cM} \sin \omega t + \frac{H_c \ell_m}{N} .$$

Neglecting the magnetizing current

$$i_1 = i_2 = \frac{N_c}{N} I_{cM} \sin \omega t$$

Substituting in Eqs. (1) and (2) and dividing by ωN

$$\frac{1}{\omega} \frac{dF_1}{dt} = [F_M - F_x(1-r)] \sin \omega t \tag{17}$$

$$\frac{1}{\omega} \frac{dF_2}{dt} = -[F_M + F_x(1-r)] \sin \omega t \tag{18}$$

Integrating from ωt_c to ωt_s

$$F_s - F_c = \left[F_M - F_x(1-r)\right] (\cos \omega t_c - \cos \omega t_s) \tag{19}$$

$$F_s - F_G = \left[F_M + F_x(1-r)\right] (\cos \omega t_c - \cos \omega t_s) \tag{20}$$

Actually the quantity $N_c I_{cM}$ need not be large, and in fact should be kept as small as Eq. (16) permits. For proper operation F_M will be much larger than F_x. Making this approximation it is seen from Eqs. (19) and (20) that $F_c = F_G$.

Then rewriting Eqs. (12) and (15) in their approximate form

$$F_G - F_o = F_M(1-r) (1 + \cos \omega t_s) \tag{21}$$

$$F_G - F_o = F_M(1 - \cos \omega t_c) \tag{22}$$

and solving for the firing angle as a function of the control angle

$$\cos \omega t_s = \frac{r - \cos \omega t_c}{1 - r}$$

for $0 < \omega t_c < \omega t_s$.

If r is very close to unity it is seen that a small change in control angle causes a large change in firing angle. Expression (23) is valid only for control angles in the range indicated since it was assumed that the control angle preceded the firing angle in this mode of operation.

Fig. MRI-13438 gives the exact theoretical wave shapes. The photographs of Fig. MRI-13439-a bear out the preceding theory. In particular, it is observed that in the photograph of the flux wave shape in Fig. MRI-13439-a, F_2 does not begin to decay right after the start of the half-cycle but must wait until the control current flows.

Expression (23) is based on the assumptions stated in section A of this chapter and was derived for the case when both magnetizing and circulating currents are negligible. The ideal magnetic amplifier to satisfy these conditions would have zero coercive force cores and infinitesimal control current. Under these conditions the result (Eq. (23)) is accurate no matter what the wave shape of the control current provided it remains "on" until the end of the half cycle. The only function of the control current is to act as a "valve" which

determine whether or not F_2 is decaying, so that regardless of its wave shape, it is of importance only when it goes on and when it goes off. As a first (and good) approximation it is seen that the control current has absolutely no effect on core No. 1, whose flux is rising during the positive half-cycle. Of course, during the other half-cycle, the control current exerts influence only on core No. 1.

It is interesting that, under the idealizations made, the relationship between the control and firing angles is dependent only on the ratio of load resistance to total mesh resistance.

D. Information for Analyses of Other Modes

Some general rules for determining the flux equations for any mode whatsoever can be set forth with reference to Fig. MRI-13440-a and Fig. MRI-13440-b. i_c is taken at random to "go on" and "go off" several times in the interval shown. It goes off whenever its magnitude drops below the minimum specified by Eq. (16). It was seen in the preceding section that the control current doesn't affect a core in its positive half-cycle operating along $H = H_c$, but does act as a valve for the core whose flux is decreasing.

If magnetizing and circulating currents are negligible, F_2 (the decaying flux) will decrease sinusoidally whenever the control current is "on". The amplitude of the decay depends on whether or not core No. 1 is saturated. When core No. 1 is unsaturated (and therefore its mesh current is negligible), the entire line voltage will appear across core No. 2 and will cause its flux to decay with amplitude F_M.

$$\frac{1}{\omega}\frac{dF_2}{dt} = -F_M \sin \omega t \qquad (24)$$

but when core No. 1 is saturated the current in mesh No. 1 is strong and the voltage across core No. 2 has an amplitude $V_M(1-R_L/R^*)$ because of the drop across the load resistance. Then

$$\frac{1}{\omega}\frac{dF_2}{dt} = -F_M(1-r) \sin \omega t \qquad (25)$$

Of course, if i_c is "off"

$$\frac{1}{\omega}\frac{dF_2}{dt} = 0 \qquad \text{in either case,} \qquad (26)$$

and the operating point of core No. 2 makes a horizontal excursion (such as AB - Fig. MRI-13440-a and Fig. MRI-13440-b).

When the control current is either "on" or "off", as long as core No. 1 is unsaturated, its flux rises with amplitude F_M along H-H_c and

$$\frac{1}{\omega}\frac{dF_1}{dt} = F_M \sin \omega t \tag{27}$$

E. Firing Angle Preceding Control Angle

The region BC (Fig. PRI-13437-c) is obtained when the control angle is increased beyond the point where it meets the firing angle. The rules of section D can be applied without going through the analysis in detail. The assumptions in section A and the equations in section B are applicable to this mode also.

From the beginning of the forward half-cycle to the firing angle, ωt_s, F_2 cannot decay because the control current is "off". F_1, however, builds up with amplitude F_M (Eq. (27)). Integrating Eq. (27) between the limits F_o at the start and F_S at the firing angle,

$$F_S - F_o = F_M (1 - \cos \omega t_s) \tag{28}$$

All this time F_2 is locked at F_S.

From ωt_s to ωt_c both cores are saturated and no change of flux occurs in this interval. It should be noted that although both cores are saturated only one mesh conducts since the rectifier in the other mesh blocks.

After ωt_c the control current is "on", core No. 1 is saturated, and core No. 2 decays according to Eq. (25). Thus integrating between the limits F_S at ωt_c and F_o at π gives

$$F_S - F_o = F_M (1 - r)(1 + \cos \omega t_c) \tag{29}$$

Subtracting Eqs. (28) and (29) gives the firing angle as a function of control angle.

$$\cos \omega t_s = - (1-r) \cos \omega t_c + r \tag{30}$$

$$\text{for} \quad \omega t_s < \omega t_c < \pi$$

Comparing Eq. (30) to Eq. (23), it is seen that the "cosine gain" under one mode is the reciprocal of the "cosine gain" under the other mode. The maximum gain that can be obtained under this mode is unity (for r = 0).

The next step is to convert Eqs. (23) and (30) into useful average current relationships.

F. Gain Relationships and Transfer Curves

Fig. MRI-13440-c is a set of curves relating the control and firing angles under both modes. The only parameter is "r". The curves are independent of any other parameters just so long as the magnetizing and circulating currents are negligible.

If the control current has the assumed wave shape, its average value can be expressed in terms of the control angle as

$$\bar{I}_c = -\frac{I_{cM}}{\pi}(1 + \cos \omega t_c) \tag{31}$$

and if magnetizing and circulating currents are negligible it is seen from Fig. MRI-13438 that the average rectified load current is

$$\bar{I}_L = \frac{V_M}{\pi R^*}(1 + \cos \omega t_s) \tag{32}$$

To find the current gain, G_I,

$$G_I = \frac{d\bar{I}_L}{d\bar{I}_c} = -\frac{V_M}{I_{cM} R^*}\frac{d(\cos \omega t_s)}{d(\cos \omega t_c)}$$

In the region of greatest interest (control angle preceding the firing angle) the relationship between the angles is given by Eq. (23). Differentiating Eq. (23) and solving for current gain gives

$$G_I = \frac{V_M}{I_{cM} R^* (1-r)}$$

But

$$(1-r) = (1-\frac{R_L}{R^*}) = \frac{1}{R^*}(R^* - R_L) = \frac{R_F}{R^*}$$

Therefore, the final expression for the current gain becomes

$$G_I = \frac{V_M}{I_{cM} R_F} \qquad \text{for} \quad \omega t_c < \omega t_s \tag{33}$$

It is interesting that the current gain is independent of load resistance, control turns, and load turns. Although the relationship between the angles is independent also of V_M and I_{cM}, these quantities enter into Eq. (33) in the process of averaging the load and control currents. The gain is inversely dependent on R_F, the forward mesh resistance, which is the sum of the rectifier and winding resistances. The lower I_{cM}, the greater the gain.

I_{cM}, however, must not be brought below the minimum specified by Eq. (16).

The curves of Fig. MRI-13440-c can be translated into the transfer curves of Fig. MRI-13440-d, by observing that when $\omega t_c = 0$ the control current is a negative maximum and when $\omega t_s = 0$ the average rectified load current is a maximum. Figs. MRI-13441-a, MRI-13441-b, and MRI-13441-c show the theoretical transfer curves with various parameters. In the curves note that

$$\bar{I}_{L\ MAX} = \frac{2V_M}{\pi R^*}, \qquad \bar{I}_{c\ MAX} = \frac{2I_{cM}}{\pi}$$

To find the voltage gain consider the control circuit to have a finite physical resistance, R_c. Then

$$G_V = \frac{R_L}{R_c}\frac{d\bar{I}_L}{d\bar{I}_c} = G_I \frac{R_L}{R_c}$$

and from Eq. (33)

$$G_V = \frac{V_M R_L}{I_{cM} R_F R_c} \tag{34}$$

The power gain is given by the following definition:

$$G_p = \frac{R_L}{R_c}\frac{d(\bar{I}_L^2)}{d(\bar{I}_c)^2} = G_I^2 \frac{R_L}{R_c} = \frac{V_M^2 R_L}{I_{cM}^2 R_F^2 R_c} \tag{35}$$

In a multistage amplifier I_{cM} and R_c are usually related, since actually the control circuit is excited from a voltage source as shown in Fig. MRI-13436-b.

It should be noted that Eq. (33) predicts a perfectly linear transfer curve since it involves only circuit constants and does not include the magnetic properties of the cores. Deviations from linearity are partially due to magnetizing current which Eq. (33) neglects.

Figs. MRI-13442 to MRI-13446 are transfer curves taken with the doubler circuit and using a-c excitation. The test setup is as in Fig. MRI-13436-b. The core material is Hypernik V and information regarding the cores is given in the Appendix.

It is seen by glancing at the curves that the high gain region is obtained for small control angles which correspond to large values of control current. Fig. MRI-13441-d shows the potentiometer setup used to take these readings accurately.

In general, there is very good correlation between the experimental results and Eq. (33). Fig. MRI-13442 uses different values of forward mesh resistance. It is immediately seen that the gain is an inverse function of forward mesh resistance. Also the useful range is smaller as the resistance goes up because the control angle meets the firing angle at a later value as seen in Fig. MRI-13440-c. The entire range is less because increasing the mesh resistance lowers the maximum load current. The rectifier resistance is taken as one ohm since two discs of selenium are used in each rectifier, and from the Appendix it is seen that the proper value of forward resistance based on the linear portion of the rectifier characteristics is about one ohm.

In Fig. MRI-13443 the control current amplitude is the parameter. The gain is seen to go up with decreasing amplitude in accordance with Eq. (33). There is a lower limit of control amplitude because of the necessity for the control current to jump an amount corresponding to the coercive force as dictated by Eq. (16). It is noticed that for still lower amplitudes of control current the bottom half of the transfer curve is wiped away, since now small control angles will not satisfy Eq. (16). The same effect would result if too few control turns were used. This then is one of the factors limiting the gain. The obvious solution is to use more control turns, but if too many turns are used, the control current may be affected by induced voltages from the load circuit and may no longer be assumed forced.

Transfer curves using line voltage as the parameter are plotted in Fig. MRI-13444. Again in accordance with Eq. (33), it is observed that increasing the line voltage increases the gain and of course also the range of operation. The voltages used were all under the saturation value. The effect of larger voltages will be considered in the next section. For lower voltages the curve is shifted to the right and control takes place over a region of later control angles. This shift is not explained by the idealized theory of the preceding sections and more light may be shed on this phenomenon after the discussions of Chapter II, which consider deviations from the ideal hypotheses.

In Fig. MRI-13445 the effect of load resistance changes is shown. As predicted by Eq. (33) the gain is not affected. Furthermore, the curves are not shifted from each other, which indicates that for a given control angle the amplifier behaves like a constant current source, provided operation is maintained in the linear high gain range. Naturally, the range of operation is reduced for higher values of load resistance since the maximum load current is lower.

Of interest are the curves of Fig. MRI-13446 which show that the gain is independent of both load and control turns. The only effect of varying the control turns is to shift the transfer curve. Increasing the turns shifts the curve to the right and control is obtained over a range of later control angles. Changing the load turns has only a very slight effect on the gain and does not shift the curve. The region of operation, however, is seen to be higher. This is because decreasing the turns increases the magnetizing current.

It is well if the transfer curves are shifted a little to the right without a loss of gain for two reasons. For one thing control is obtained over a region of later control angles which means that the jump of control current at the control angle will be greater and lower values of control amplitude can be used, thereby increasing the gain. Secondly, if the amplifier is operated from another stage a higher overall gain will result, because the first stage operates over a region further from the bend of its own transfer curve. For these reasons any slight shift to the right, as caused by an increase of control turns, for example, is welcome.

The transfer curves of Figs. MRI-13442 to MRI-13446, immediately bring to light two shortcomings of this type of operation. For a two-stage single-ended amplifier full control current in the second stage must be maintained when the amplifier supplies no load ($\bar{I}_L$ is low). Secondly, if operation is limited strictly to one region of the transfer curve, full output is never obtained. The entire region of control is up to control angles of the order of 20 to 50 degrees.

Nevertheless the transfer curves have excellent linearity and current gains of the order of 50 were obtained without any difficulty. Much higher gains could be expected for Hypernik V cores wound with load turns of lower resistance.

Table 1 (Fig. MRI-13474) compares the values of gain measured from the transfer curves to those calculated from Eq. (33). The results are in very good agreement despite the fact that Eq. (33) neglects magnetizing and circulating currents. The measured values of gain could only be considered accurate to within 5%.

G. Operation with Larger Voltages

In the analysis of Section C, the condition was imposed that the core never saturated negatively. This was insured by making F_M less than or equal to F_S. Since increasing the voltage increases the gain, the next logical step is to investigate what happens when $F_M > F_S$ or $V_M > \omega N F_S$.

The effect of increasing the voltage is to cause the cores to saturate negatively for values of control angle which will make the minimum flux, F_o, hit the value $-F_S$. Eq. (22) is

$$F_G - F_o = F_M (1 - \cos \omega t_c)$$

and Eq. (20) can be written in its approximate form as

$$F_S - F_G = F_M (\cos \omega t_c - \cos \omega t_s)$$

when $F_o = -F_S$, the limit of the analysis of Section C,

$$F_G + F_S = F_M (1 - \cos \omega t_c).$$

Adding

$$2F_S = F_M (1 - \cos \omega t_s)$$

or

$$\text{Min. } \cos \omega t_s = \frac{F_M - 2F_S}{F_M} \tag{36}$$

such that the analysis of Section C is valid.

Even though F_M is greater than F_S, the analysis of Section C is valid as long as Eq. (36) is satisfied. If, however, the control angle is brought so low that it causes the cosine of the firing angle to go below the minimum specified by Eq. (36), then the cores saturate negatively and the analysis is no longer valid.

At the start of the positive half-cycle core No. 1 is at pt. B (Fig. MRI-13447-a) and ready to start its rise. Core No. 2 is at pt. A and is not ready to decay because the control current is "off" (see Section D). It is clear because F_2 cannot decay until the control current goes "on", and since after that the fluxes rise and decay with the same amplitude, F_M, that core No. 1 must saturate positively before core No. 2 saturates negatively. That is, $\omega t_s < \omega t_L$ where ωt_L is when F_2 hits $- F_S$.

F_1 rises with amplitude F_M from zero to ωt_s over the range from $-F_S$ to $+ F_S$, and by the rules of Section D,

$$2F_S = F_M (1 - \cos \omega t_s) \tag{37}$$

and solving for the firing angle

$$\cos \omega t_s = \frac{F_M - 2F_S}{F_M} \tag{38}$$

a result which is independent of the control angle. Thus, the firing angle is constant and equal to the maximum value as specified by Eq. (36) whenever the core saturates negatively. This will occur for all values of control angle which when substituted in Eq. (23) give a value of cos ωt_s below that of Eq. (36). For larger control angles the firing angle is determined by Eq. (23).

Fig. MRI-13447-b shows the relationship between the cosines of the control and firing angle for the case where F_M is larger than F_S for diffsrent values of r. The theoretically expected transfer curves for different values of voltage are drawn in Fig. MRI-13447-c.

The effect of overdriving the amplifier was observed experimentally and the results are plotted as transfer curves in Fig. MRI-13448. Although the gain increases somewhat with increasing voltage, as predicted, the load current cannot be brought below a minimum corresponding to the firing angle as given by Eq. (38). For this reason application of the overdriven amplifier is more or less limited.

II. Deviations from the Basic Assumptions

A. Justification of the Basic Assumptions

Certain assumptions were made in Section A of Chapter I to simplify the derivation of the basic steady state modes of operation of the a-c excited doubler circuit. These gave rise to an idealized theory the accuracy of which was checked to some extent by the transfer curves and wave form photographs. The close correlation between the experimental results and the theory is itself evidence that the assumptions made were good ones for a sensitive core material, such as Hypernik V.

That the d-c hysteresis loop for the Hypernik V cores can be represented as rectangular as in Fig. MRI-13437-b is seen from a study of the actual loop taken from hysteresis loop measurements using the ballistic method described by Spooner[11]. The loop is plotted in the Appendix. Now, if magnetizing current is neglected anyway, the slope of the vertical portions of the loop in no way affects the wave shape of the load current. Furthermore, the firing angle using a-c excitation should not be affected by a change in the slope of the loop. This is in contrast to the d-c excited amplifier where the minimum flux (which determines the firing angle) is determined by the d-c current in the control circuit and is critically dependent on the slope. In the a-c case, however, the minimum flux is not set by a d-c MMF but rather is determined by the amount of flux decay that the "valve action" of the control current permits. It can therefore be concluded that the analysis is valid also for the less sensitive core materials provided the knee of the B-H curve remains sharp and the magnetizing current does not become too large. More will be said regarding less sensitive core materials in Section F of this chapter.

The photograph of Fig. MRI-13449-a shows a minor loop traced out by a Hypernik V core and is in accord with Fig. MRI-13437-b.

It was assumed that the rectifier forward resistance was linear. The rectifier characteristics plotted in the Appendix show this to be true only for sizable currents through the rectifier. The only way the rectifier forward

resistance enters into the idealized theory is in determining the quantity $F_M(1 - r)$ which is the amplitude of the flux decay of core No. 2 while core No. 1 is saturated. This expression enters through Eq. (12). "r" is defined as R_L/R^* where R^* is partially determined by the rectifier resistance. But in the derivation of Eq. (12), R^* refers to the total resistance of mesh No. 1. During the interval for which Eq. (12) applies this mesh is fully conducting and therefore the rectifier resistance can be assumed as linear.

Rectifier leakage exercises its influence by tending to unlock the core from its zero MMF position from the beginning of the negative half-cycle to the control angle. It is thus expected that if the leakage is not pronounced, it will be insufficient to release the core and the operation should hardly be affected. Section G of this chapter studies the influence of leakage experimentally.

The third major assumption had to do with the control current. The main factor preventing forcing of the assumed current through the control windings is the EMF induced from the load meshes. Before the control angle one core is saturated and no voltage is induced across it. The other core, however, is rising with amplitude F_M and a voltage will be induced in the control windings tending to send current circulating in the same direction as the physical control current, and this may unlock the first core before the control angle. If, however, sufficient resistance is used in the control circuit and if the control turns are a fraction of the load turns, then the induced voltage is minimized. During the experimental runs, a control resistance of the order of 200 ohms was used together with a turns ratio of 6 to 1 and no appreciable induced currents were present. This was seen by observing the control current wave shape with and without shorted control windings and no significant change in the shape occurred. The photographs of Fig. MRI-13449-c and d bear this out.

To obtain the sharply truncated control current a sensitive core material with a sharp knee, such as Hypernik V, must be used in the first stage. Also the magnetizing current in the first stage must be low or else the control current will be "on" before the control angle.

B. A-C Excitation Shifted in Phase

It was implicitly supposed heretofore that the source of the a-c excitation was in phase with the load voltage. Out of phase operation of the doubler circuit will now be considered mainly for completeness but would seldom merit practical use, for reasons that will become apparent.

The angle by which the excitation source lags the load voltage is symbolized as "ωtp", and called the "phase angle". The phase angle introduces extra complications into the analysis and reference should be made to Fig. MRI-13450 and the rules of Section D of Chapter I applied. Four modes are

possible and are represented by the different diagrams. It is clear that the maximum phase angle is 180 degrees since the control current is full-wave rectified. A phase angle of 180 degrees is equivalent to one of zero degrees.

As illustrated in Fig. MRI-13450, mode (a) is when the control angle precedes the firing angle and occurs in the first half cycle after the phase angle.

In the ideal analysis the wave shape of the control current is irrelevant. It is important only when the control current is "on" and "off" as explained in Section D of Chapter I and illustrated in Fig. MRI-13440-a and Fig. MRI-13440-b.

From the start of the half-cycle up to the phase angle the control current is "on". Then F_2 decays from F_S according to Eq. (24). Defining the value of F_2 at the phase angle as F_P and integrating in the interval,

$$F_S - F_P = F_M (1 - \cos \omega t_p) \tag{39}$$

Then F_2 locks at F_P because the control current is "off". After ωt_c, however, it can once more decay and

$$F_P - F_G = F_M (\cos \omega t_c - \cos \omega t_s) \tag{40}$$

where F_G is defined just as in Chapter I as F_2 at the firing angle. After the firing angle Eq. (25) applies because F_1 is saturated. Then

$$F_G - F_o = F_M (1 - r)(1 + \cos \omega t_s) \tag{41}$$

All the while F_1 builds up unhampered according to Eq. (27). Thus,

$$F_S - F_o = F_M (1 - \cos \omega t_s) \tag{42}$$

Combining Eqs. (39) through (42) and solving for the firing angle gives

$$\cos \omega t_s = \frac{\cos \omega t_p - \cos \omega t_c - 1 + r}{1 - r} \tag{43}$$

It is seen from this that when the control angle occurs at the phase angle, then the firing angle is at the close of the half-cycle.

In mode (b) of Fig. MRI-13450, the firing angle precedes the control angle. Going through the same procedure as for mode (a) the flux relationships can be shown to be:

$$F_S - F_P = F_M (1 - \cos \omega t_p) \tag{44}$$

$$F_P - F_o = F_M (1 - r)(1 + \cos \omega t_c) \tag{45}$$

and

$$F_S - F_o = F_M (1 - \cos \omega t_s) \tag{46}$$

solving gives

$$\cos \omega t_s = -(1-r)(1+\cos \omega t_c) + \cos \omega t_p \tag{47}$$

It is seen that when $\omega t_c = \pi$, $\omega t_s = \omega t_p$.

In mode (c) the control angle is increased beyond π. When the control angle minus π precedes the firing angle the flux equations can be written. Since $\cos (\omega t_c - \pi) = -\cos \omega t_c$, the equations for this mode are:

$$F_S - F_G = - F_M (\cos \omega t_c + \cos \omega t_s) \tag{48}$$

$$F_G - F_o = F_M (1 - r)(\cos \omega t_s - \cos \omega t_p) \tag{49}$$

and

$$F_S - F_o = F_M (1 - \cos \omega t_s) \tag{50}$$

Solving:

$$\cos \omega t_s = \frac{1 + \cos \omega t_c + (1-r) \cos \omega t_p}{1 - r} \tag{51}$$

In mode (d) the firing angle comes first and:

$$F_S - F_o = - F_M (1-r) (\cos \omega t_p + \cos \omega t_c) \tag{52}$$

$$F_S - F_o = F_M (1 - \cos \omega t_s) \tag{53}$$

Solving:

$$\cos \omega t_s = 1 + (1-r) \cos \omega t_c + (1-r) \cos \omega t_p \tag{54}$$

Equations (43), (47), (51), and (54) give the theoretical relationship between the control and firing angles for the four different modes. When the phase angle is zero, there are only two different modes and the equations reduce to Eqs. (23) and (30). The theoretical relationship between firing and control angles for a given phase angle and different values of "r" is drawn in Fig. MRI-13451-a.

Although the cosine relationships are linear, the transfer curve will in general not be. Whereas the average load current is a linear function of cos ωt_g, the average control current is given by

$$\bar{I}_c = \frac{\bar{I}_{cMAX}}{2}\left[1 + \cos(\omega t_c - \omega t_p)\right]$$

and is not a linear function of cos ωt_c. It is also observed from Fig. MRI-13451-a that in general there are three discontinuities in the transfer curves.

To predict a transfer curve with ωt of phase operation requires the solution of a transcendental equation. This is done numerically for r = .9 and the results are plotted as broken lines for phase angles of 60 and 120 degrees in Fig. MRI-13452. The solid lines are experimental curves. A comparison of the results indicates that the theory is correct and can be used with fair reliability to predict the trend of any transfer curve for any phase angle, regardless of the shape of the control pulse.

C. A-C Excitation Plus D-C Bias

From the point of voiew of an a-c excited stage alone the transfer curves of Figs. MRI-13442 to MRI-13446 are in a rather awkward position. The use of a d-c bias comes to mind, the direction of which being "negative"; that is, in the same direction as the control pulses. From a theoretical standpoint the bias (if perfectly constrained) should allow the decaying core to slip out of saturation even before the control angle and instead cause it to lock at some other value of flux along the slope of the B-H loop. This would mean a reduction in F_o and a corresponding later firing angle. The delay in the firing angle is manifested by a shift of the transfer curve to the right. The flux where the core locks can be determined from the d-c control magnetization curve[12] of the circuit.

The first thing that is observed in attempting to take transfer curves of the a-c excited doubler circuit with bias is the instability illustrated in Fig. MRI-13451-b and so often encountered in underdriven magnetic amplifiers. The extent of the instability increases with the bias and for the ordinary unbiased case only a very slight instability is observed. This instability can be eliminated entirely by slightly overdriving the amplifier. To sidestep this difficulty all the transfer curves of Fig. MRI-13453 are taken for decreasing values of load current.

It is seen from Fig. MRI-13453 that although the bias shifts the transfer curves into a more accessible position, the gain is reduced by a factor of 2 or 3. Also the useful linear range is reduced since there is a discontinuity when the firing angle reaches the control angle. The condition of full saturation throughout the half-cycle is never reached because of the presence of the demagnetizing d-c MMF.

In view of these disadvantages, the use of d-c bias would be limited. Instead, however, there is nothing wrong with biasing the first stage which is d-c excited.

D. Control with "Positive" A-C Excitation

Control by varying the angle of truncation can also be achieved by applying the control pulses in a positive sense. This requires a large negative bias (larger than that required to shift the curves with "negative" control), since the positive pulses alone will keep both cores saturated throughout the cycle.

With "positive" control, the firing and control angles vary in the same direction, whereas with "negative" control they vary in opposite directions and meet somewhere along the way. Now the firing angle precedes the control angle as shown in Fig. MRI-13451-c, and the high gain region is obtained for control angles late in the half-cycle.

Fig. MRI-13454 is a plot of transfer curves for different values of d-c bias. The gain is of the same order of magnitude as with "negative" control for the same parameters, but the curves do not exhibit quite the linearity enjoyed by the amplifier with "negative" control. Also, it is observed that low values of load current are not in the linear range and this - plus the necessity of a large d-c bias - would limit the use of "positive" control to applications where the average control Current must be kept at low values for no a-c signal.

E. Effect of Shunting Additional Windings with Resistances

A very interesting property of the a-c excited doubler circuit is observed when a low resistance is shunted across an additional winding on each core. In the d-c excited self-saturating amplifier, the effect of this resistance is to pivot the transfer curve to the left about the upper knee of the original curve.[5] This results in a severe reduction in gain inversely proportional to the shunting resistance.

It is seen from the transfer curves of Fig. MRI-13455 that no such reduction takes place when a-c excitation - varying the angle of truncation - is applied. Even when the auxiliary winding of ten turns is shorted out completely, so that only the winding resistance of less than one ohm remains, the

gain is hardly affected. Only the minimum point is raised. On the other hand, shorting the winding for the d-c excited amplifier was observed to reduce the gain by a factor of thirty.

Dissipation in a resistance shunting a winding can be used to simulate the eddy-current loss in a core.[13] Conclusions should not be hastily drawn from Fig. MRI-13455, however, concerning the independence of the a-c excited amplifier from eddy-currents, since with a-c operation the eddy-currents may behave in an entirely different way, but these results should at least indicate the order of the effect.

F. The Use of a Less Sensitive Core Material

In Section A of this Chapter it was explained why it is expected that the operation of the a-c excited self-saturating amplifier should be independent (if magnetizing current is still negligible) of a change in the slope of the vertical portions of the B-H loop.

Consider a core material such as Hypersil, a major d-c hysteresis loop of which is in the Appendix. A minor loop is photographed in Fig. MRI-13449-b. The decaying core locks in at the zero MMF value as in the case of Hypernik V, but now this point is below saturation. The material is seen to be much less sensitive than Hypernik V. Not only is the slope considerably reduced but there is also no distinct transition between the "saturated" and "unsaturated" regions. Thus, in both the a-c and d-c excited cases, there is no longer the cleanly truncated load wave form observed with Hypernik V. Also the magnetizing current is considerable because of the lower unsaturated inductance.

It is therefore expected that the transfer curves exhibit a high degree of nonlinearity, in both the a-c and d-c cases, when Hypersil is used. Furthermore, in the d-c case the "gain" (taken arbitrarily as the maximum slope) is seriously affected, mainly because of the reduction in the slope of the B-H loop.

With a-c excitation, however, it is not the slope itself but rather the other factors (round knee, magnetizing current) which alter the shape of the transfer curves. Refer to Fig. MRI-13456. Curves K-1 and K-2 compare Hypersil to Hypernik V for equal forward mesh resistances, and it is seen that over a small range the gain with Hypersil comes very close to the gain using Hypernik V. At any rate, the difference is many times less than was observed with d-c excitation and in comparison to more sensitive core materials Hypersil would stand up very much better with a-c excitation.

When the forward mesh resistance is lowered as for curve K-3 of Fig. MRI-13456, the gain using Hypersil, is very high and this indicates that it is the winding resistance rather than core properties which imposes a practical limitation on the gain.

From these considerations it is concluded that in many cases Hypersil can be used as the core material for the last stage of a multistage amplifier with but little reduction in overall gain. However, because of the rounded wave forms, the output cannot be used to excite further stages in the same manner.

G. . The Effect of Rectifier Leakage

Leakage of the mesh rectifiers, when a negative voltage is applied, exerts its greatest influence during the short interval before the control angle. With only slight leakage the flux of the decaying core remains practically locked in at a constant flux, as shown in Fig. MRI-13449-e, up to the control angle. However when additional leakage is introduced (by shunting the rectifiers with resistors), there is a demagnetizing effect because of the negative mesh currents, and the MMF varies, preventing the locking of the cores at a fixed value of flux. A large amount of leakage, as caused by 1000 ohm shunting resistors, results in the flux wave form of Fig. MRI-13449-f, where it is seen that the core does not lock at all.

The effect on the transfer characteristics is shown in Fig. MRI-13457. Unlike the case with d-c excitation[4], there seems to be no appreciable reduction in linearity. The gain, however, is reduced quite a bit. The reduction in gain seems to begin after a critical value of leakage. This value probably corresponds to the demagnetizing MMF just required to unlock the core past the knee of the B-H loop. For lesser leakage the demagnetization results in no change of flux and does not affect the operation much.

A comparison of curves L-4 and L-6 indicates that the amount of leakage is independent of load resistance.

Equation (33) states that as the voltage is halved, the current gain should also be halved. Comparing curves L-4 and L-5, which are for large amounts of leakage, shows the gain to be little changed by halving the voltage. The conclusion is that halving the voltage also halves the leakage current which compensates for the drop in gain predicted by Eq. (33).

H. Effect of Lowering Control Circuit Resistance

It was previously mentioned that the assumption of control current "forcing" can always be fulfilled by using a large enough control circuit resistance. If this resistance is decreased, the effect of induced voltages from the load windings to the control windings will become pronounced, and as explained in Section A of this Chapter, a circulating current will flow before the control angle in the same direction as the applied control current.

Fig. MRI-13460-a and Fig. MRI-13460-b show photographs of the control current with a low control resistance (ten ohms) for shorted and unshorted control windings. Compare these with Fig. MRI-13449-c and Fig. MRI-13449-d. With the control windings shorted, there are no induced voltages. It is seen, however, that the control current wave shape is far from the ideal anyway, there being no sharp truncation. This is because the first stage is operated with a low resistance and a low voltage (to keep the current amplitude fixed). When the shorting is removed from the control windings, the effect of the induced voltages on the control current is observed.

The curves of Fig. MRI-13458 show the effect of insufficient forcing. As the resistance was lowered, the voltage of the first stage was also lowered in order to keep the same current amplitude. It is seen that if the control circuit resistance is lowered too much, the gain decreases.

III. Transient Behavior

A. Background

In general any amplifier, whether magnetic or electronic, has associated with it a certain delay, the extent of the delay usually being directly related to the magnitude of the gain. In terms of a sinusoidal input the delay is interpreted as a frequency and phase response. With a step input the delay is measured in terms of a "rise time" or "time constant".

Since a magnetic amplifier is essentially a d-c amplifier, it is convenient to express its delay as a response due to a step signal within its linear range of operation. The "time constant" of the amplifier is defined as the time required for the completion of an output change of 63% after a step signal is applied.[14] The "output" refers to the average output over a cycle and the time response is pictured as taking place over a large number of cycles. The transient can never be less than one cycle since it requires at least that long to reach a steady state condition.

The term "time constant" implies that the output changes as a simple exponential. This is only true in the case of a linear single-delay system. In general, there may be several stages which introduce several independent delays. In addition, magnetic amplifiers do not behave linearly within each cycle. However, if the operation is restricted to a straight line portion of the transfer curve, and if the time response is long enough, the response is very close to an exponential.

The time constant is often expressed in cycles of line frequency instead of seconds.

B. Method of Transient Observation

In order to obtain a stationary pattern of the transient on an oscilloscope, the step must be applied repetitively and periodically. This is done by switching the d-c input to the first stage by means of a fast acting relay which is operated from a chain of electronic frequency dividers driven from line frequency. Details of this instrument are given in the Appendix. This is the same as applying a square wave input whose half period is long enough to allow the transient to settle. It is important that the impedance the amplifier sees looking back into the switching circuit is not much different when the switch is open or closed, since the time response is in general a function of this impedance.

The test setup is seen in Fig. MRI-13459-a. The oscilloscope sweep must be made a very low frequency since the transients are slow. This is accomplished by means of the external condenser as shown. A sweep period of two seconds is a typical value. Since the sweep is slow, the scope screen should be long persistent.

Since only the average value of output is of interest, the output is first averaged by means of a Cyclic Integrator,[15] which, by electronic integration, gives a pulse for each cycle the height of which is proportional to the average output. Photographs of the resulting displays are seen in Figs. MRI-13460-c, d, e, f, and Fig. MRI-13461.

C. Overall Transient Response of Two-Stage Magnetic Amplifier

The second stage of a two-stage magnetic amplifier is a-c excited from the rectified output of the first stage, which itself is d-c excited. For proper operation the control current to the second stage must be forced by using a large enough control circuit resistance. Thus, the control windings are fed from an effective current source which means that the time response of the first stage is unaffected by the presence of the second stage. This was checked experimentally by observing the response of the first stage when the control windings of the second stage were connected and when they were shorted. No difference was observed.

In the a-c excited amplifier stage, a step signal means that the control angle jumps from one value to another instantaneously. This is possible if the current is forced. Unlike the d-c situation this does not mean that the minimum flux within a cycle must jump from one cycle to the next. The minimum flux is not determined from a d-c MMF and is set by the control angle in the steady state only. During a transient the minimum flux changes gradually and the second stage has a delay despite the fact that the control current may jump. The time constant of the second stage will be considered in the following sections. At present, let it suffice to say that the second stage alone has a time constant denoted by T_2.

The question arises in what manner the two-stage amplifier responds to a step signal to the first stage if the stages have time constants of T_1 and T_2, respectively. The problem consists of determining the response of the second stage of time constant T_2 to an exponential of time constant T_1 which is the output of the first stage when a step is applied thereto. This can be solved using the Laplace Transforms.

The resulting response is of the same form as the current obtained when an exponential voltage wave shape, of time constant T_1, is applied to a deenergized resistance-inductance series circuit of time constant T_2.

Thus

$$I(p) = \frac{E(p)}{Z(p)}$$

where, if K_1 is a constant, the impressed voltage is

$$K_1 \left(1 - \varepsilon^{-\frac{t}{T_1}}\right)$$

which transforms into

$$E(p) = K_1 \left(\frac{1}{p} - \frac{1}{p + \frac{1}{T_1}}\right) = \frac{K_1}{T_1} \frac{1}{p\left(p + \frac{1}{T_1}\right)}$$

and

$$Z(p) = K_2 \left(p + \frac{1}{T_2}\right)$$

Then

$$I(p) = \frac{K}{T_1 T_2} \frac{1}{p\left(p + \frac{1}{T_1}\right)\left(p + \frac{1}{T_2}\right)} \tag{55}$$

where K is another constant. The inverse transform of Eq. (55) yields the solution for the response

$$K\left[1 - \left(\frac{T_1 \varepsilon^{-\frac{t}{T_1}} - T_2 \varepsilon^{-\frac{t}{T_2}}}{T_1 - T_2}\right)\right] \tag{56}$$

This is valid if the two time constants are different. If $T_1 = T_2$, Eq. (55) becomes

$$I(p) = \frac{K}{T_1^2} \frac{1}{p(p + \frac{1}{T_1})^2} \tag{57}$$

the inverse transform of which gives the response as

$$K\left(1 - \frac{t}{T_1} \varepsilon^{-\frac{t}{T_1}} - \varepsilon^{-\frac{t}{T_1}}\right) \tag{58}$$

for $T_1 = T_2$

Eq. (56) gives the response of a two-stage amplifier to a step input in terms of the individual time constants. Fig. MRI-13459-b shows the response for two different cases.

D. Transient Response of A-C Excited Stage - Observation

The determination of the time response of the d-c excited self-saturating circuit is discussed elsewhere.[7] It is the second or a-c excited stage with which this work is concerned. As mentioned previously, a step input to an a-c excited amplifier means that the control angle jumps from one value to another. Direct switching cannot be used to accomplish this. Instead the test stage is fed from a d-c excited amplifier where switching can be accomplished easily as described in the Appendix.

It is seen from Eq. (56) that if the time constant of the first stage is small compared to that of the second stage, the overall response approximates a simple exponential and the observed "time constant" is but little greater than that of the second stage alone. All measurements are taken with the doubler circuit of Fig. MRI-13436-a. The core material is Hypernik V. In all observations the switching rate is 1/64 of the line frequency. The time constant in cycles is read directly by counting the number of pulses (see Section B of this Chapter) up to the 63% point.

The photographs of Fig. MRI-13460-c, d, e, f are taken for varying parameters. It is seen that the time constant is practically independent of control circuit resistance, control turns, and load turns. It is not so surprising that the response is independent of control resistance and control turns since the control current is forced through them anyway. At first, however, it is startling that the response is independent of load turns, since the cores are the seat of the delay and their influence should be felt in

relation to the number of turns through which they are introduced into the load meshes. Nevertheless, it is shown in the following section that the result is theoretically correct.

It is further observed (but no photos are shown) that the time constant is virtually independent of line voltage and control amplitude. In addition, the time constant is not related to the operating range as long as it remains in the linear region. Another point to be made is that no difference can be detected upon rise and decay of the transient. In the d-c excited doubler circuit such a difference has been observed and explained.[7]

For the given circuit only two quantities are seen to influence the time constant to any extent. They are load resistance, R_L, and forward mesh resistance, R_F. Fig. MRI-13461 shows various response patterns as these parameters are varied. Clearly the time constant is observed to increase as the load resistance increases but decreases as the forward mesh resistance is made higher.

E. Transient Response of A-C Excited Stage - Theory

It is extremely difficult to derive an exact theory of the transient response of a magnetic amplifier, but if one speaks of relatively longer time constants and considers only average quantities where operation is restricted over linear portions of the transfer curves, the problem can be attacked more easily.

A method used by Storm[16] for a simple d-c excited amplifier, which gave good correlation between theory and observed results, will be applied here. It must be remembered that the solution involves many approximations, but even if the results are not mathematical certainties, they can be used to show a qualitative trend. As it turns out, however, the theory is in close agreement with the previously observed results.

An "average" or "effective" inductance is defined for each core as the change in average flux linkages per change in average amperes; that is,

$$L = N \frac{\Delta \bar{F}_1}{\Delta \bar{I}_1} \tag{59}$$

Consider the doubler circuit of Fig. MRI-13436-a. If the control current is forced and a step is applied (meaning a jump of the control angle), the only effect of the control circuit is to induce a step driving function in the load windings. Then the equivalent circuit with the elements linearized is as in Fig. MRI-13459-c where only average quantities are considered.

It is known from the steady state theory (Chapter I, Section C) that the rectifiers conduct nearly throughout the whole cycle, the only time they block being during the short portion of the negative half cycle before the control angle. It will therefore be assumed that the rectifiers can be represented in Fig. MRI-13459-c by a constant forward resistance and this lumped with the winding resistance is the quantity called R_F.

The mesh equation for the upper loop is

$$e = (R_L + R_F + pL)\,\bar{I}_1 - R_L\bar{I}_2$$

But by the symmetry of operation $\bar{I}_1 = \bar{I}_2$, therefore

$$e = (R_F + pL)\,\bar{I}_1$$

and since e is a step the time constant is

$$T_2 = \frac{L}{R_F} \tag{60}$$

It remains to determine "L". It should be noted that Eq. (60) is valid only for the doubler circuit. Note that in the full-wave circuit of Fig. MRI-13462-b the time constant would be $\frac{L}{2R_L + R_F}$ since the currents add in the load resistance.

Now if magnetizing current is neglected, the current $\bar{I}_1$ has two components, namely, one-half the load current plus the average circulating current. Then

$$\Delta\bar{I}_1 = \frac{1}{2}\Delta\bar{I}_L - \Delta\frac{N_c}{N}\bar{I}_c$$

where I_c is itself negative. But $\Delta\bar{I}_c = \Delta\bar{I}_L/G_I$, thus

$$\Delta\bar{I}_1 = \Delta\bar{I}_L\left(\frac{1}{2} - \frac{N_c}{N}\,\frac{1}{G_I}\right)$$

The second term in the parenthesis is ordinarily much less than a half. Hence, $\Delta\bar{I}_1 \approx \frac{1}{2}\Delta\bar{I}_L$, and Eq. (59) becomes

$$L = 2N\,\frac{\Delta\bar{F}_1}{\Delta\bar{I}_L} \tag{61}$$

At this point another approximation is made. The average flux in core No. 1 is taken to be the mean of the minimum flux, F_o, and the saturation flux, F_s. In other works, $\bar{F}_1 \approx \frac{F_s + F_o}{2}$, and

$$\Delta \bar{F}_1 \approx \frac{\Delta F_o}{2}$$

Now from Eqs. (15) and (19) with F_x negligible

$$F_s - F_o = F_M (1 - \cos \omega t_s)$$

and

$$\Delta \bar{F}_1 = \frac{\Delta F_o}{2} = \frac{F_M}{2} \Delta \cos \omega t_s$$

but from Eq. (32),

$$\Delta \cos \omega t_s = \frac{\pi R^*}{V_M} \Delta \bar{I}_L$$

therefore,

$$\Delta \bar{F}_1 = \frac{\pi F_M R^*}{2V_M} \Delta \bar{I}_L$$

but

$$F_M = \frac{V_M}{\omega N}$$

thus,

$$\Delta \bar{F}_1 = \frac{\pi R^*}{2\omega N} \Delta \bar{I}_L = \frac{R^*}{4fN} \Delta \bar{I}_L$$

Substituting back into Eq. (61), the effective inductance is seen to be

$$L = \frac{1}{2} \frac{R^*}{f} \qquad (62)$$

This gives the rather interesting result that the effective or average inductance seen by the load mesh is independent of the turns and is related to the total mesh resistance directly. Substituting in Eq. (60) the time response is seen to be

$$T_2 = \frac{1}{2f}\,\frac{R^*}{R_F} \quad \text{in seconds}$$

or

$$T_2 = \frac{1}{2}\,\frac{R^*}{R_F} = \frac{1}{2}\,\frac{(R_L + R_F)}{R_F}, \quad \text{in cycles} \qquad (63)$$

Thus, as previously observed, the time constant is determined only by the load and forward mesh resistances. Expression (63) can be rewritten as

$$T_2 = \frac{1}{2}\,\frac{R^*}{R^* - R_L} = \frac{1}{2}\,\frac{1}{(1-r)}$$

Thus, the time constant is seen to be inversely related to the cosine gain given by Eq. (23).

A comparison of the measured results of the preceding section and the values of time constant calculated from Eq. (63) is given in Table 2, Fig. MRI-13475. The results are seen to be in very good agreement. The observations in Fig. MRI-13461 could only be made within a certain accuracy and a range rather than a fixed value is given as the result.

In all photographs the time constants on rise and decay of the transient are indistinguishable. In the d-c excited doubler there is a difference due to a circulating current on decay.[7] In the a-c case, however, the circulating currents are already considered and they are not affected by the direction of the step signal.

F. Figure of Merit

The figure of merit of a magnetic amplifier is defined as the ratio of gain to time constant in cycles.

At this point the multistage amplifier shows a great advantage, since the overall gain is the product of the gains of the individual stages, whereas it can be said with tongue in cheek that the total time constant is only the sum of the individual time constants. Thus, the figure of merit is greater than would be obtained with but one stage.

From Eqs. (23) and (63) the "cosine" figure of merit of the a-c excited stage is:

$$M_{cos} = \frac{G_{cos}}{T_2} = 2 \qquad (64)$$

The "current" figure of merit is from (33),

$$M_I = \frac{G_I}{T_2} = \frac{2 V_M}{I_{cM} R^*} \tag{65}$$

The "voltage" figure of merit is from (34),

$$M_V = \frac{G_v}{T_2} = \frac{2 V_M R_L}{I_{cM} R^* R_c} \tag{66}$$

The "power" figure of merit is from (35),

$$M_P = \frac{G_P}{T_2} = \frac{2 V_M^2}{I_{cM}^2 R_F R_c} \tag{67}$$

if $R_L = R^*$ approximately.

Most often the performance is expressed in terms of the power figure of merit. To maximize it the winding and rectifier forward resistance should be kept small. To raise the voltage, either the load turns must be increased in order to keep the "minimum point" on the transfer curves, or else cores with larger cross-sectional area used to raise the saturation flux. However, increasing the load turns raises the winding resistance. To minimize the control amplitude in Eq. (67), more control turns must be used to satisfy Eq. (16). The control resistance must not be lowered so much that the control current can no longer be assumed as forced. In addition, it should be kept in mind that it is the overall figure of merit that is important in a multistage amplifier and increasing the figure of merit of the a-c excited stages should not be done at the expense of that of the first stage unless the overall figure of merit is greater.

The gain, time response, and hence the figure of merit of the a-c excited self-saturating circuit is to a first approximation independent of core characteristics. This is in contrast to the d-c excited self-saturating circuit, where the figure of merit is seriously contingent on core characteristics and dimensions.[17] The upper practical limit to gain and figure of merit obtainable is, however, definitely determined by the cores.

IV. Application to Various Circuits

A. Half-Wave Circuit

Until now the entire discussion was limited to the voltage doubler circuit, since it reacts most favorably to a-c excitation as present comparison

will reveal. As a special case of the doubler, consider the situation when r = 0. This means that the entire mesh resistance is in series with the windings and there is no coupling between the two meshes.

The half-wave circuit of Fig. MRI-13462-a represents one mesh of the doubler circuit when r = 0. Useful load current flows only during one half-cycle. Referring to the ideal cosine relationships of Fig. MRI-13440-c, it is seen that the cosine gain for r = 0 is unity, and that there is no discontinuity in the characteristic.

Since the control current has no effect on a core whose flux is rising, it is necessary to have control only during the negative half-cycle. The ideal wave forms are drawn in Fig. MRI-13462-c. Note that now both the maximum average control current and maximum average load current are reduced by a factor of two for the same voltage, control amplitude, and total mesh resistance as for the doubler.

For the half-wave circuit the previous gain relationships can be applied with $R_F = R^*$. Hence, if control current is used over only one-half of the cycle, it follows from Eq. (33) that

$$G_I = \frac{V_M}{I_{cM} R^*} \tag{68}$$

which means that the gain is the ratio of the load current amplitude to the control current amplitude.

This result is valid for all control angles since there is no discontinuity of modes. An actual transfer curve is plotted in Fig. MRI-13464 and the result is in agreement with the above.

Although the half-wave circuit gives good linear operation and its range encompasses all control angles, its usefulness is seriously impaired by the fact that it has an inherent low gain about which not much can be done.

The theoretical time constant can be found in the same way as for the doubler circuit (Chapter III, Section E). The "effective inductance" is again given by Eq. (62). The effective resistance is now, however, R^* instead of R_F. Hence

$$T_2 = \frac{L}{R^*}$$

and substituting R^* for R_F in Eq. (62),

$$T_2 = \frac{1}{2} \text{ cycle} \tag{69}$$

which is a bad approximation since the transient analysis is valid only for longer time constants. However, the photograph of Fig. MRI-13467-a shows the time response to be close to one cycle which is considerably faster than for the doubler circuit.

B. Full-Wave Circuit

The only difference in the basic equations for the full-wave circuit of Fig. MRI-13462-b is that Eqs. (1), (2), and (3) should be rewritten as

$$V_M \sin \omega t = (R_L + R_\omega)\, i_1 + e_1 + N \frac{dF_1}{dt} + R_L\, i_2$$

$$-V_M \sin \omega t = (R_L + R_\omega)\, i_2 + e_2 + N \frac{dF_2}{dt} + R_L\, i_1$$

and

$$i_L = i_1 + i_2$$

Thus, in computing the voltage across core No. 2, dF_2/dt, when core No. 1 is saturated, as was done in Eq. (11), the quantity $(1-r)$ becomes $(1+r)$ and if magnetizing and circulating currents are once again neglected, Eq. (23) becomes

$$\cos \omega t_s = \frac{-r - \cos \omega t_c}{1 + r} \quad \text{for } 0 < \omega t_c < \omega t_s$$

The cosine gain in the range when the control angle is less than the firing angle is thus seen to be less than unity and have a minimum value of one half (when $r = 1$). Fig. MRI-13463-a shows the cosine relationships for different values of r. It is seen that the cosine gain for the full-wave circuit is greater when the control angle follows the firing angle, its value being the reciprocal of the cosine gain when the control angle occurs earlier. Thus, the useful range for the full-wave circuit has a maximum cosine gain of two. In particular

$$G_{cos} = (1-r) \quad \text{for } 0 < \omega t_s < \omega t_c \tag{70}$$

and the current gain is readily found to be

$$G_I = \frac{V_M}{I_{cM} R^*} (1+r) \tag{71}$$

Since usually the winding resistance is a small part of the total mesh resistance, r is nearly unity and $(1+r) \approx 2$. Thus,

$$G_I \approx \frac{2 V_M}{I_{cM} R^*} \quad .$$

To determine the theoretical time constant when operating within the basic mode, the exact same method can be applied as was used in Chapter III, Section E for the doubler circuit. Now, however, the currents through the common load resistance add and as a result the time constant is given by

$$T_2 = \frac{L}{2R_L + R_F} \tag{72}$$

Since the derivation of the quantity "L" made no specification of the relative position of the control and firing angles, its value is the same in the full-wave circuit even though the basic mode is for a firing angle preceding the control angle. Thus, the time constant is found to be

$$T = \frac{1}{2} \frac{R^*}{(2R_L + R_F)} \tag{73}$$

since R_L is considerably greater R_F, $R^* \approx R_L$, and $T \approx \frac{1}{4}$ cycle.

Of course, the actual time constant cannot be less than one cycle, so that Eq. (73) is written only for purposes of consistency. Fig. MRI-13467-b is a typical response pattern for the full-wave circuit.

Table 3, Fig. MRI-13475, lists values of theoretical gain and time constant for the three basic circuits. At first glance it seems that the theoretical value of time constant for the full-wave circuit of 1/4 is not in accord with the consistency of the other two circuits where the time constant is one-half the cosine gain. It must be remembered, however, that the full-wave circuit is operating in a different region (ωt_s before ωt_c), and that actually the cosine gain of the full-wave circuit is 1/2 when the control angle precedes the firing angle.

A transfer curve for the full-wave circuit is plotted in Fig. MRI-13464 and the trend once again justifies the theory. Control in the high-gain region is obtained over values of control angles late in the half-cycle which may be a distinct advantage as far as overall gain of two stages is concerned. The gain itself, however, is ordinarily much lower than that of the doubler circuit and in addition the range of operation has a rather high "minimum point".

The full-wave circuit does, however, have an intrinsically fast response time. If the time constant is taken as the minimum of one cycle, the figure of merit is equal to the power gain.

$$M_p = \frac{4 V_M^2}{I_{cM}^2 R_c R^*} \tag{74}$$

Thus, although the response of the full-wave circuit is much faster than that of the doubler circuit, the figure of merit of the doubler, as given by Eq. (67), can be made a good deal higher than that of the full-wave circuit.

C. The Multistage Amplifier

The possibilities of combining a-c and d-c stages using doublers, full-wave, or half-wave circuits, with or without feedback (see Section E of this Chapter) are indeed numerous and offer much "meat" for further investigation.

The schematic of a tested two-stage amplifier is drawn in Fig. MRI-13465. The cores used in both stages are of Hypernik V, those of the first stage having somewhat smaller dimensions. A d-c excited full-wave circuit is used as the first stage so that the input to the second stage requires no rectification. The second stage is a doubler circuit - to give a high gain - the input to which is the output current of the first stage. Fig. MRI-13466 is a transfer curve of the entire amplifier. The polarity of the gain is reversed from the single stage since two stages are used. The measured current gain is 720 corresponding to a power gain of 1.73 million. The measured overall "time constant" from the photograph of Fig. MRI-13467-c is about 30 cycles and thus the figure of merit is 57,600 - a figure much higher than would ordinarily be obtained from a single stage.[17] The regions of operation of each stage are depicted in Fig. MRI-13468-a. Note that although the first stage operates over a region close to the bend of its transfer curve, no appreciable loss in linearity results since the excursion of the first stage is small. If necessary the composite transfer curve can easily be shifted to give minimum output for zero d-c input by applying a small d-c bias to the first stage. It is noted that there is a power dissipation in the control circuit of the second stage, but this could conceivably be made use of by utilizing the control circuit to drive an auxiliary noninductive load.

The high figure of merit obtained with two stages could be multiplied many times by employing three stages, since the current gains multiply, whereas the individual time constants sort of add. It should be possible to obtain figures of merit of the order of several million without difficulty by hooking another doubler to the output of the circuit of Fig. MRI-13465. A problem arises here, however, since if both the second and third stages had identical transfer curves, the input excursion to the third stage would not

correspond to an output swing of the second stage over its own high gain region. Instead the second stage would operate with very early firing angles corresponding to a portion of the region BC of Fig. MRI-13437-c which gives low gain (or even an attenuation). The remedy is to somehow shift the high gain region of the third stage to the right as shown in Fig. MRI-13468-b. This can be done in several ways. One method is to apply a small d-c bias to the last stage. Another consists of operating the last stage at a lower voltage. The shifting effect of a reduced voltage was observed in the curves of Fig. MRI-13444. The possibility of substituting a full-wave circuit for the intermediate stage comes to mind since its high-gain region is obtained over a range of early firing angles (see Section B of this Chapter). This, however, results in a lower gain. Any attempt to increase the gain of the intermediate stage by raising the amplitude of the output of that stage reduces the gain of the third stage since its gain is inversely proportional to its control amplitude. Despite this, the method may be applicable because the intermediate cores can be of smaller size than those of the last stage and consequently require less control amplitude (see Eq. (16)).

Thus, by using sufficient stages very small d-c signals can be amplified to give large power changes with a relatively quick response. The practical limit is determined by the smallest signal that can be amplified without being drowned out by pickup and drift. The overall stability of the amplifier can be improved by incorporating some kind of negative feedback or by using a push-pull arrangement.

The fact that the control current of an a-c excited stage is unidirectional prevents the combination of two such units in a push-pull arrangement by themselves if the angle of truncation is to be varied. However, an overall push-pull scheme, such as illustrated in the block diagram of Fig. MRI-13469-a, is feasible. Each "half" of the push-pull is a multistage amplifier, the d-c input being fed to both halves in series. The outputs are then mixed to give wave forms such as in Fig. MRI-13469-b. The transfer characteristic of each multistage portion of the push-pull (such as those of Figs. MRI-13468-a and MRI-13468-b) is biased to the position where a zero d-c input corresponds to about one-half full output. This is done by applying a d-c bias current to the first stage of each half. The input windings are arranged so that an increase in the output of one-half section decreases the output of the other. The net output is the difference. The overall characteristics of the entire circuit is sketched in Fig. MRI-13469-c. If doublers are used as output stages, the negative values of output should be interpreted as a phase reversal of 180 degrees.

This arrangements, just as for a single stage push-pull circuit, gives zero output for zero input when perfectly balanced (biasing adjusted). The output range and the gain are greater than with just a single ended multistage amplifier of the same parameters. Also the linearity is considerably improved. Small variations in line voltage tend to cancel since both halves are affected simultaneously. This is also true for any common variation in core or circuit parameters due to such factors as heating, rectifier creep, etc.

Two possibilities of harmful interaction between the halves are in the d-c control mesh and through the common load. The use of a sufficiently high control circuit impedance will prevent coupling through the control mesh. The influence of the common load is to change the effective R_L that each output stage sees during the portion of the half-cycle after both halves have reached their firing angle. Thus, the quantity "r" takes on two different values and this will alter the individual transfer curves to some extent. There is also a reduction in current gain due to the mixing resistors drawing power themselves.

D. Frequency of the Power Source - Discussion

The 60 cycle line was used as the power source in all experimental work in the preceding sections. It is interesting to speculate on the use of a power source of a higher frequency, say in the audio range, for application to an a-c excited amplifier.

A magnetic amplifier is essentially a modulating system, the "carrier" being obtained from the power source and modulated by the average value of the signal. The signal (meaning a fluctuation in the average value of the truncated control current in the a-c excited case) must be of a frequency appreciably lower than the carrier, since the delay discussed in Chapter III results in a frequency response characteristic analogous to the drop in gain caused by stray and interelectrode capacities in electronic amplifiers at higher frequencies.

It is sometimes, but by no means always, necessary to demodulate the irregular wave forms obtained from the magnetic amplifier to give a fairly smooth d-c output. Two simply circuits to accomplish this are shown in Fig. MRI-13470-a. The arrangement using the condenser gives a d-c output, the condenser charging to the peak of the amplifier wave form. This, however, is not a reproduction of the average value. The use of the inductive scheme gives a true average. One immediate advantage arising from the use of a higher carrier frequency is to require smaller demodulating components for the same smoothness of output.

Another advantage lies in the fact that the time response in cycles is theoretically independent of frequency, but the response in seconds becomes correspondingly quicker with higher frequencies.

Not only does the response quicken with higher frequencies but the voltage applied can be greater for the same saturation flux and load turns. Thus, it is seen from Eq. (33) that the a-c excited amplifier can have a higher ultimate gain. Of course, Eq. (33) neglected any effects the frequency might have on the cores.

It is known that core losses, due partly to eddy-currents, increase with frequency. This may change the core characteristics to such an extent that Eq. (33) must be modified. However, it was shown in Section F of Chapter II that the a-c excited amplifier is not directly affected by core characteristics, the influence of the core properties on the gain being felt to a second

order only. Thus, it is expected that the effects of a higher frequency on the circuit are not as severe in an a-c stage as in the d-c excited amplifier.

Other difficulties may arise at higher frequencies because of winding leakage inductance and rectifier and winding capacity. Also a source supplying sufficient power at higher frequencies may present a practical difficulty.

E. Regenerative Circuits - Oscillator, Flip-Flop

Although the behavior of a magnetic amplifier is nonlinear within each carrier cycle, a consideration of only average rectified values of signal and output leads to the approximation of the device as a linear active element provided the operation is restricted to linear portions of the transfer characteristic and there is no "cutting off" at either end.

The analogy to a vacuum tube amplifier then comes forth, the latter being a voltage amplifier with a 180 degree phase reversal, and the magnetic amplifier acting as a current amplifier with arbitrary phase reversal since the windings are isolated. Fig. MRI-13470-b shows the linear equivalent circuit for each. The internal inductance shown in the magnetic amplifier plays the same role as the stray capacity in the electronic circuit, except that the effect of the inductance is felt at a much lower signal (modulating) frequency when speaking in terms of a sinusoidal input. The inductance is determined among other things by the type of circuit, and its value is such that when divided by R_L the result is the time constant in seconds. It is assumed that the amplifier is excited from a current source in the control circuit, a condition which should be approached in the a-c excited amplifier.

In Fig. MRI-13470-c the output of a magnetic amplifier of any number of stages is fed back to supply its own input. The circuit will be unstable and oscillate at a modulating frequency (frequency by which the angles vary) where the net "phase shift" is 360 degrees around the loop provided the loop cosine gain is equal to or exceeds unity in magnitude at that frequency, since then the amplifier supplies sufficient input for itself. There are two possible sources of phase shift. Each amplifier section itself gives either an in or out of phase output. There is an additional phase shift in each stage due to the inductance-resistance divider shown in the equivalent circuit of Fig. MRI-13470-b. Each divider has a theoretical maximum attainable shift of 90 degrees (at infinite frequency).

Applying these principles an oscillator was set up with three stages of doubler circuits using Hypernik V cores, each stage giving 180 degrees phase shift. The additional 180 degrees required for oscillation were provided by the effective inductances of the circuits, each delay giving 60 degrees. The block diagram is shown together with its electronic analogy in

Fig. MRI-13471. Fig. MRI-13467-d is a photograph of the oscillatory wave form as obtained across the load resistance of any of the stages. The frequency is seen to be about 7 cycles a second. Thus, the circuit can supply a low frequency oscillation of considerable power. Care was taken so the high gain regions of each circuit overlap, otherwise the circuit would not oscillate, and this required proper adjustment of the circuit parameters. Six cores were necessary (two for each stage).

Using two stages, 360 degrees phase shift is obtained only at a steady signal or at infinite frequency of modulation. The attenuation at higher frequencies due to the inductance-resistance divider will bring the loop gain down below unity. Thus, the two stage circuit (using negative control) with the output fed back into the input is unstable at d-c only. That is what is called a "flip-flop" circuit. Fig. MRI-13472 shows a magnetic flip-flop circuit, using Hypernik V cores, with its electronic analogy, the Eccles-Jordan trigger circuit. Half-wave circuits are used since their response time is rapid and their cosine gain at d-c is unity (see Section A of this Chapter) which gives just sufficient loop amplification to cause instability. Care must be taken so that control current in each stage flows during the negative half-cycle of the corresponding core, since only then is the control effective.

The operation can best be explained with reference to a transfer characteristic of the half-wave circuit as shown in Fig. MRI-13473-a. The control current of one stage is the load current of the other. A temporary increase in the control current of one stage decreases the control current of the other which in turn increases further the first control current. Thus the circuit is unstable, and this "run-away action" or "vicious cycle" continues until one stage cuts off (no longer on high-gain region). Then the circuit comes to rest with the stages operating at points A and B (Fig. MRI-13473-a), respectively. The circuit remains in this state until the stability is disturbed, whereupon the two stages interchange operating points. "Flipping" can be accomplished in many ways. One simple method is to inject a negative d-c bias pulse in the stage which is carrying full current, or a positive pulse in the other stage. This has the effect of temporarily shifting the transfer curve of one stage to where the circuit is again unstable. The duration of the pulse need be only so long that it insures that the run-away action is well under way. The rapidity of the run-away action is directly related to the time constant of the circuit, just as the stray capacity in the electronic flip-flop determines its flipping speed. Thus, in the half-wave circuit the pulse need only last for one cycle, as shown in Fig. MRI-13473-b.

The circuit of Fig. MRI-13472-b is by no means the only possibility of a flip-flop arrangement. Doublers could also be used for each stage but the speed of response would be much slower and more components are required. A one stage doubler could be used with positive control since this gives zero phase shift at d-c, but this requires the maintenance of a large d-c bias current (see Section D, Chapter II). The half-wave flip-flop circuit is relatively fast and requires only two cores, two rectifiers, and two resistors.

It can be plugged directly into the a-c line, requiring no d-c power supply. There is also no need for the stages to be symmetrical. One control amplitude can be reduced to the point where it still satisfies Eq. (16), thereby saving considerable power in one load.

It is noteworthy that at higher frequencies of the carrier the circuit is faster acting and the trigger pulses can be of a shorter duration.

Conclusions

Some of the more important results can be summarized as follows:

(1) By cascading several magnetic amplifier stages, a much greater figure of merit is obtainable than when but one d-c excited stage is used. The most favorable arrangement employes voltage doublers as the a-c stages, with "negative", in-phase, unbiased control current pulses. All stages except the very last should use a core material which saturates sharply. The winding resistance of the a-c excited stages should, in general, be kept down to a minimum.

(2) The minimum flux during a cycle is determined by the amount of flux decay that the "value" action of the control current permits.

(3) Therefore, the transfer characteristics are to a first approximation independent of the slope and width of the B-H loop, whereas the d-c excited operation is critically dependent on core characteristics. Thus, using less sensitive core materials will not seriously hamper the operation of the a-c excited amplifier. Also changes in core characteristics arising from the use of higher line frequencies should not severely influence the transfer characteristics.

(4) The ideal analysis of the a-c excited doubler with zero forward mesh (winding) resistance predicts infinite gain regardless of the slope of the B-H loop, whereas the ideal analysis of the d-c excited self-saturating circuit predicts a gain proportional to the slope, the forward mesh resistance not being a critical factor.

(5) The gain and time response of the a-c excited self-saturating circuit are both independent of load and control turns, as well as of core characteristics. The practical limit of gain and time response are, however, determined by the cores and windings. The expressions for gain and time response are summarized in Table 3, Fig. MRI-13475.

(6) There is close correlation between experimental and theoretical results throughout.

APPENDIX I-

$$G_I = \frac{V_M}{I_{CM} R_F} = \frac{2\sqrt{2}\, V}{\pi \bar{I}_{CMAX} R_F}$$

A- RESULTS WITH R_F AS PARAMETER (MRI-13442)

R_F	Calculated Gain	Measured Gain	% Dev.
7.5	58	54	-6.9%
18.5	23.4	20	-14.5%
29.5	14.7	11.5	-21.8%

B- RESULTS WITH I_{CM} AS PARAMETER (MRI-13443)

I_{CM}	Calculated Gain	Measured Gain	% Dev.
.393	29	26	-10.4%
.196	58	53	- 8.6%
.157	72	68	- 5.6%
.133	85	80	- 6.3%

C- RESULTS WITH V AS PARAMETER (MRI-13444)

V	Calculated Gain	Measured Gain	% Dev.
60	58	52	-10.3%
45	43.5	41	- 5.8%
30	29	29	-

D- RESULTS WITH R_L AS PARAMETER (MRI-13445)

R_L	Calculated Gain	Measured Gain	% Dev.
100	58	56	-3.5%
200	58	56	-3.5%
300	58	56	-3.5%

E- RESULTS WITH TURNS AS PARAMETER

N	N_C	Calculated Gain	Measured Gain	% Dev.
300	50	14.5	11	-29.1%
300	20	14.5	11	-29.1%
180	50	14.5	12	-17.2%

Table 1. Tabulation of Measured and Calculated Values of Current Gain

$$T_2 = \frac{1}{2} \frac{(R_L + R_F)}{R_F}$$

	R_L (ohms)	R_F (ohms)	MRI-13461 T_2 Observed	T_2 Calculated
1	50	7.5	4	3.8
2	100	7.5	7-8	7.2
3	200	7.5	12-14	13.8
4	200	27.5	4	4.2
5	200	17.5	5-6	6.2
6	200	12.5	8-9	8.6

Table 2. Comparison Between Observed and Calculated Time Constant for Doubler Circuit with A.C. Excitation Core Material-Hypernik V

	Time Constant	Cosine Gain	Current Gain
Doubler	$\frac{1}{2}(1-r) = \frac{1}{2}\frac{R^*}{R_F}$	$1-r$	$\frac{V_M}{I_{cM}R^*}(1-r) = \frac{V_M}{I_{cM}R_F}$
Half-Wave	$\frac{1}{2}$	1	$\frac{V_M}{I_{cM}R^*}$
Full-Wave	$\frac{1}{4}$ (approx.)	$1+r$ 2	$\frac{V_M}{I_{cM}R^*}(1+r)$ $\frac{V_M}{I_{cM}R^*}$

Table 3. Theoretical Relationships in Region of Highest Gain

APPENDIX II

Method of Switching the Transient

To study the transient response of a system experimentally, a satisfactory means for initiating the transient is necessary. One way to do this is to simply open or close a switch and record the response on a device such as a Brush Recorder or photograph it from an oscilloscope with a driven sweep.

It is usually more desirable, however, to obtain a stationary pattern on the oscilloscope. This requires that the switch opens and closes at a fixed rate. An electronic switch (square wave generator) accomplishes this and is very good for many purposes, but it has several restrictions. This "switch" has a comparatively high output impedance and is thus limited by the current that it can pass, unless additional power amplification is employed. This method also presents problems when a slow switching rate is desired.

At lower frequencies switching can be done by mechanical means. This investigation uses an instrument which opens and closes a fast acting relay thereby effecting repetitive switching. A schematic of the particular type of relay is shown in Fig. MRI-13430-a. If the current through winding AB is adjusted properly, the relay contacts will be open when no current flows in winding CD. But when the current through winding CD rises to a certain value, I_t, the contacts close, and when the current drops below a value, I_r, the relay reopens. Thus, by applying a square wave signal to winding CD, the contacts can be made to open and close at the frequency of the square wave. The frequency, however, must be low enough for the relay to handle and is limited to about 100 cycles a second.

The tripping coil CD is connected directly to one of the load resistances of an Eccles-Jordan Trigger Circuit. The amplitude of the pulses which trigger the circuit is fixed so that the circuit flips on negative pulses only, the pulses (both positive and negative) being obtained from the output of any one of a chain of frequency dividers (also Eccles-Jordan circuits), the choice depending on which frequency division of the reference voltage is desired to operate the relay. A block diagram is shown in Fig. MRI-13428. Fig. MRI-13429 is the actual circuit diagram.

The reference voltage is taken directly from the a-c line and may be 60 or 400 cycles. This input sine wave is sent through a clipper which is a high-mu triode that cuts off at -4 volts on the grid. The peak to peak value of the sine wave input is a few hundred volts so that a fast rise is obtained at the output of the clipper (Fig. MRI-13430-b). The clipped wave is then differentiated through a small condenser to give positive and negative pulses (Fig. MRI-13430-c), the negative pulses activating the first of the frequency dividers, the output of which (Fig. MRI-13430-d) is again differentiated and fed into the next divider giving an output (Fig. MRI-13430-e) which is once

again differentiated, and so forth. Thus, the relay contacts can be made to switch at 1/2, 1/4, 1/8, 1/16, 1/32, or 1/64 of line frequency. The phase of the switching relative to the line can be varied by the phase shift control.

A circuit diagram of the divider stage containing the relay tripping coil is drawn in Fig. MRI-13431-a. The tripping coil must not be connected directly in series with the plate of either tube because its inductance would slow down the run away action of the circuit when a negative pulse is applied to either grid and thus prevent tripping. Instead the coil is shunted by a 2200 ohm resistor so that the run away action can take place and after a transient the current in the coil will rise to its full value (about 10 ma).

Referring to Fig. MRI-13431-b, it is seen that the open and closed time of the relay will, in general, be of different duration. However, by properly adjusting the value of the critical tripping current, I_t, and release current, I_r, the relay can be made to have equal open and closed durations. The values of I_t and I_r are determined only by the bias current in coil AB (Fig. MRI-13430-a), and by varying the current the symmetry of the switching is controlled.

If a circuit as in Fig. MRI-13431-c is connected to the contacts, a square wave voltage appears across the resistor R which can be used to initiate a transient.

There is a small capacity associated with the relay contacts and lead wires, and this will cause the "switching time" to be longer when the relay opens than when it closes. Referring to Figs. MRI-13431-d and MRI-13431-e, it is seen that the time constant due to the relay capacity is $(\frac{RR_o}{R+R_o})C$ when the relay closes, and RC when it opens. R_o (the resistance of the contacts) is very small and therefore voltage across R jumps almost instantaneous upon closing, but a faint trace can be seen when the relay opens (Fig. MRI-13431-f). The value of R for Fig. MRI-13431-f is very high (.5 Meg) and if a more normal value is used the trace cannot be seen (Fig. MRI-13431-g), and the switching occurs almost instantaneously. This excludes the effect of any loading by the system to which the switching is applied.

List of Parts for Frequency Divider (see Fig. MRI-13429)

S_1, S_2	SPST Switch
S_3	Six Throw Selector Switch
P_1	Pilot Light 6.3 v.
F_1	50 ma. Fuse
T_1	117 - 6.3 v. Filament Transformer - 3 amps.
T_2	117 to 250-0-250 v. Power Transformer at 50 ma. with 6.3 v. Filament tap at 2.5 amps.
R_1	20 K, 1/2 Watt
R_2	10 K, 1/2 Watt
R_3	2.2 K, 1/2 Watt
R_4, R_{10}	1 Meg., 1/2 Watt
R_5	560 K, 1/2 Watt
R_6	2.5 K, 10 Watts
R_7	1 Meg. Potentiometer - 2 Watts.
R_8	2.0 K, 10 Watts
R_9	27 K, 1/2 Watt
R_{11}	82 K, 2 Watts
R_{12}	500 K Potentiometer - 2 Watts
C_1	330 μμf - 200 v.
C_2	33 μμf - 200 v.
C_3	1000 μμf - 200 v.
C_4	100 μμf - 200 v.
C_5, C_7	8 μf electrolytic - 300 v.
C_6	.005 μf - 600 v.
C_8	.04 μf paper - 450 v.

REFERENCES

1. W. J. Dornhoeffer, "Self-Saturation in Magnetic Amplifiers", AIEE Trans., Vol. 68, 1949.

2. W. H. Esselman, "Straight Line Analysis of Full-Wave Magnetic Amplifier", Polytechnic Institute of Brooklyn, Report R-223-49, PIB-168, Sept. 8, 1949.

3. E. J. Smith, "A Study of Self-Saturating Magnetic Amplifiers", Part I, Polytechnic Institute of Brooklyn, Report R-229-49, PIB-174, Dec. 30, 1949.

4. E. J. Smith, "A Study of Self-Saturating Magnetic Amplifiers", Part II, Polytechnic Institute of Brooklyn, Report R-230-50, PIB-175, Feb. 20, 1950.

5. E. J. Smith, "A Study of Self-Saturating Magnetic Amplifiers", Part III, Polytechnic Institute of Brooklyn, Report R-231-50, PIB-176, Mar. 27, 1950.

6. E. J. Smith, "Determination of Steady-State Performance of Self-Saturating Magnetic Amplifiers", AIEE Technical Paper, 50-206.

7. E. J. Smith, "A Study of Self-Saturating Magnetic Amplifiers", Part IV, Polytechnic Institute of Brooklyn, Report R-238-50, PIB-183, Dec. 11, 1950.

8. A. Erkmen, "The Steady State and Transient Analysis of the Doubler and Full-Wave Magnetic Amplifier with Free Excitation for 'Rectangular' Hysteresis Core Material and Resistive Load", Polytechnic Institute of Brooklyn, Report R-260-51, PIB-201, Oct. 25, 1951.

9. R. A. Ramey, "On the Mechanics of Magnetic Amplifier Operation", AIEE Trans., Vol. 70, 1951.

10. Vickers, Inc., "The Use of Rectified Pulses for Control Current in Magnetic Amplifiers", Summary Report, Index NS-678-059, Contract No. bs-46768, VED S.O. 48-1002, Aug. 20, 1949.

11. T. Spooner, "Properties and Testing of Magnetic Materials", McGraw-Hill, New York, 1927.

12. H. Lehmann, "Predetermination of Control Characteristics of Half-Wave Self-Saturating Magnetic Amplifiers", AIEE Trans., 1951, 70, pg. 2097.

13. R. Zarouri, "The Influence of Eddy Currents Upon the Performance of A-C and D-C Controlled Magnetic Amplifiers", Polytechnic Institute of Brooklyn, Report R-288-52, PIB-227, Dec. 15, 1952.

14. E. L. Harder and W. F. Horton, "Response Time of Magnetic Amplifiers", AIEE Technical Paper 50-177.

REFERENCES (Cont.)

15. S. Roman, "A Cyclic Integrator", Thesis for M.E.E., Polytechnic Institute of Brooklyn, June 1951.

16. H. F. Storm, "Transient Response of Saturable Reactors", Conference Paper, AIEE, Jan. 1950.

17. J. T. Carleton and W. F. Horton, "The Figure of Merit of Magnetic Amplifiers", Conference Paper, AIEE, June 1952.

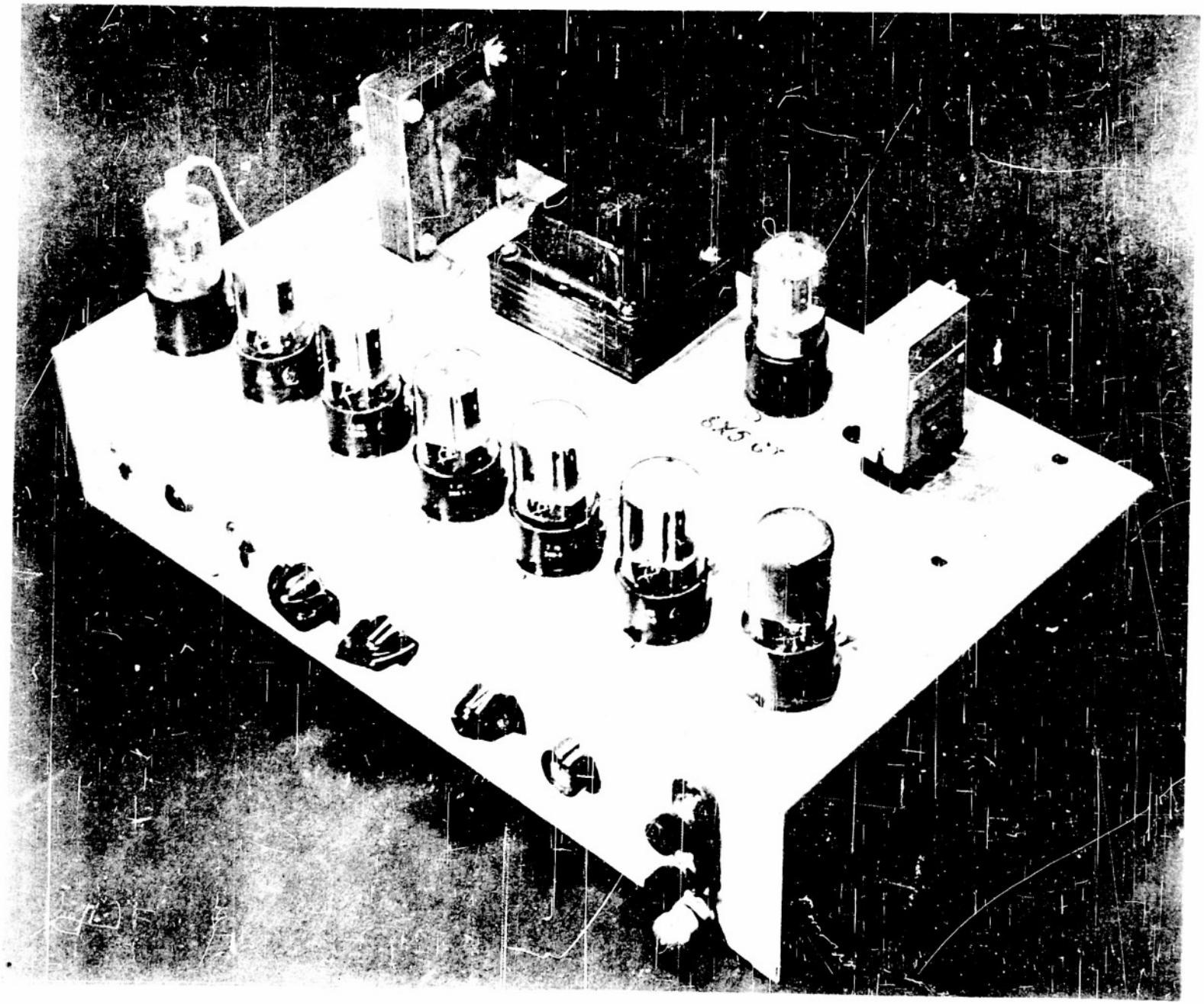

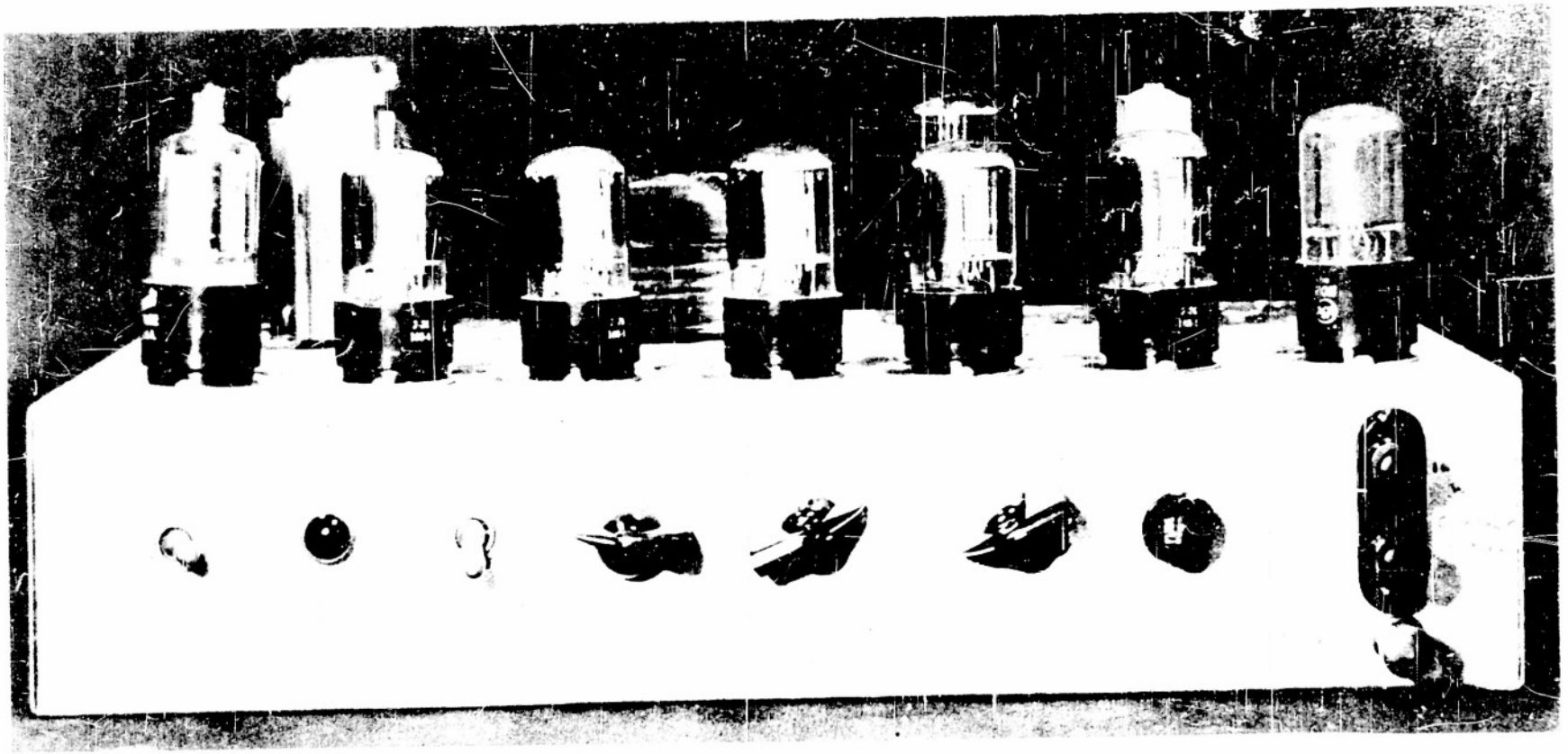

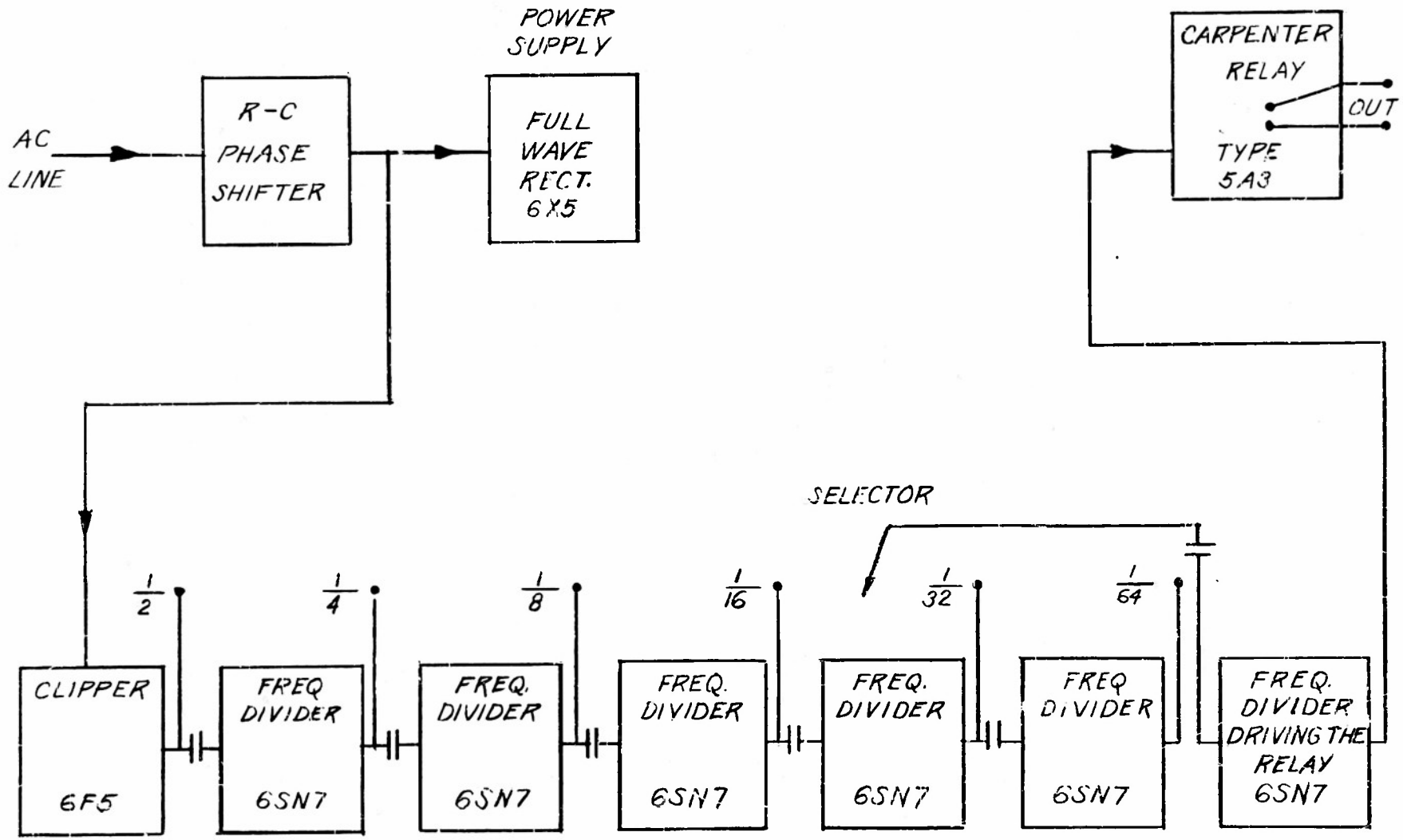

SYNCHRONIZED RELAY FOR MEASURING TRANSIENT RESPONSE

9-53

MRI 13428

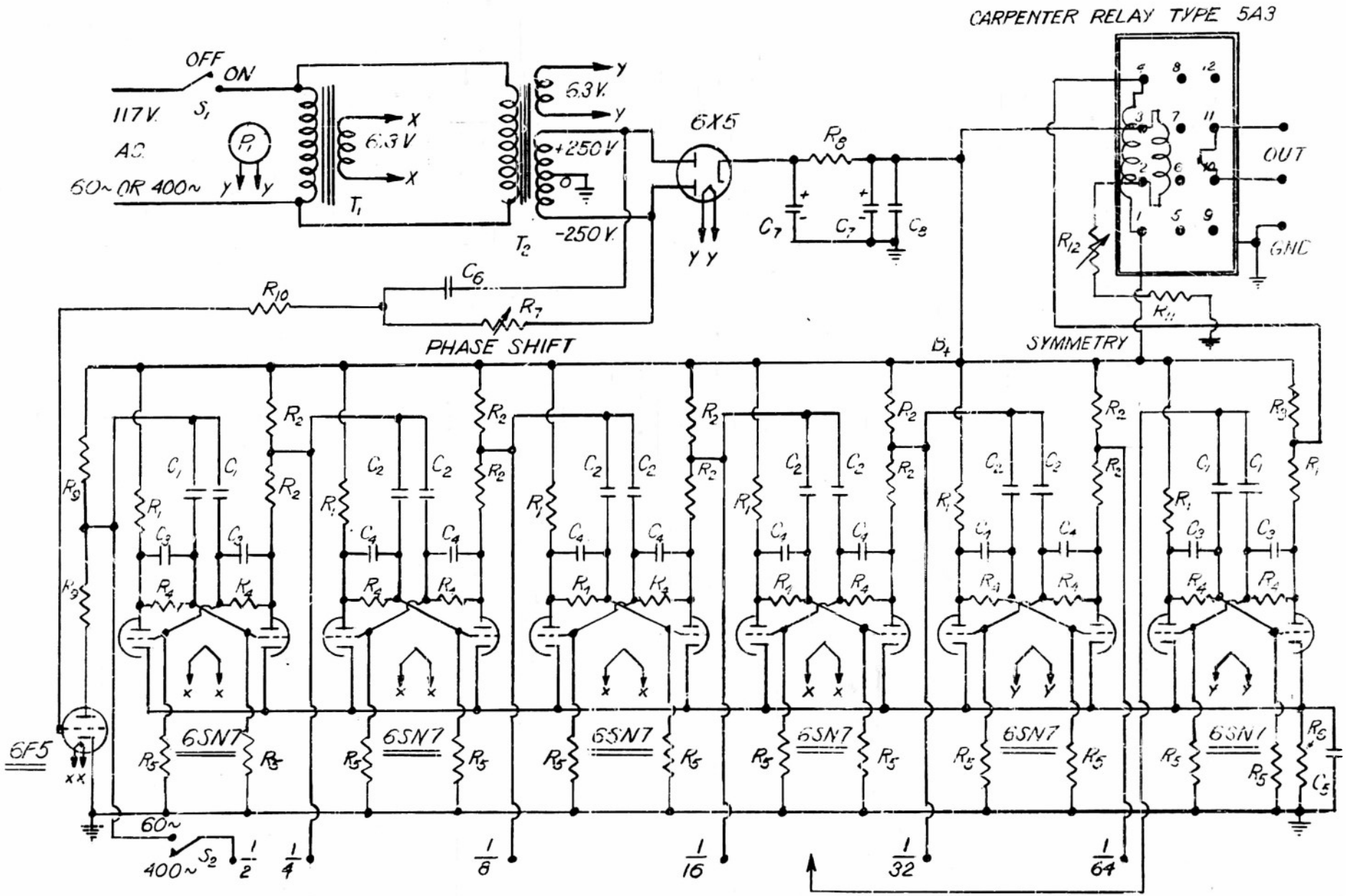
CARPENTER RELAY TYPE 5A3
OFF
ON
117V.
AC.
60~ OR 400~
S_1
P_1
T_1
T_2
6.3V.
6.3V.
+250V.
-250V.
6X5
R_8
C_7
C_8
OUT
GND
R_{12}
R_{11}
C_6
R_{10}
R_7
PHASE SHIFT
SYMMETRY
6F5
6SN7
60~
400~
S_2
1/2
1/4
1/8
1/16
1/32
1/64
10-53
FREQUENCY SELECTOR
MRI 13429

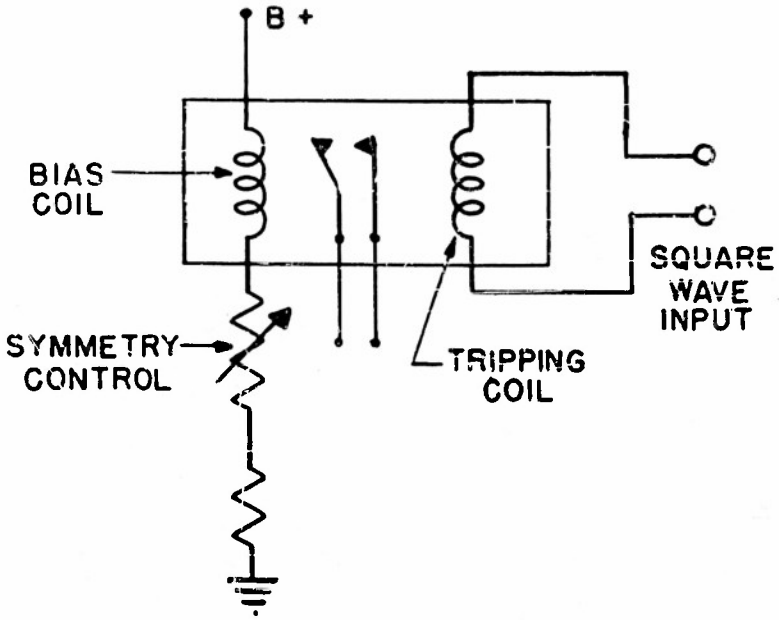

(a) Schematic of Relay

(b) Clipped Input Wave

(c) Pulses Formed From Clipped Wave

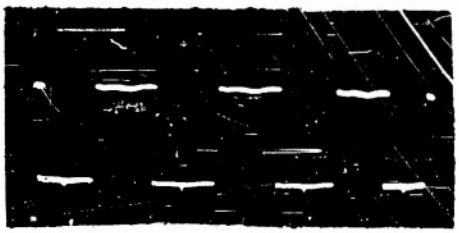

(d) Output From 1st Divider

(e) Output From 2nd Divider

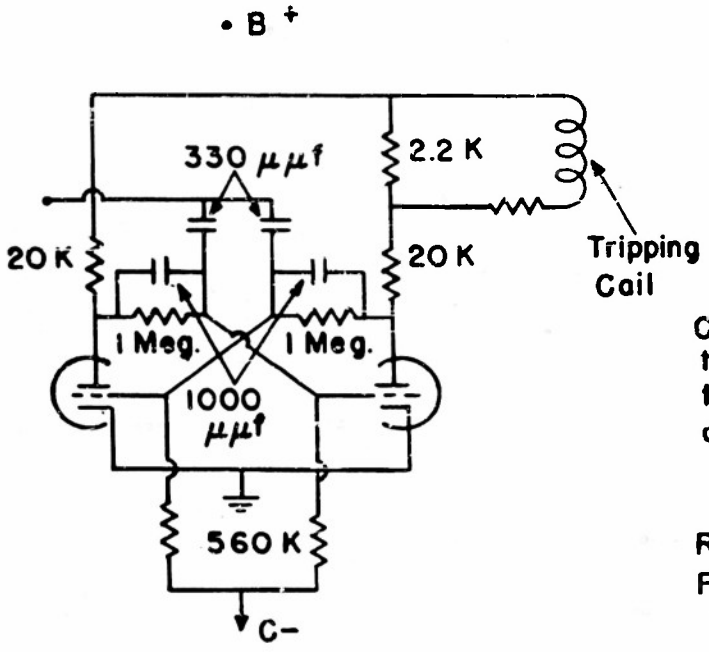

(a)

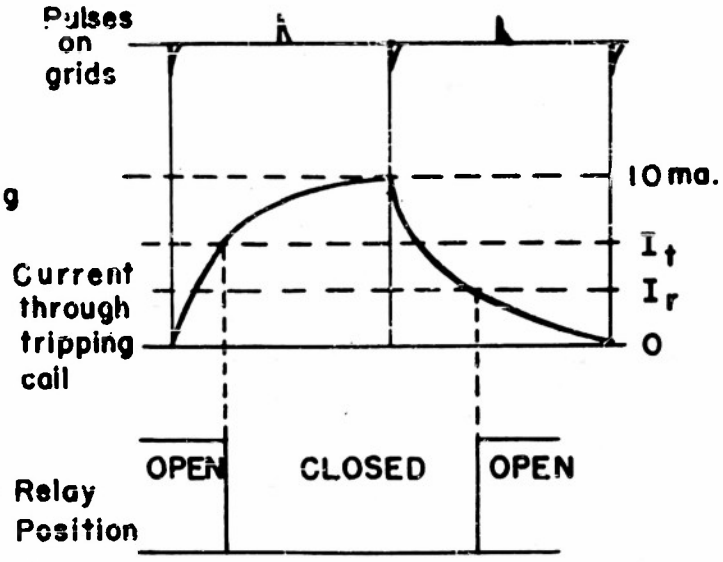

(b)

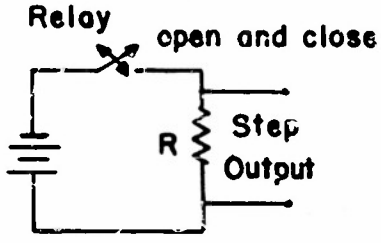

(c)

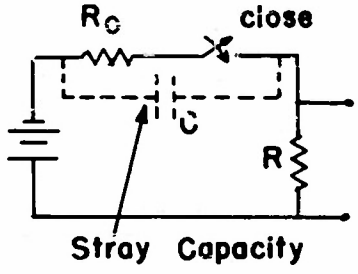

(d)

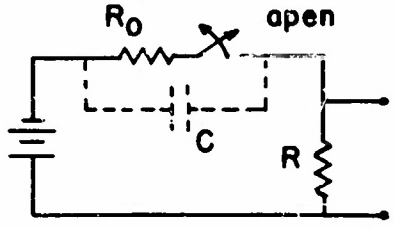

(e)

(f) Output across R
R = 500 K

(g) Output across R
R = 2 K

APPENDIX C

CORE DATA

HYPERNIK V

TORROIDAL WOUND .002" STRIP

OXIDE INSULATION

l_m = 77"

EFFECTIVE AREA = 0.8 IN^2 RESISTIVITY = 45×10^{-8} OHM-METERS

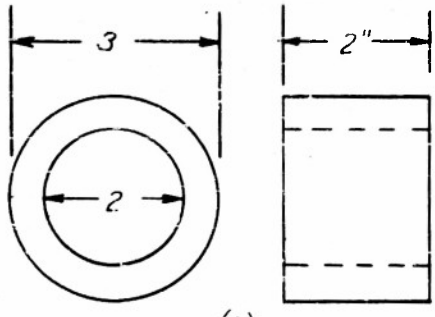

(A)

HYPERSIL

TORROIDAL WOUND - .005" STRIP

LACQUER INSULATION

l_m = 11.5"

EFFECTIVE AREA = 1.48 IN^2

RESISTIVITY = 47×10^{-8} OHM-METERS

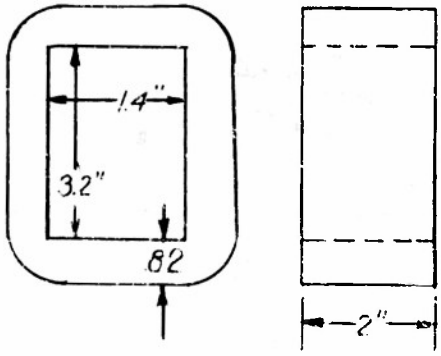

(B)

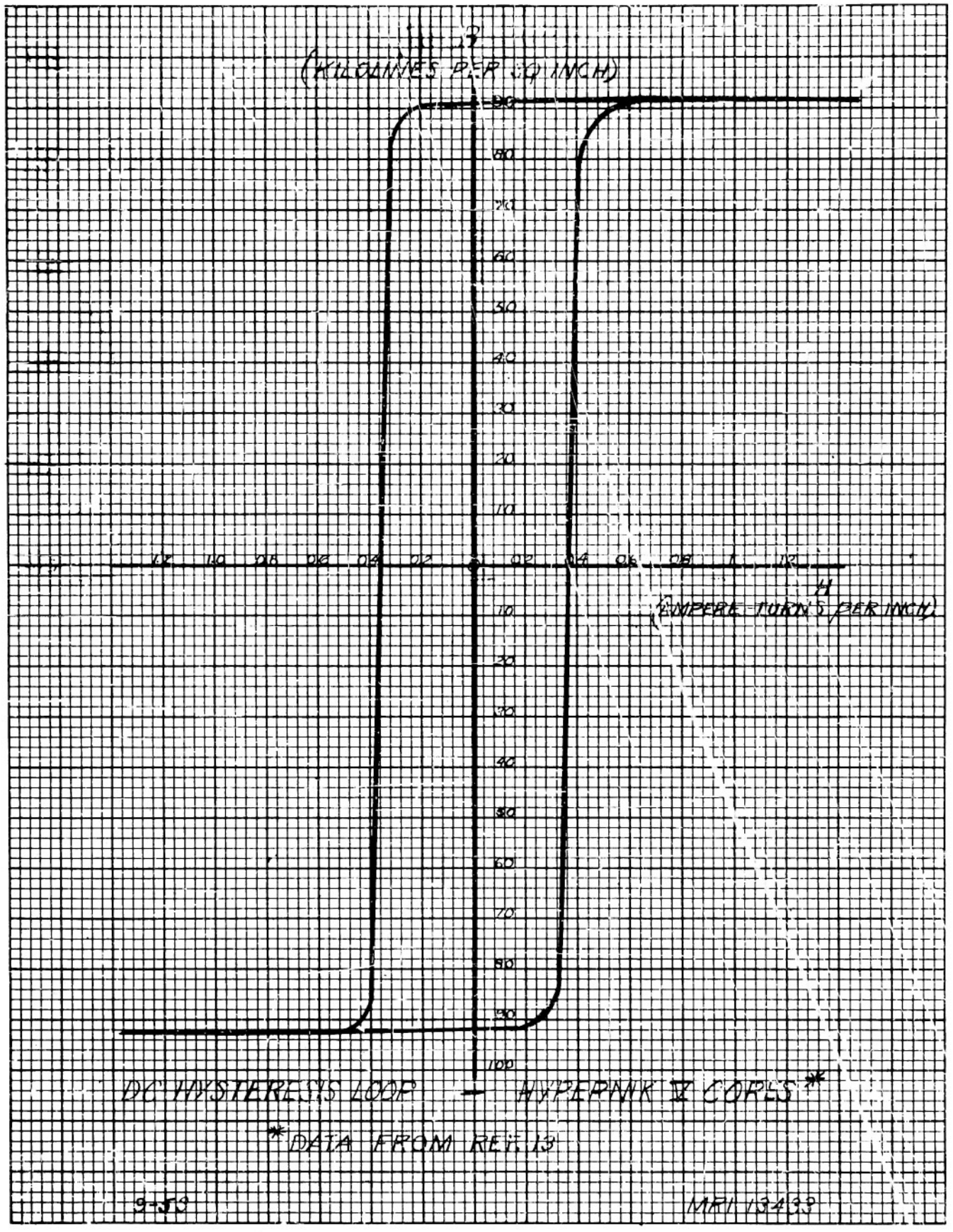

DC HYSTERESIS LOOP — HYPERNIK V CORES *

* DATA FROM REF. 13

MFN 134-33

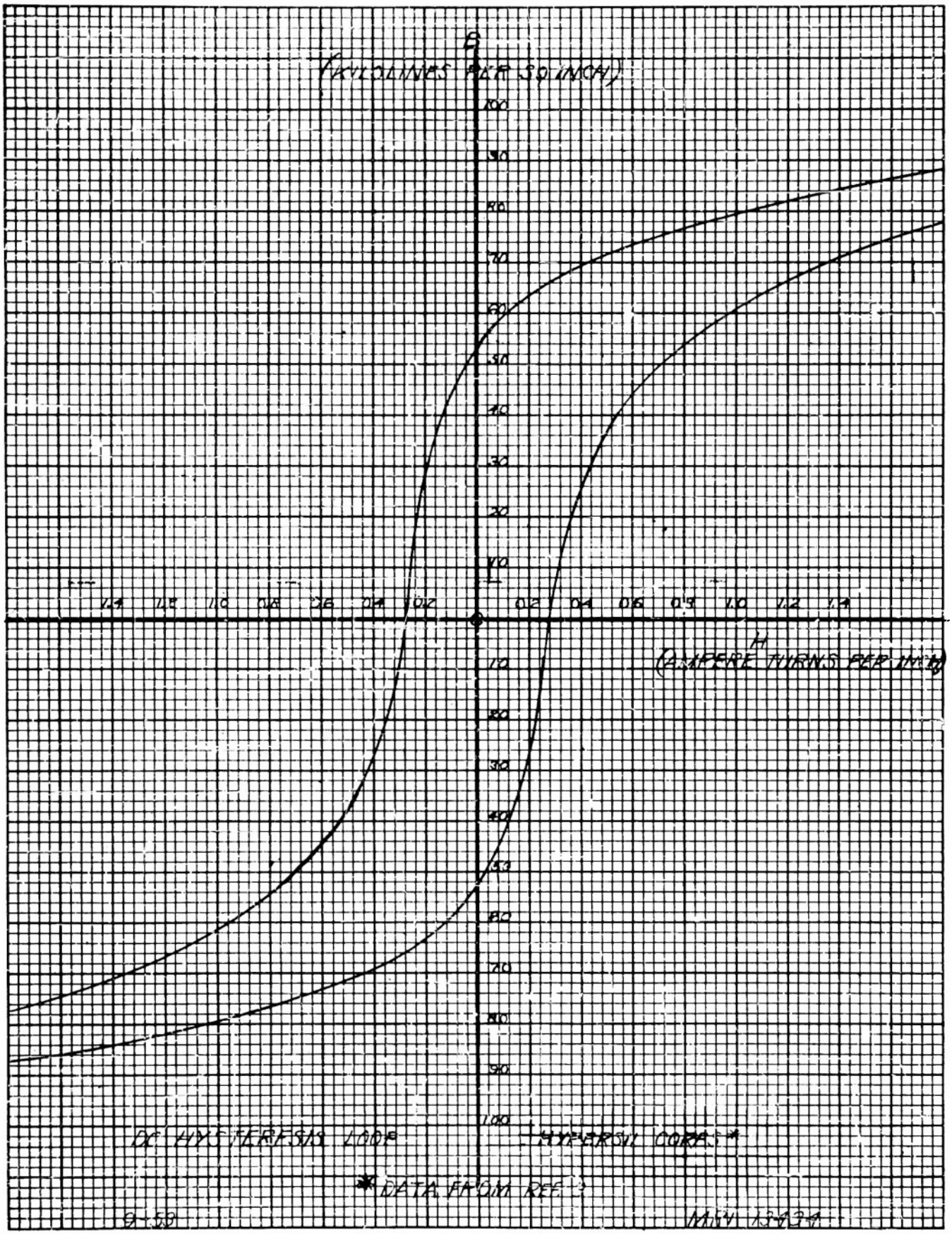
B
(KILOLINES PER SQ INCH)
100
90
80
70
60
50
40
30
20
10
1.4
1.2
1.0
0.8
0.6
0.4
0.2
0.2
0.4
0.6
0.8
1.0
1.2
1.4
H
(AMPERE TURNS PER INCH)
10
20
30
40
50
60
70
80
90
100
DC HYSTERESIS LOOP
HYPERSIL CORE *
* DATA FROM REF 3
9-59
MSV 13434

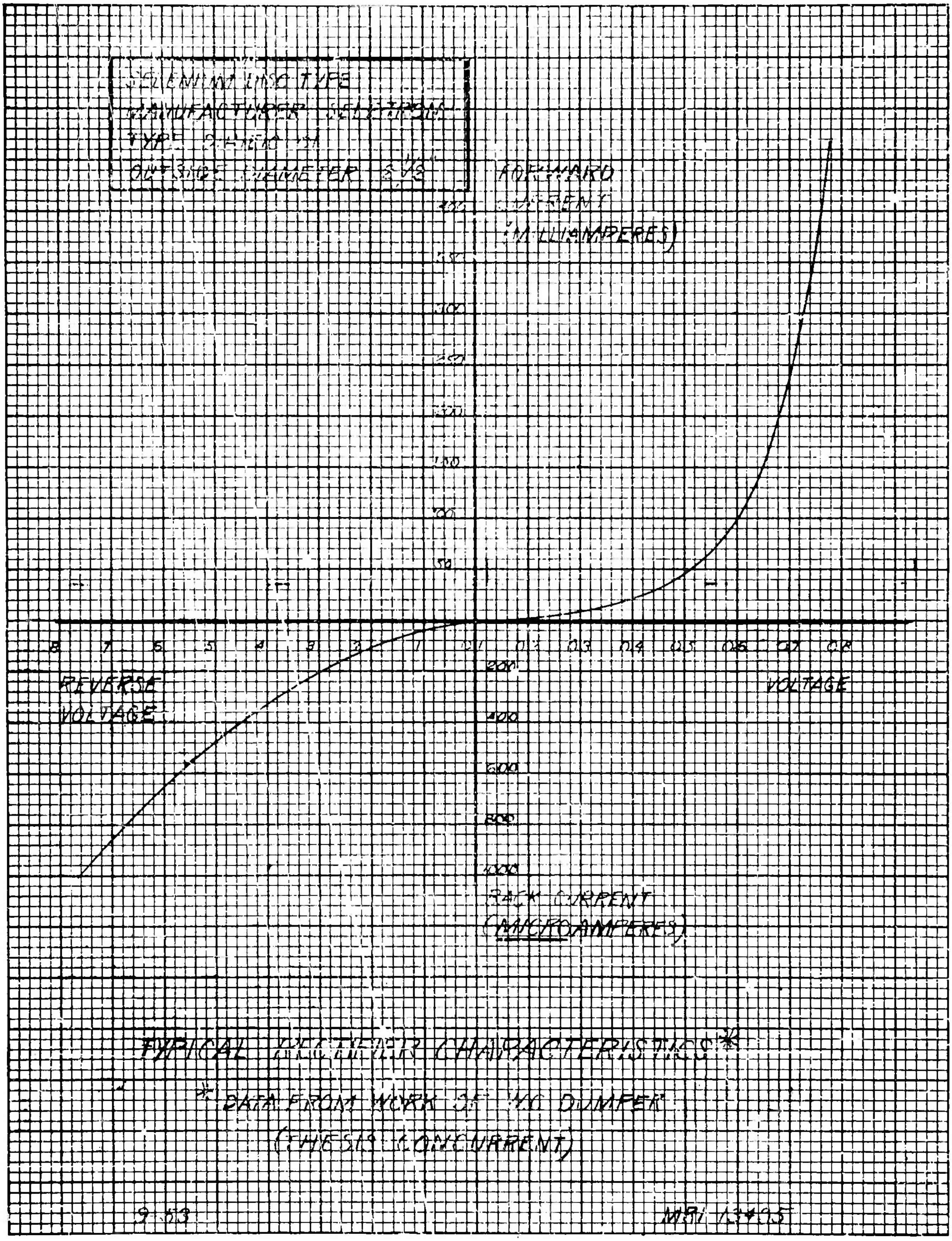

(MILLIAMPERES)
50
200
400
600
800
1000
.03
.04
.05
.06
.07
.08
REVERSE
VOLTAGE
VOLTAGE
CHARACTERISTICS*
(THESIS CONCURRENT)

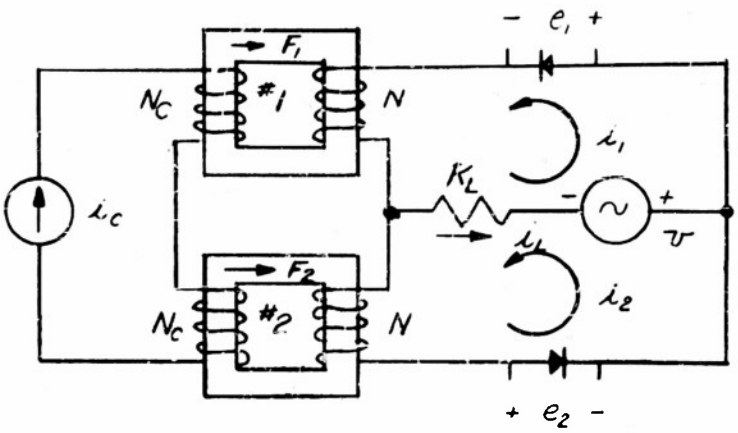

(A)

VOLTAGE DOUBLER CIRCUIT

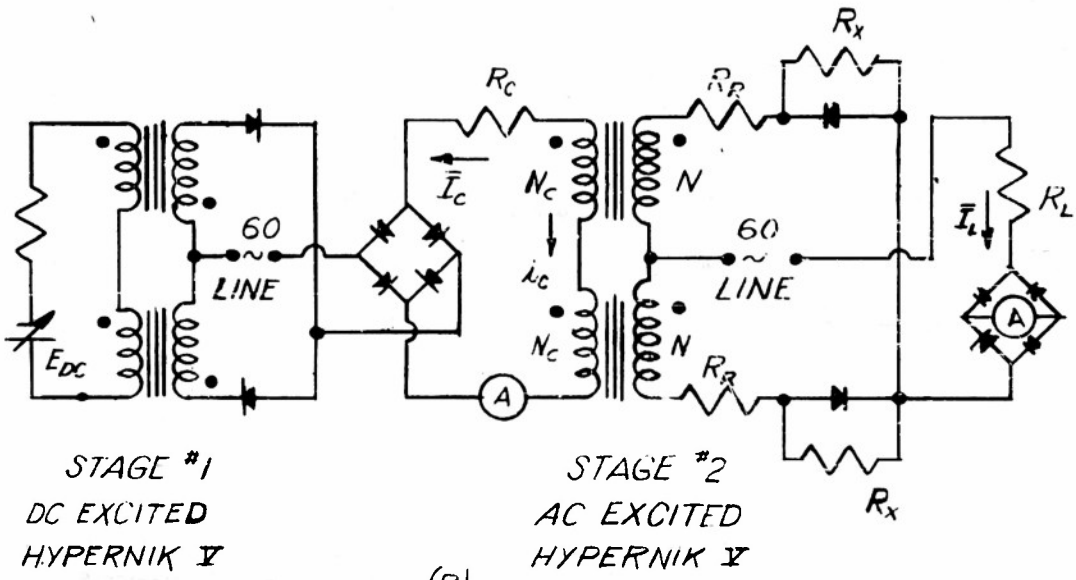

(B)

SCHEMATIC DIAGRAM OF TEST SET-UP

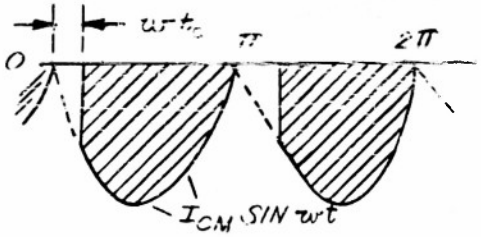

(A)

CONTROL CURRENT WAVE IN AC EXCITED STAGE

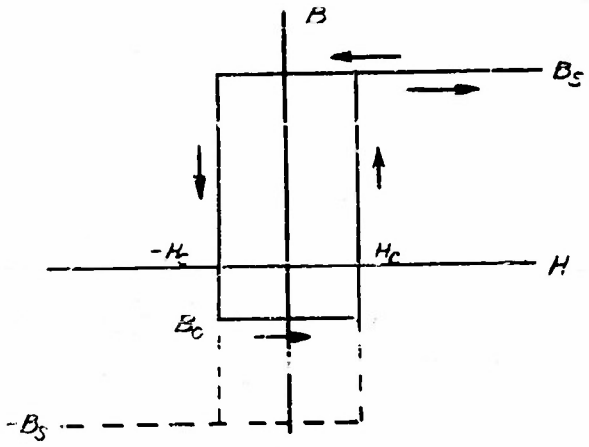

(B)

STRAIGHT LINE APPROXIMATION OF DC. B-H LOOP

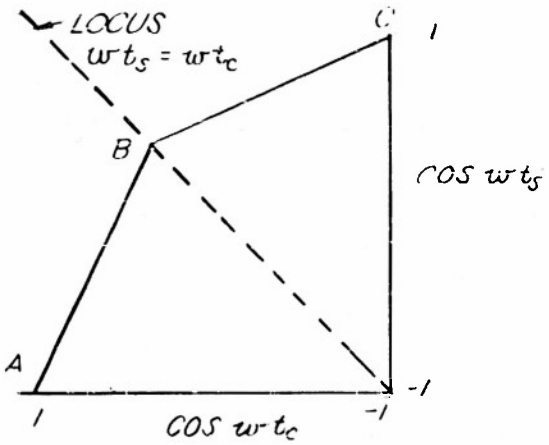

(C)

THEORETICAL RELATION BETWEEN CONTROL AND FIRING ANGLES FOR DOUBLER CIRCUIT.

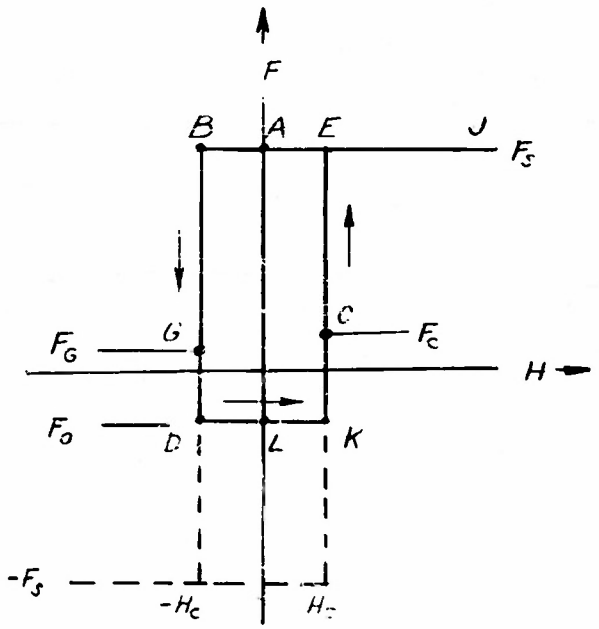

(D)

PATH OF OPERATION

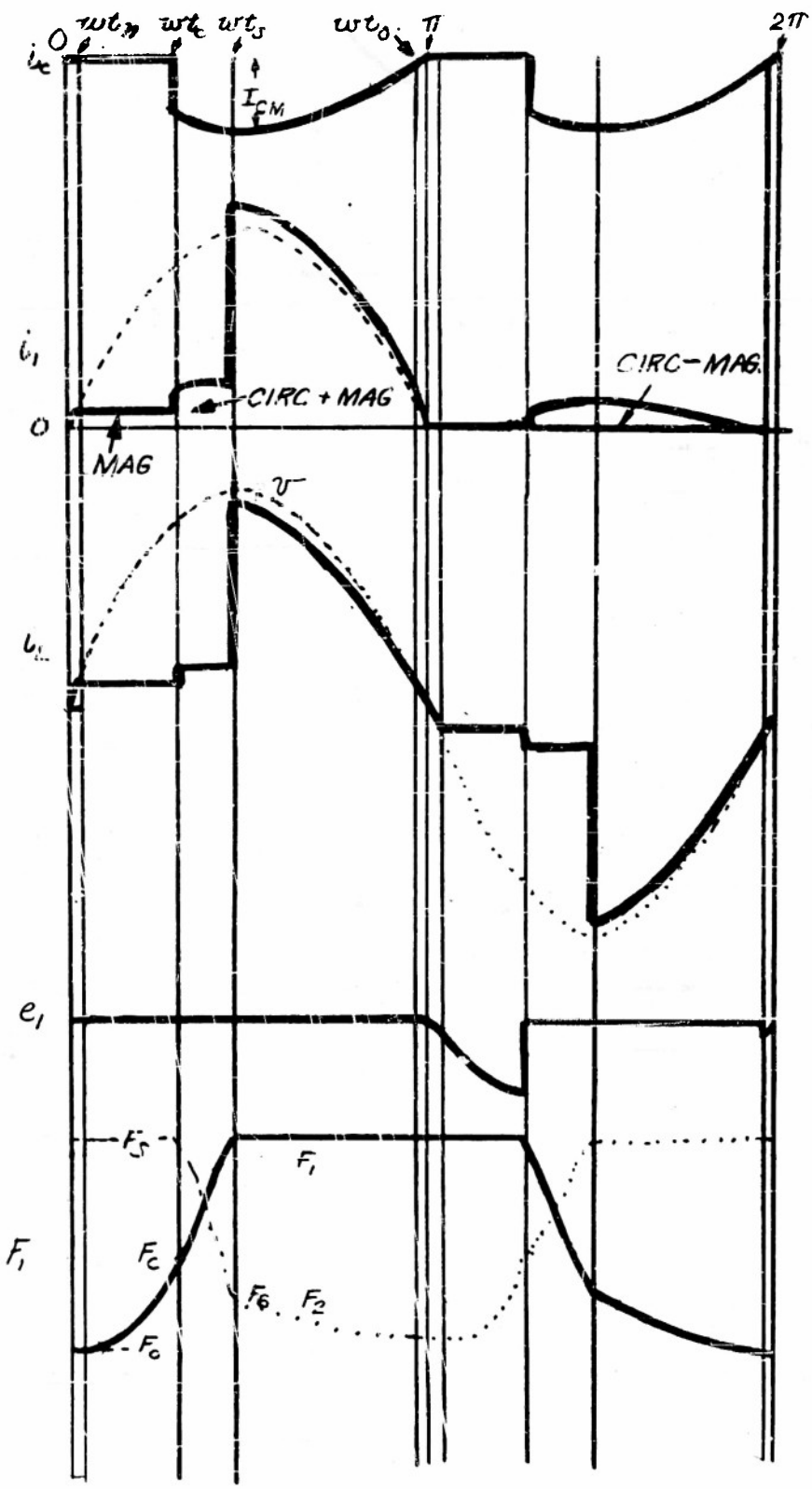

THEORETICAL EXACT WAVE FORMS FOR DOUBLER CIRCUIT

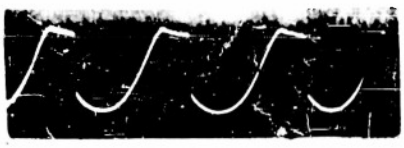

Control Current

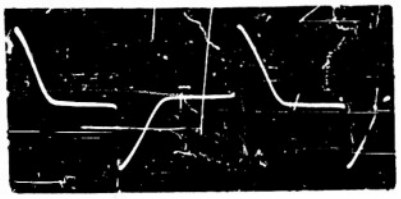

Load Current

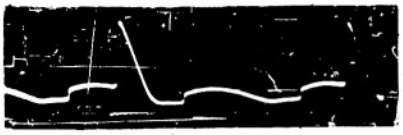

Mesh No. I Current

Rectifier No. I Voltage

Flux No. I

(a)

Actual Waveforms

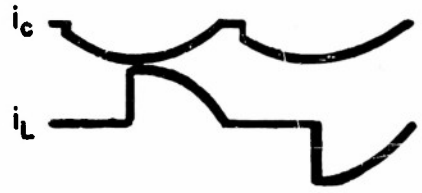

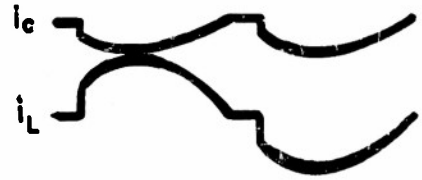

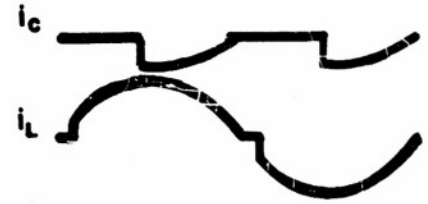

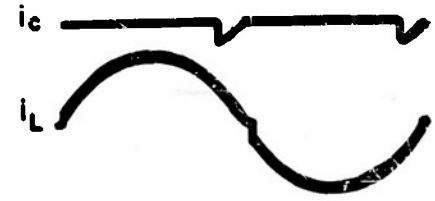

(b)

Control and Load Currents for Different Control Angles

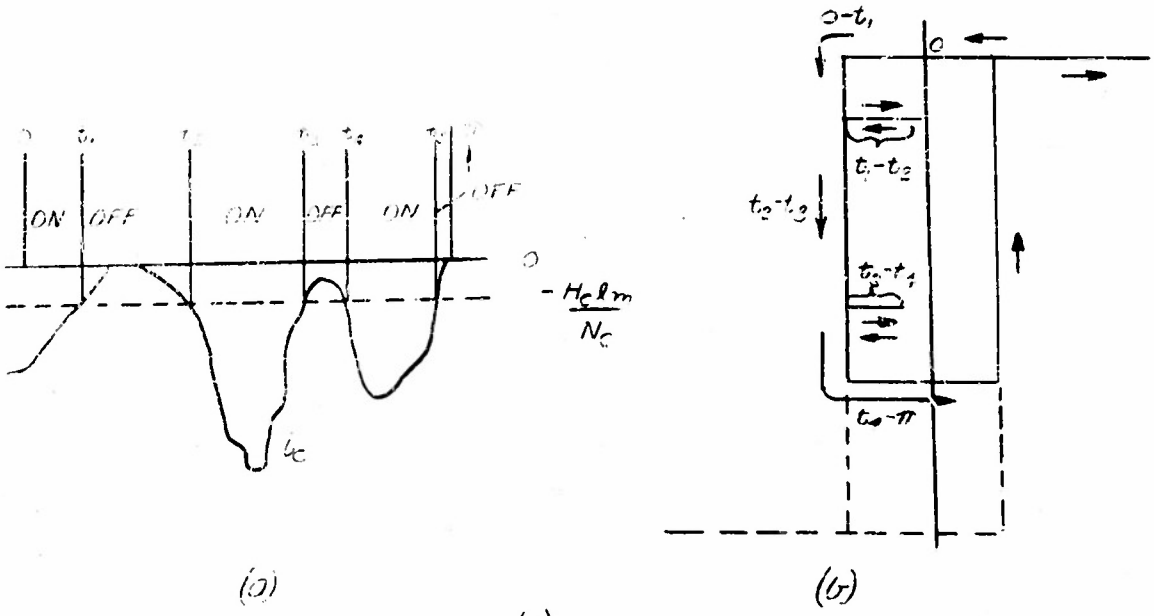

(A)

PATH OF OPERATION DUE TO RANDOM NEGATIVE CONTROL CIRCUIT

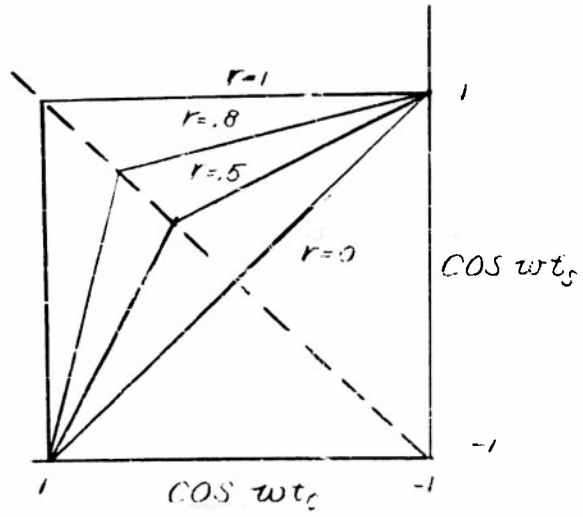

(B)

THEORETICAL COSINE RELATIONS FOR DOUBLER CIRCUIT WITH DIFFERENT VALUES OF "r"

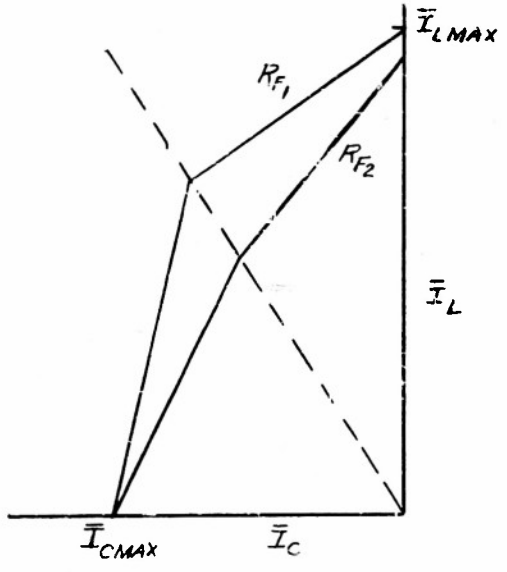

(C)

THEORETICAL TRANSFER CURVES WITH R_F AS PARAMETER

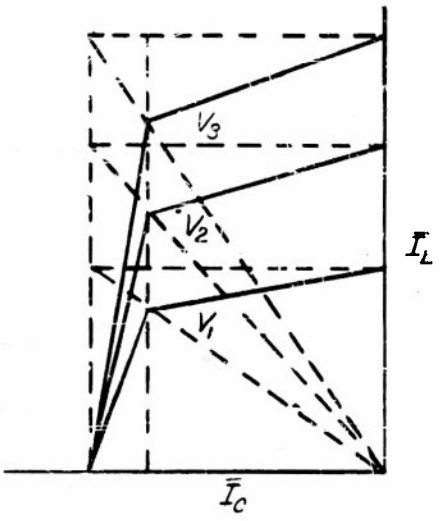

(A)

THEORETICAL TRANSFER CURVES FOR DIFFERENT VOLTAGES ($F_M < F_S$)

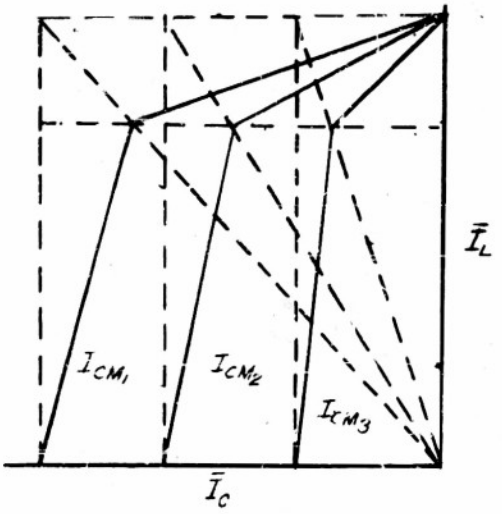

(B)

THEORETICAL TRANSFER CURVES FOR DIFFERENT CONTROL AMPLITUDES.

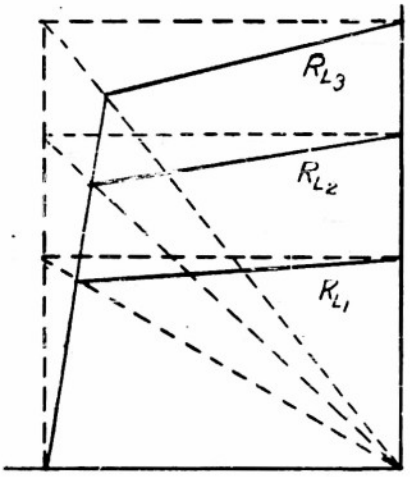

(C)

THEORETICAL TRANSFER CURVES, FOR DIFFERENT LOAD RESISTANCES

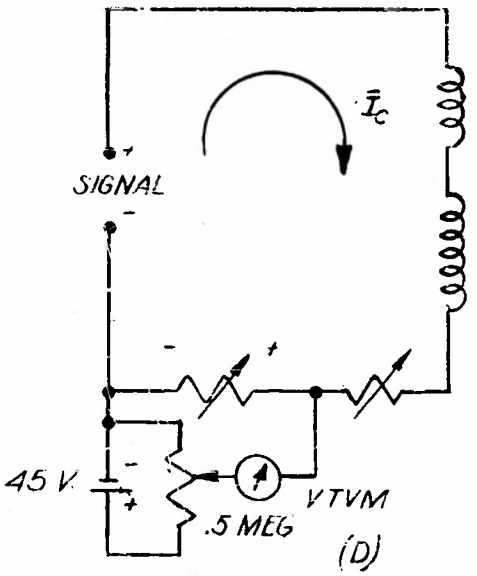

(D)

POTENTIOMETER SCHEME TO MEASURE SMALL PERCENTAGE CHANGES OF CONTROL CURRENT

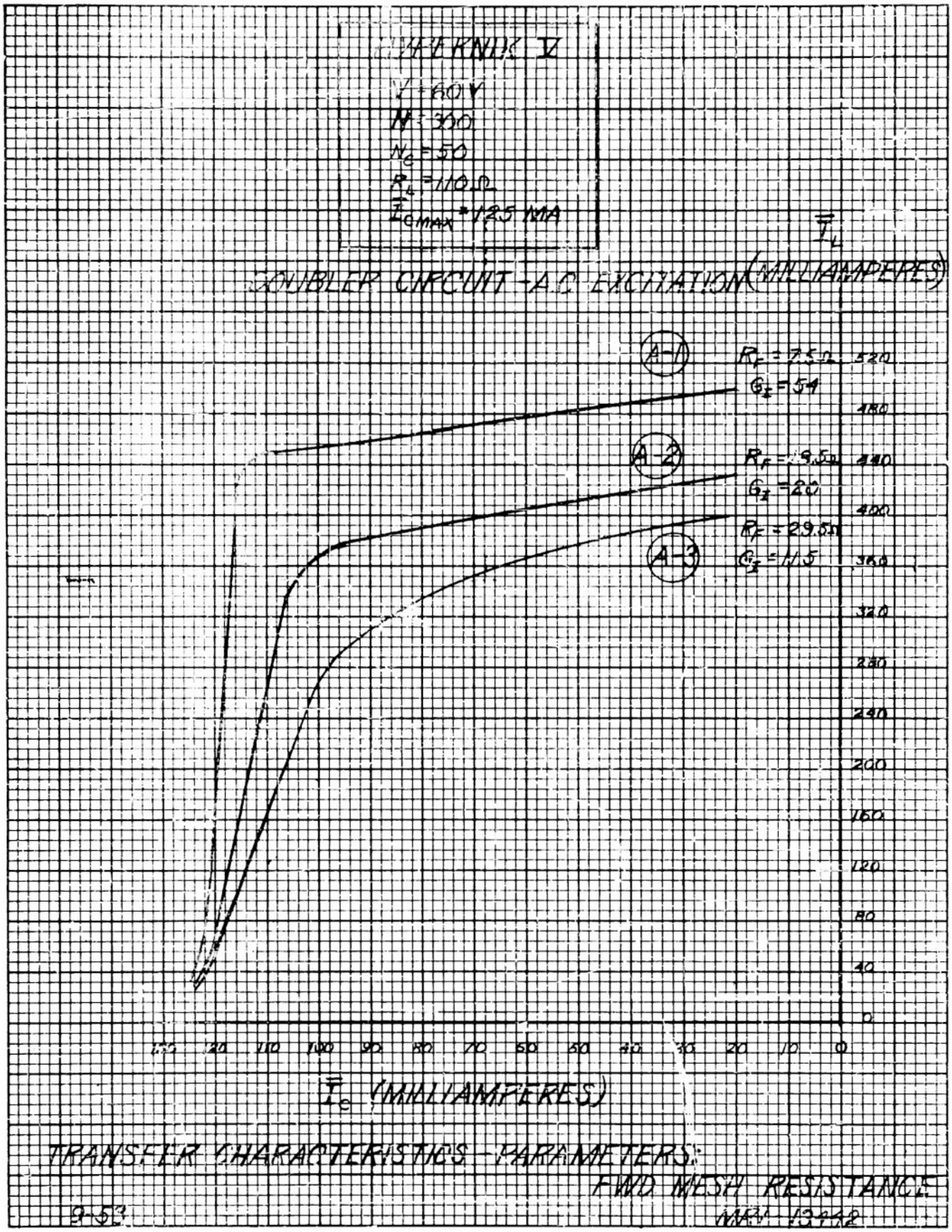
TYPE KW1C V
V_b = 60 V
N = 300
N_c = 50
R_L = 110 Ω
$I_{c\,MAX}$ = 125 MA
I_L
SQUIRLER CIRCUIT - A.C. EXCITATION (MILLIAMPERES)
A-1
R_f = 7.5 Ω
G_z = 54
A-2
R_f = 9.5 Ω
G_z = 20
A-3
R_f = 29.5 Ω
G_z = 11.5
520
480
440
400
360
320
280
240
200
160
120
80
40
0
120 110 100 90 80 70 60 50 40 30 20 10 0
I_c (MILLIAMPERES)
TRANSFER CHARACTERISTICS - PARAMETERS:
FWD MESH RESISTANCE
9-53
MAY 1942

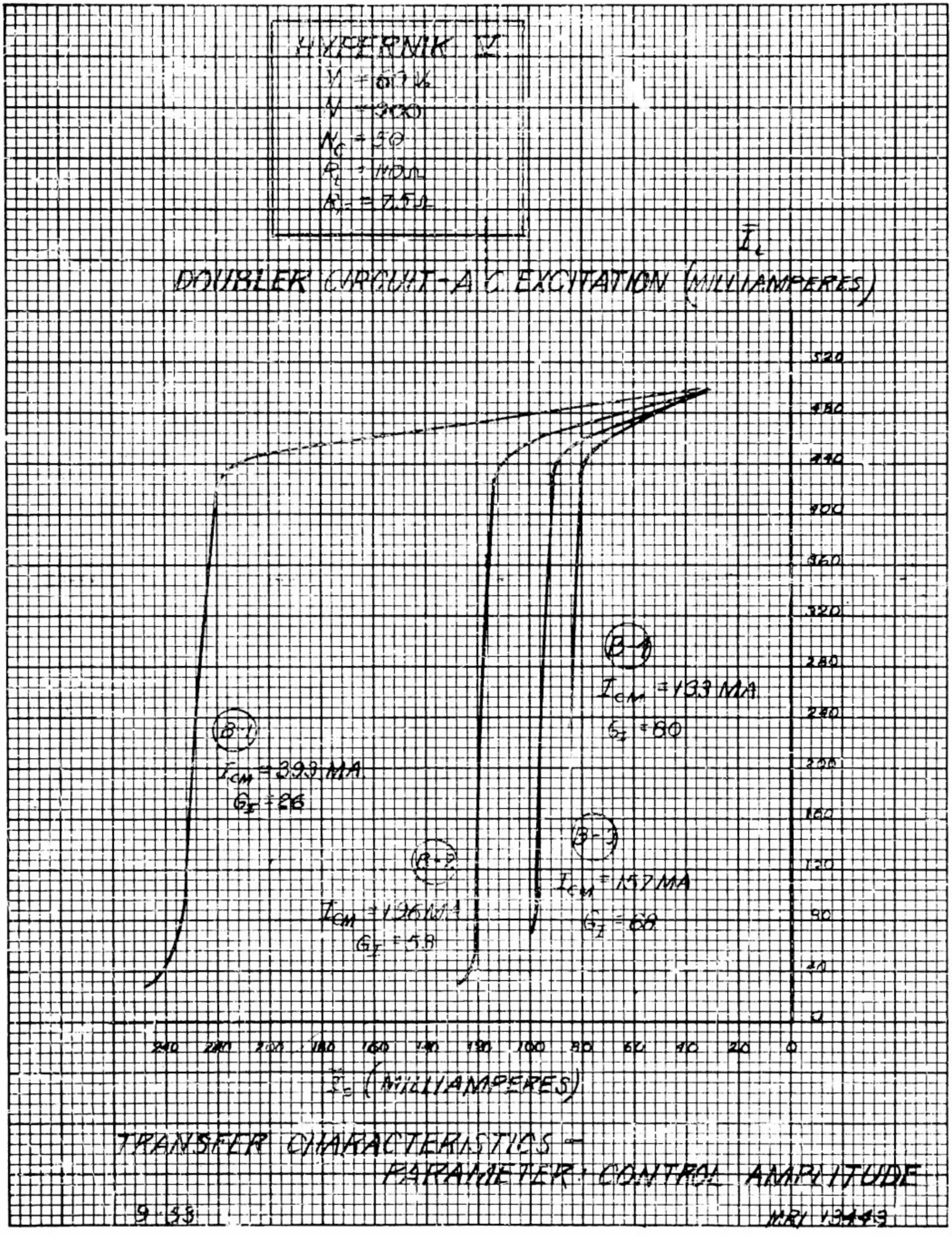

HYPERNIK V
N_C = 50
R_C = 7.5Ω
DOUBLER CIRCUIT - A.C. EXCITATION
I_L (MILLIAMPERES)
520
480
440
400
360
320
280
240
200
160
120
80
40
0
B-1
I_{CM} = 393 MA
G_I = 26
B-2
I_{CM} = 196 MA
G_I = 58
B-3
I_{CM} = 157 MA
G_I = 68
B-4
I_{CM} = 133 MA
G_I = 80
240
220
200
180
160
140
120
100
80
60
40
20
0
I_C (MILLIAMPERES)
TRANSFER CHARACTERISTICS —
PARAMETER: CONTROL AMPLITUDE
9-53
MRI 13449

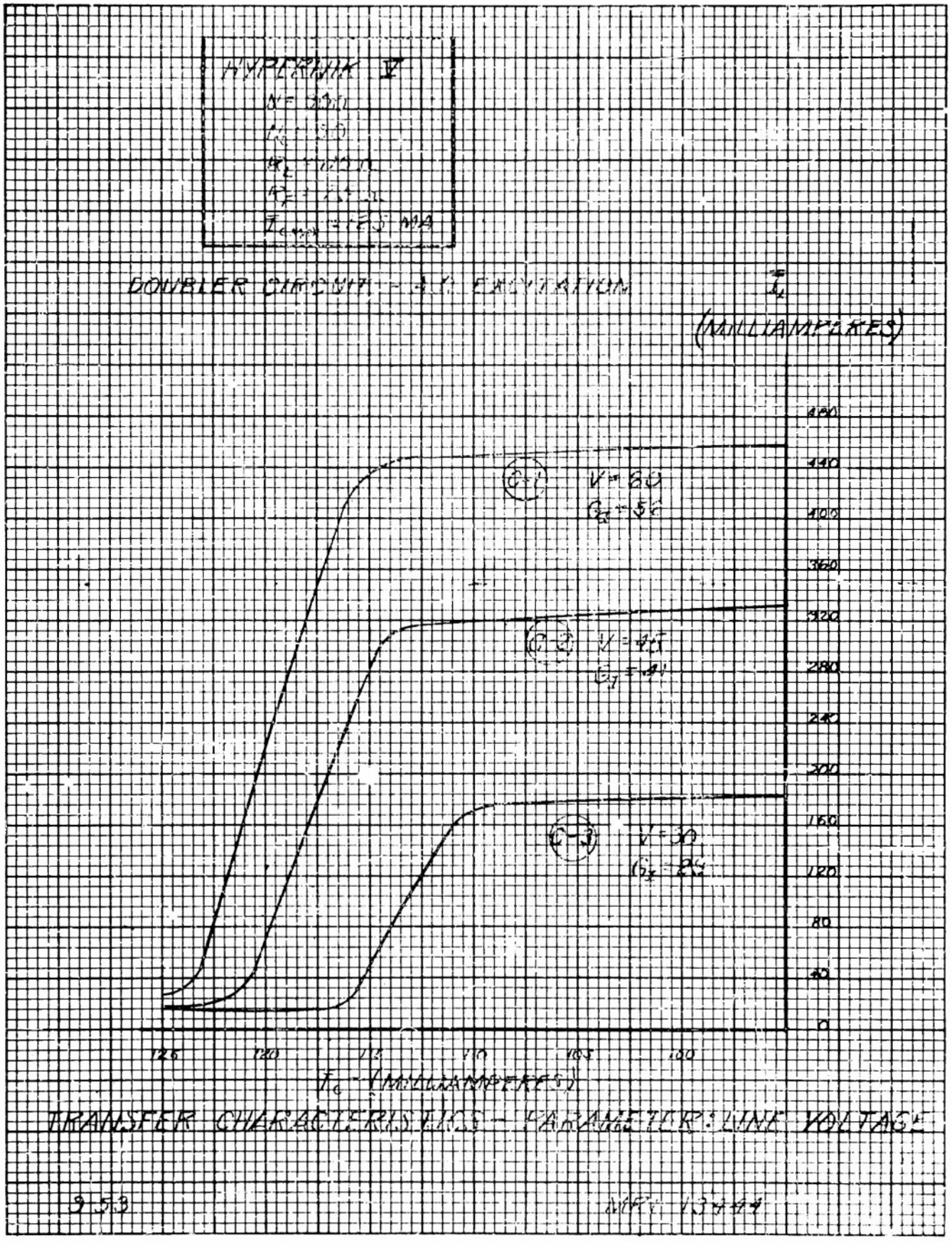
DOUBLER CIRCUIT - AVALANCHE
I_b
(MILLIAMPERES)
$V = 80$
$E_{c2} = 5$
$V = 40$
$E_{c1} = 4$
$V = 30$
$E_{c1} = 2$
160
140
120
100
80
60
40
20
0
125
120
115
110
105
100
I_c - (MILLIAMPERES)
TRANSFER CHARACTERISTICS - PARAMETER: LINE VOLTAGE
9-53

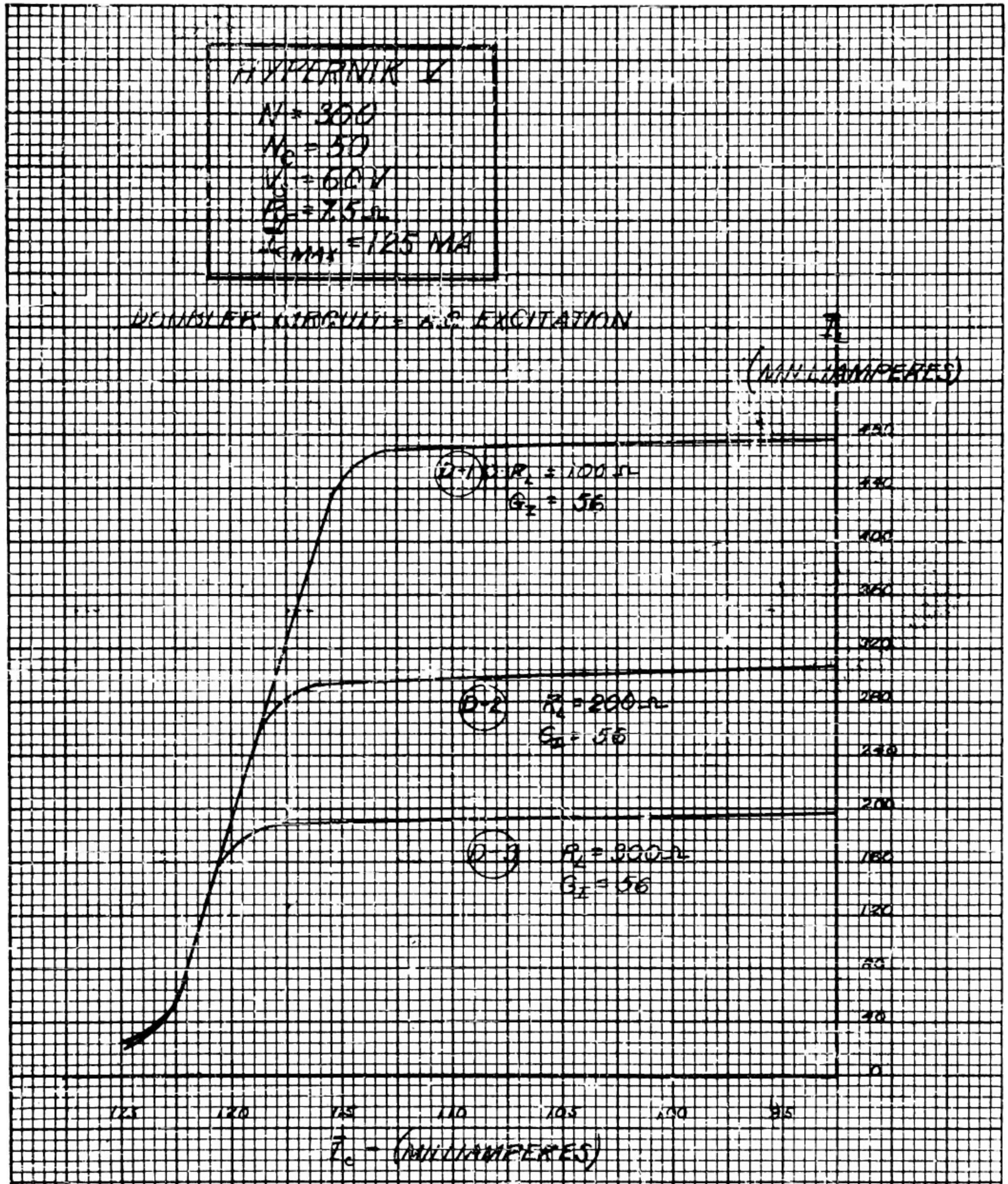

TRANSFER CHARACTERISTICS - PARAMETER: LOAD RESISTANCE

3-63

HYPERNIK V

$V = 30\ V$

$R_L = 100\ \Omega$

$R_F = 7.5\ \Omega$

$I_{c\,max} = 250\ MA$

DOUBLER CIRCUIT – A.C. EXCITATION

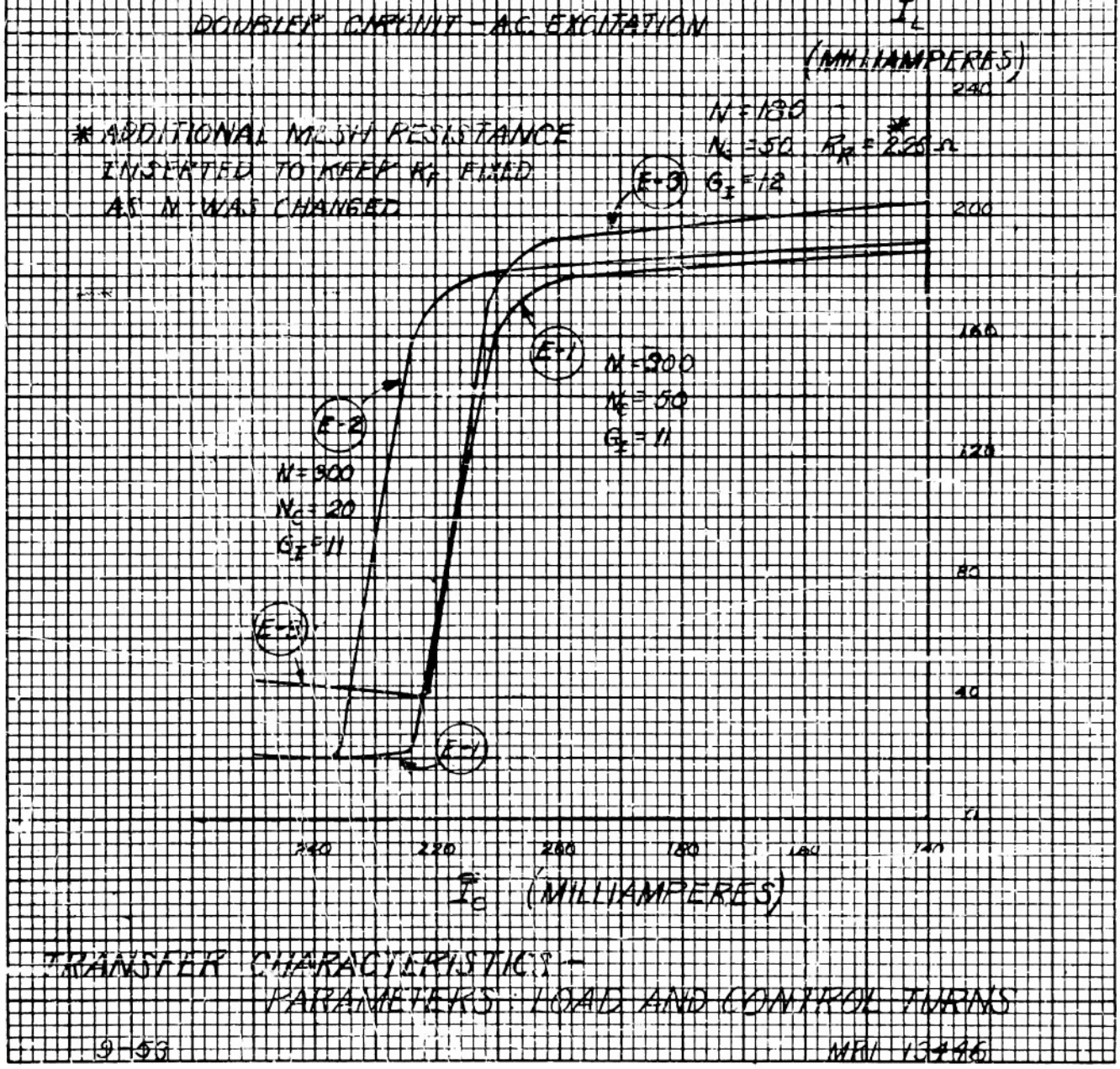

* ADDITIONAL MESH RESISTANCE INSERTED TO KEEP R_F FIXED AS N WAS CHANGED

TRANSFER CHARACTERISTICS – PARAMETERS: LOAD AND CONTROL TURNS

9-56

MRI 13446

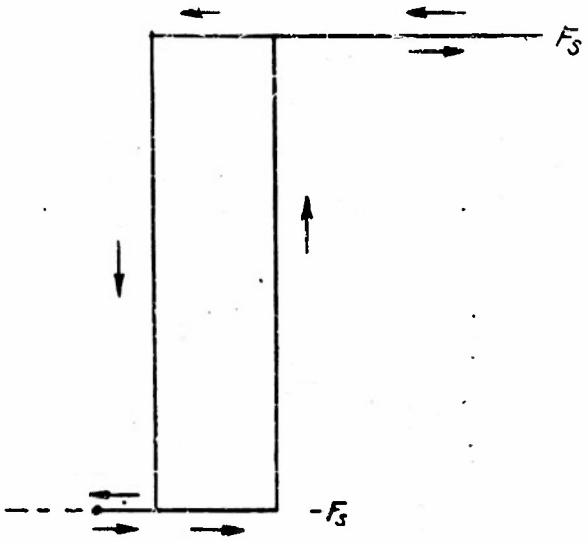

(A)

PATH OF OPERATION WHEN CORE SATURATES NEGATIVELY

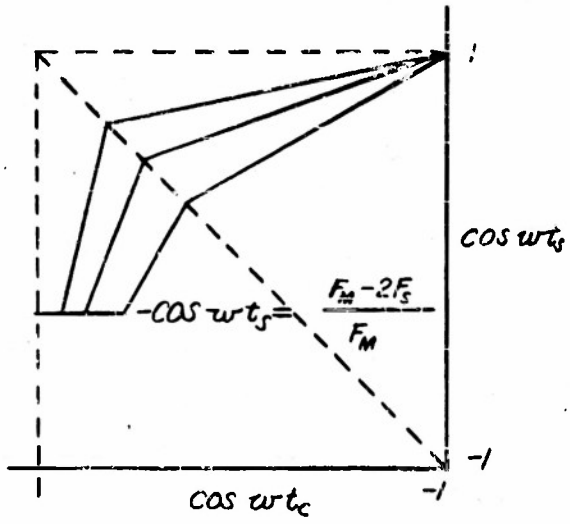

(B)

COSINE RELATIONS FOR OVERDRIVEN AMPLIFIER ($F_M > F_S$)

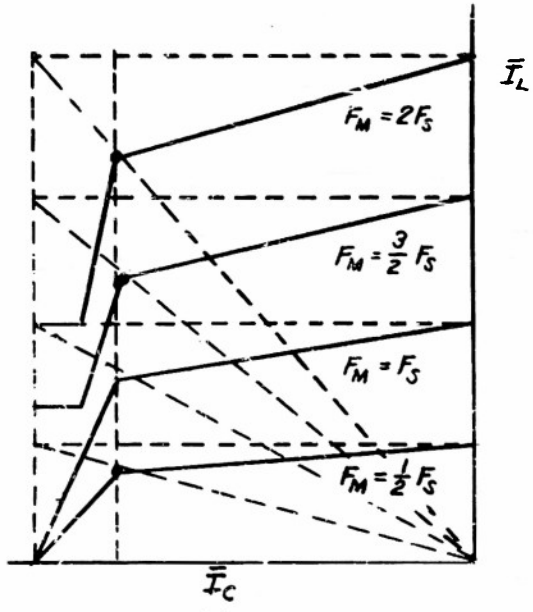

(C)

THEORETICAL TRANSFER CURVES FOR DIFFERENT VOLTAGES (INCLUDING $F_M > F_S$.)

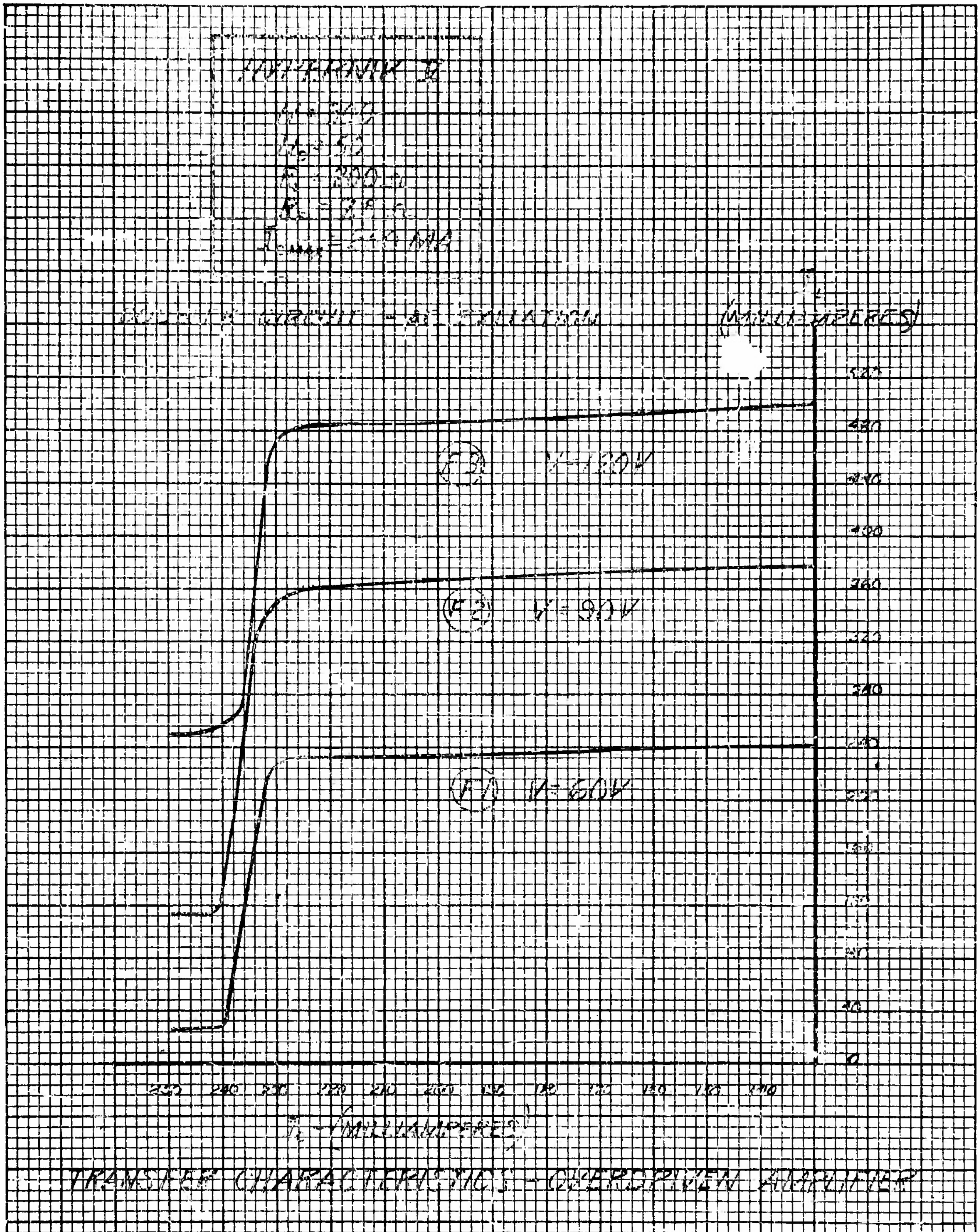

TRANSFER CHARACTERISTICS - OVERDRIVEN AMPLIFIER

MFL 13448

(a)
Minor A.C. Path of Operation
Hypernik V

(b)
Minor A.C. Path of Operation
Hypersil

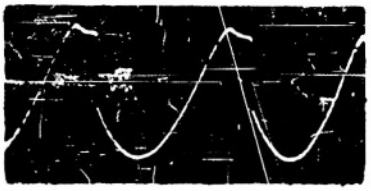

(c) Normoi

(d) Control Bias Shorted

Control Current Waveform

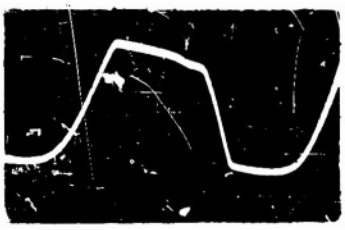

(e) Flux Waveform with Small Amount of Leakage

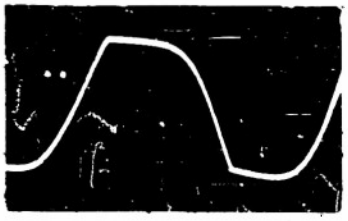

(f) Flux with 1000 Ohm Leakage Resistors Across Rectifiers

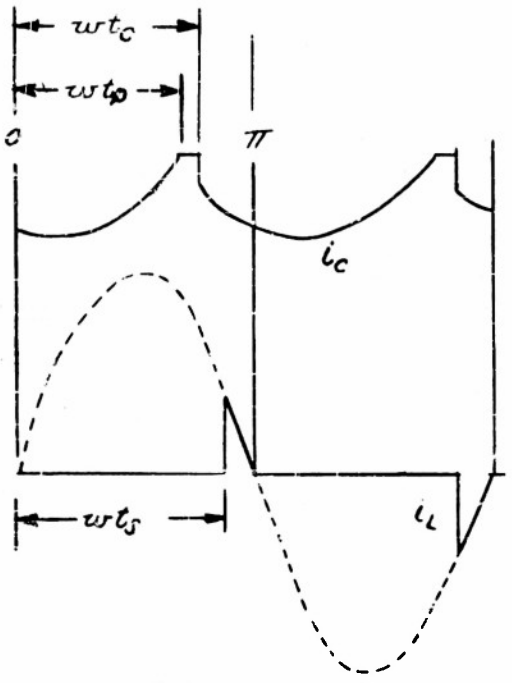

MODE (a) - $\omega t_p < \omega t_c < \pi$
$\omega t_c < \omega t_s$

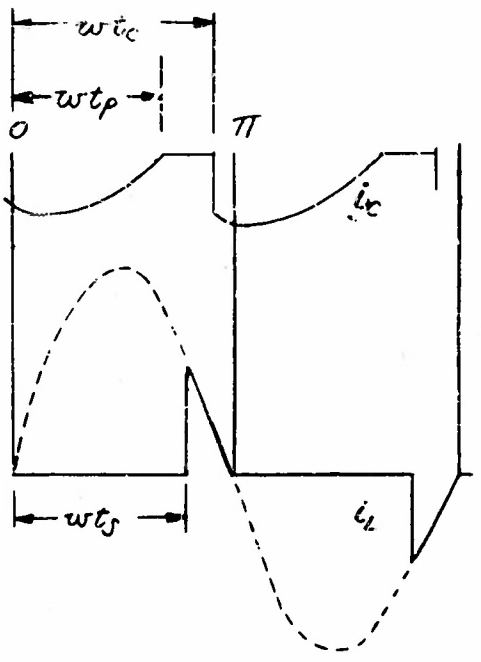

MODE (b) - $\omega t_p < \omega t_c < \pi$
$\omega t_c < \omega t_s$

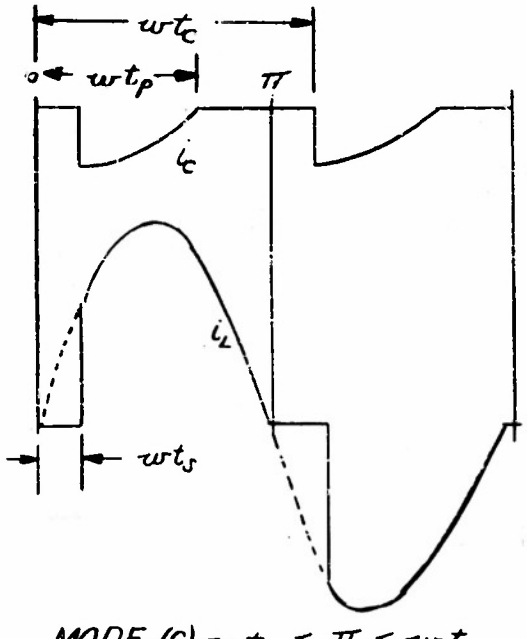

MODE (c) $\omega t_p < \pi < \omega t_c$
$(\omega t_c - \pi) < \omega t_s$

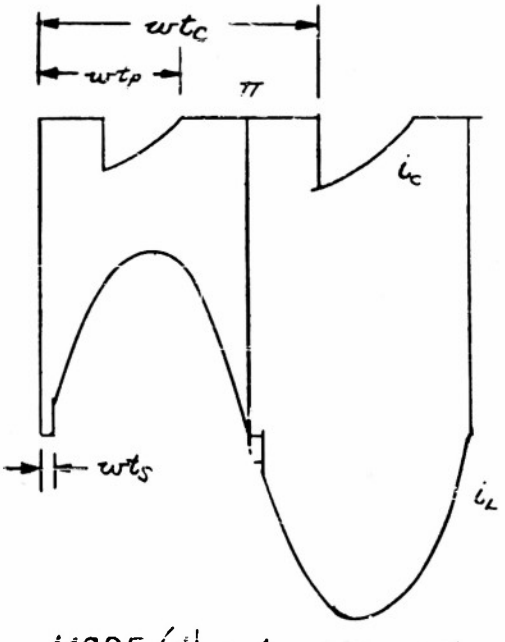

MODE (d) $\omega t_p < \pi < \omega t_c$
$\omega t_s < (\omega t_c - \pi)$

DIFFERENT POSSIBILITIES OF OUT OF PHASE OPERATION

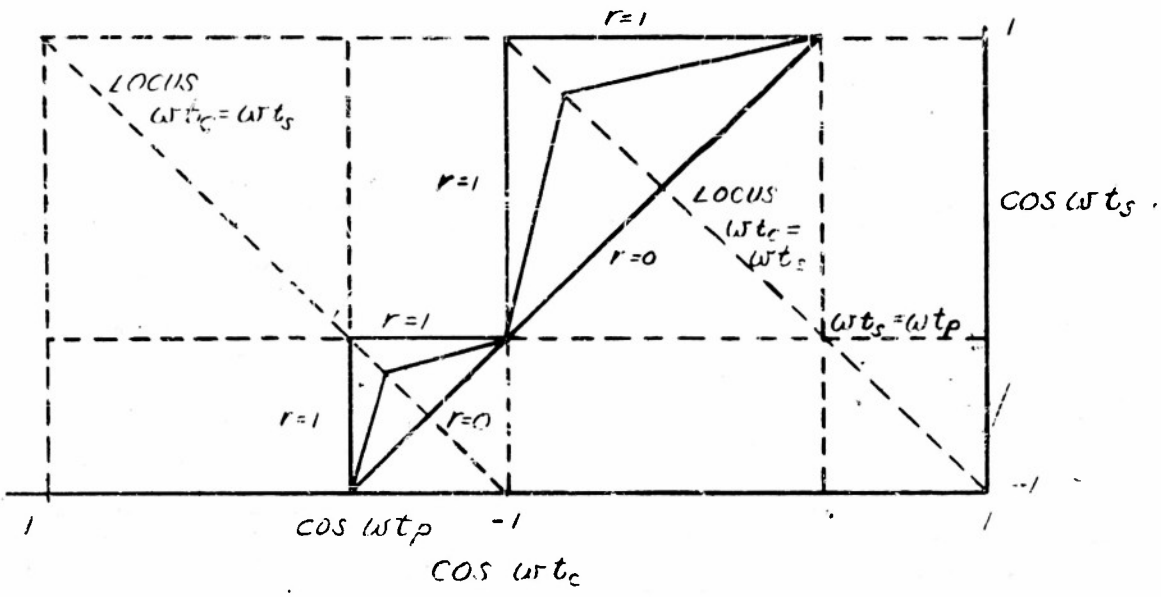

(A)

THEORETICAL COSINE RELATIONS FOR GIVEN PHASE ANGLE

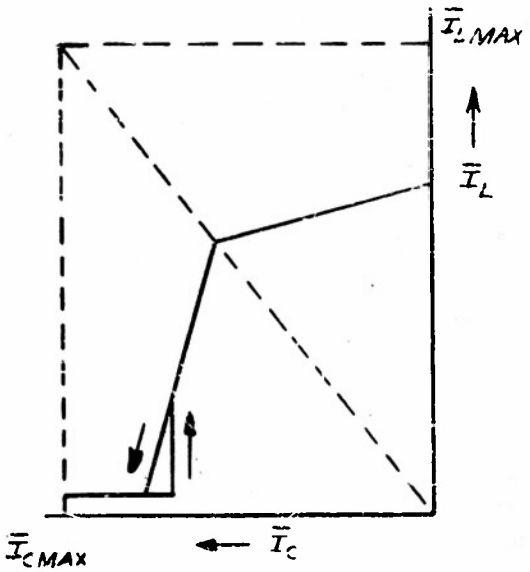

(B)

TRANSFER CHARACTERISTIC IN PRESENCE OF DC BIAS

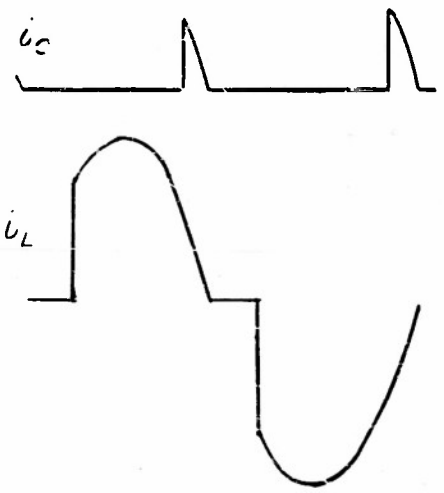

(C)

BASIC MODE WITH "POSITIVE" CONTROL

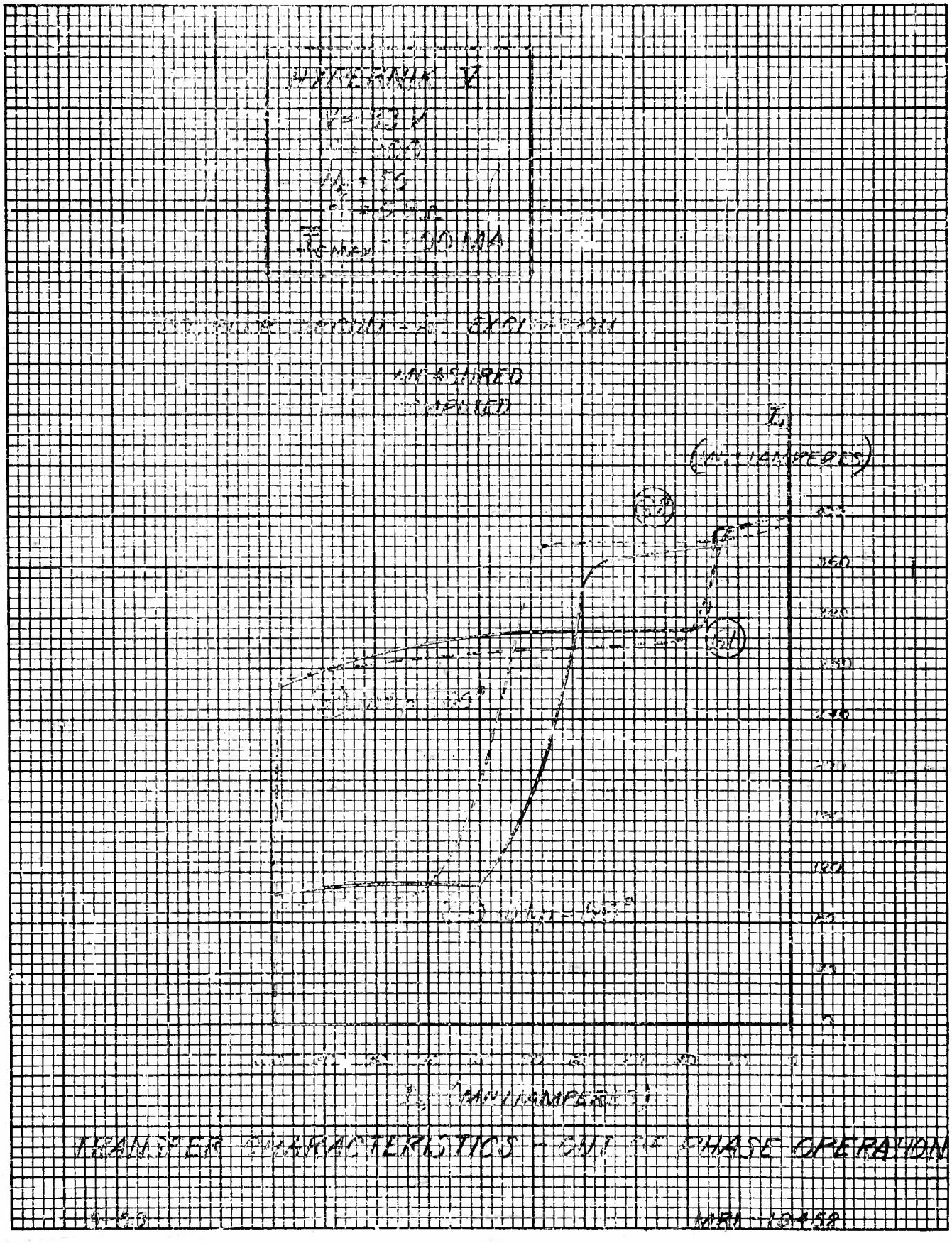
(MILLIAMPERES)
TRANSFER CHARACTERISTICS - ONE PHASE OPERATION
MRA-10458

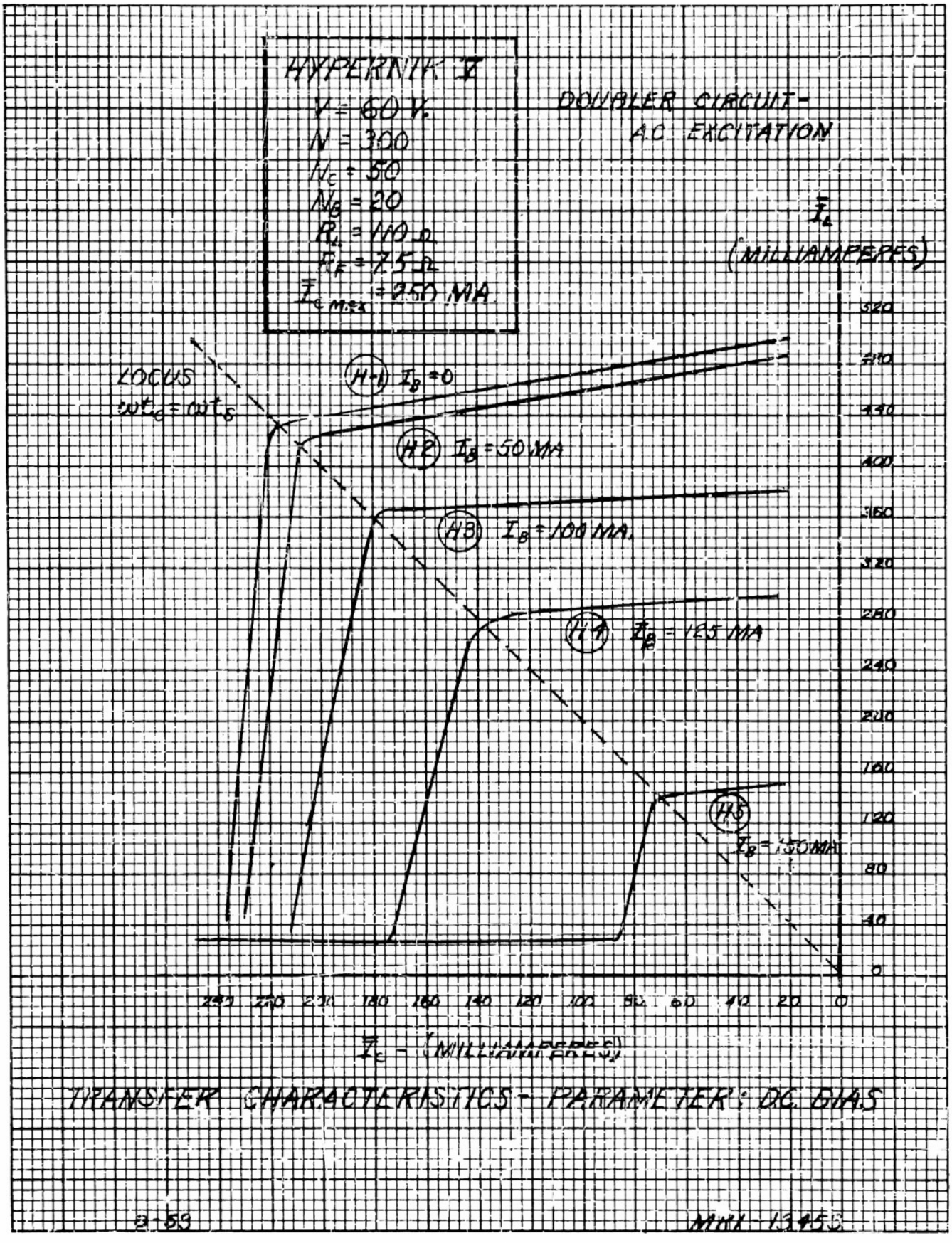

TRANSFER CHARACTERISTICS - PARAMETER: DC. BIAS

MIT 13455

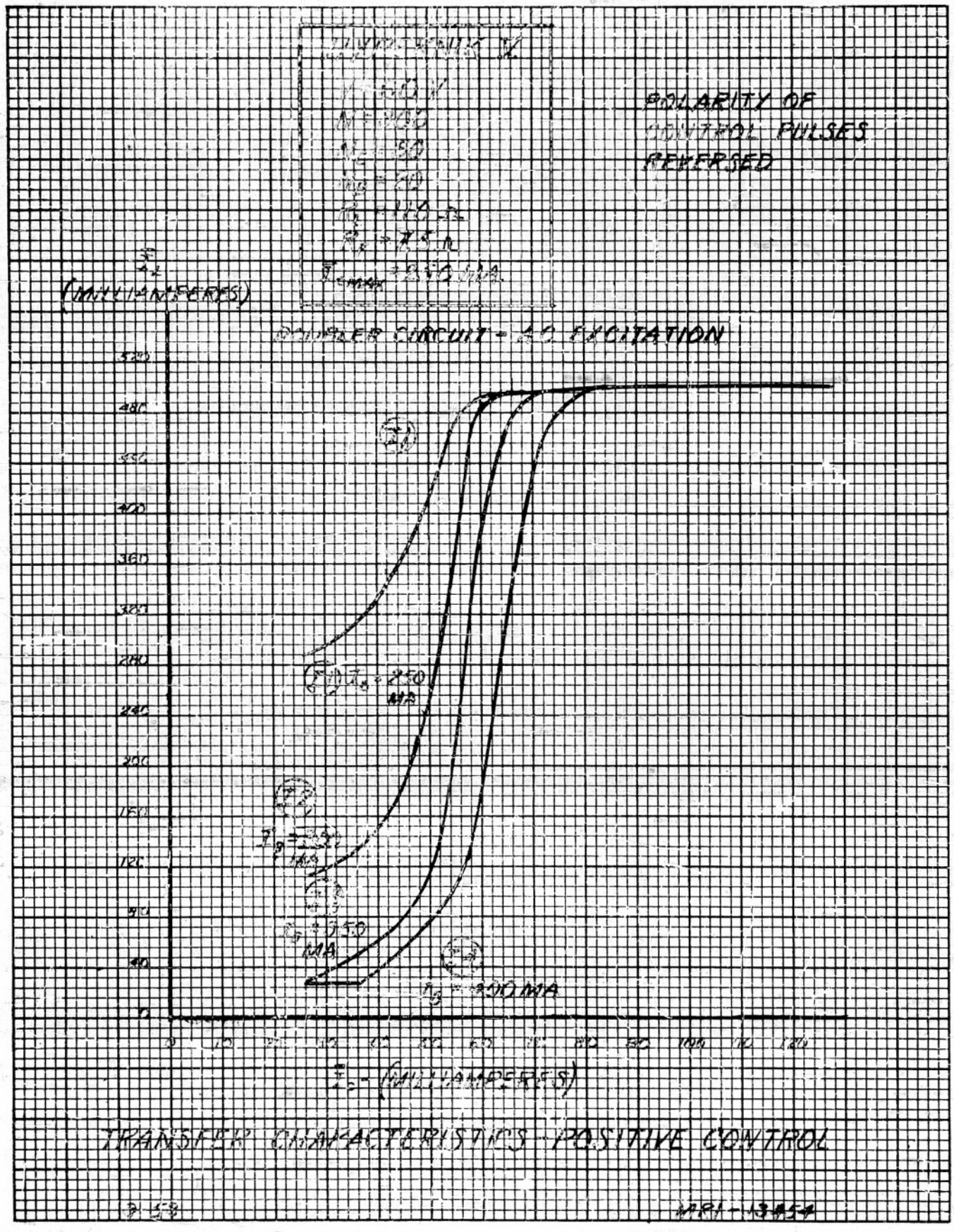
POLARITY OF CONTROL PULSES REVERSED
(MILLIAMPERES)
(MILLIAMPERES)
TRANSFER CHARACTERISTICS - POSITIVE CONTROL

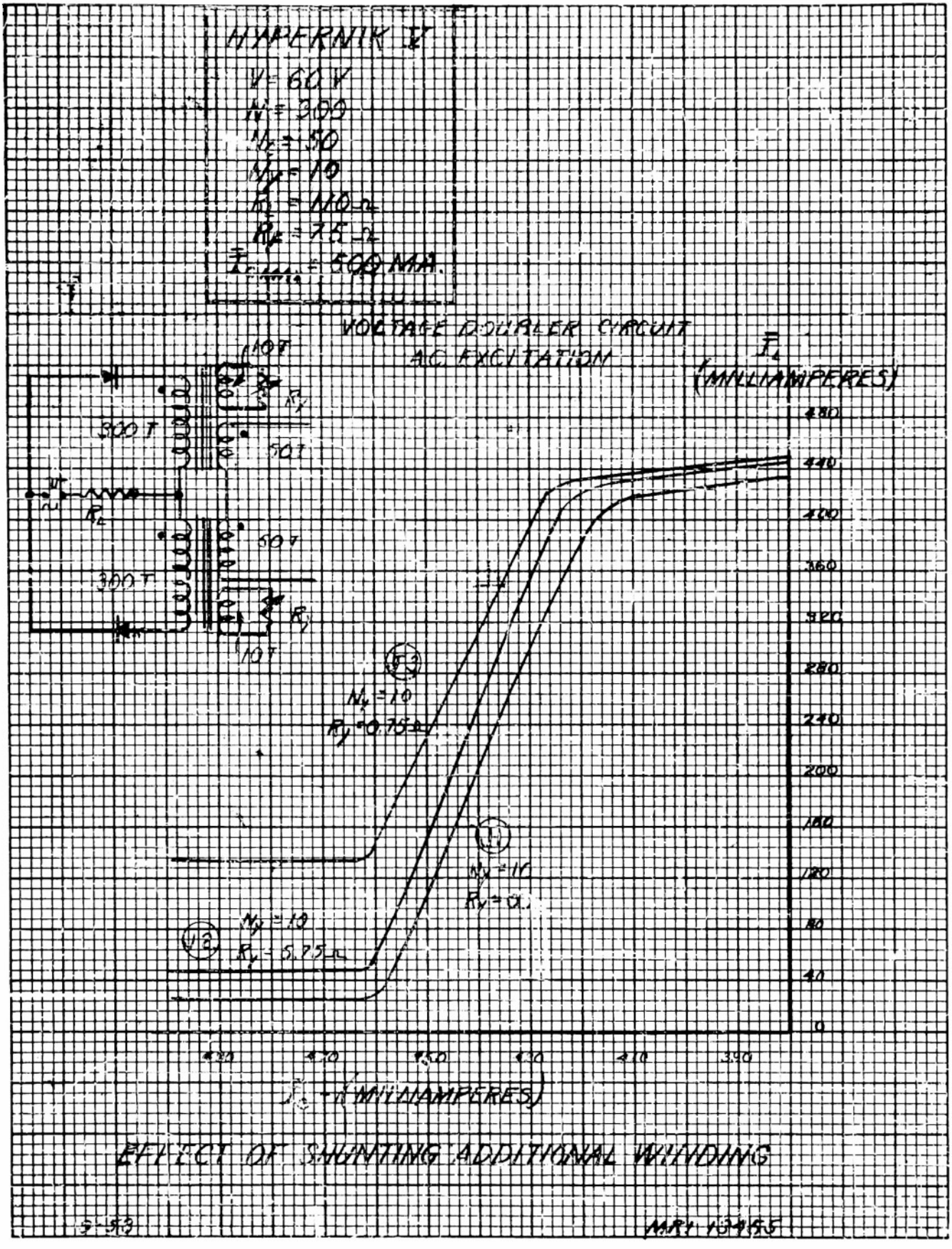
HYPERNIK IV
V = 60 V
N1 = 300
N2 = 50
N3 = 10
R1 = 110 Ω
R2 = 75 Ω
Fc max = 500 MA.
VOLTAGE DOUBLER CIRCUIT
A.C. EXCITATION
Fc (MILLIAMPERES)
500
440
400
360
320
280
240
200
160
120
80
40
0
300 T
50 T
10 T
R1
R2
N2 = 10
R2 = 0.75 Ω
N3 = 10
R3 = 0.
N3 = 10
R3 = 5.75 Ω
420
470
450
430
410
390
Fc (MILLIAMPERES)
EFFECT OF SHUNTING ADDITIONAL WINDING
5-53
MAY 1955

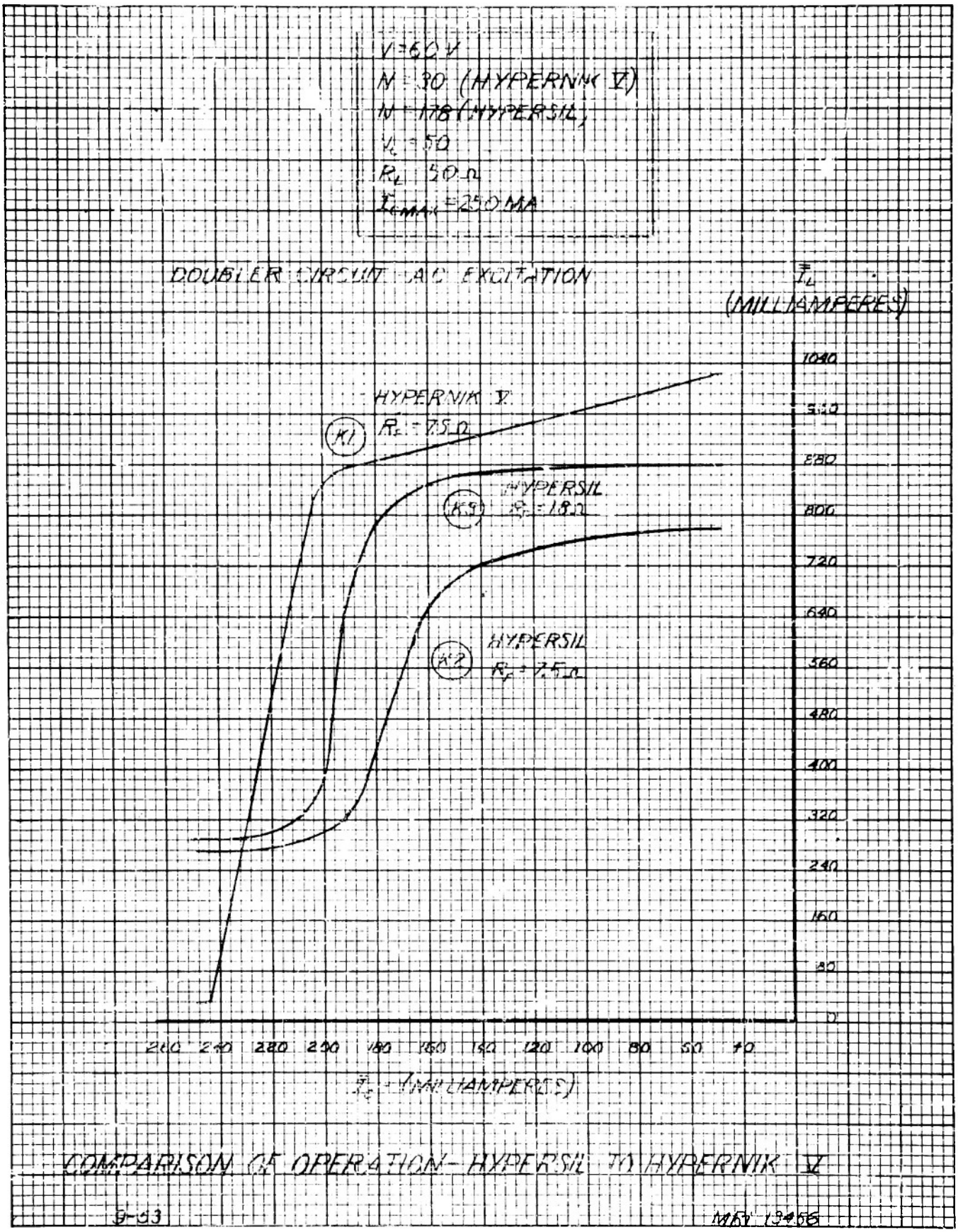
V=6.2 V
N 30 (HYPERNIK V)
N 178 (HYPERSIL)
V_c = 50
R_L 50 Ω
$I_{c\,MAX}$ = 250 MA
DOUBLER CIRCUIT A.C. EXCITATION
I_L (MILLIAMPERES)
HYPERNIK V
R_c = 75 Ω
K1
HYPERSIL
R_c = 18 Ω
K3
HYPERSIL
R_c = 75 Ω
K2
1040
960
880
800
720
640
560
480
400
320
240
160
80
0
240 240 220 200 180 160 140 120 100 80 50 40
I_c (MILLIAMPERES)
COMPARISON OF OPERATION - HYPERSIL TO HYPERNIK V
9-53
MBV 13456

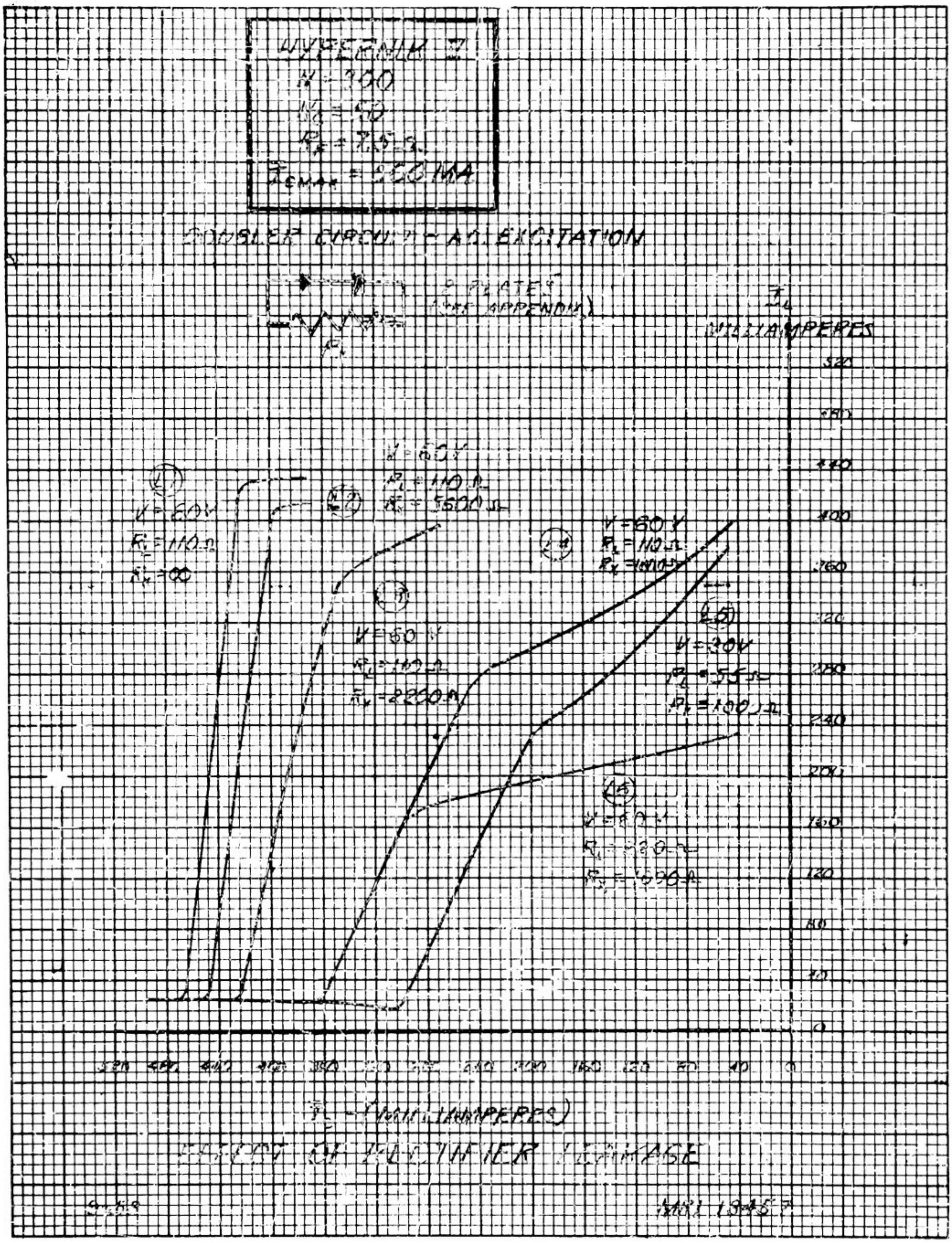

DOUBLER CIRCUIT – AC EXCITATION
(SEE APPENDIX)
MILLIAMPERES
V = 60V
R_L = 110 Ω
R_x = ∞
V = 60 V
R_L = 110 Ω
R_x = 5600 Ω
V = 60 V
R_L = 110 Ω
R_x = 2200 Ω
V = 60 V
R_L = 110 Ω
V = 30V
R_L = 55 Ω
R_x = 1000 Ω
520
480
440
400
360
320
280
240
200
160
120
80
40
0

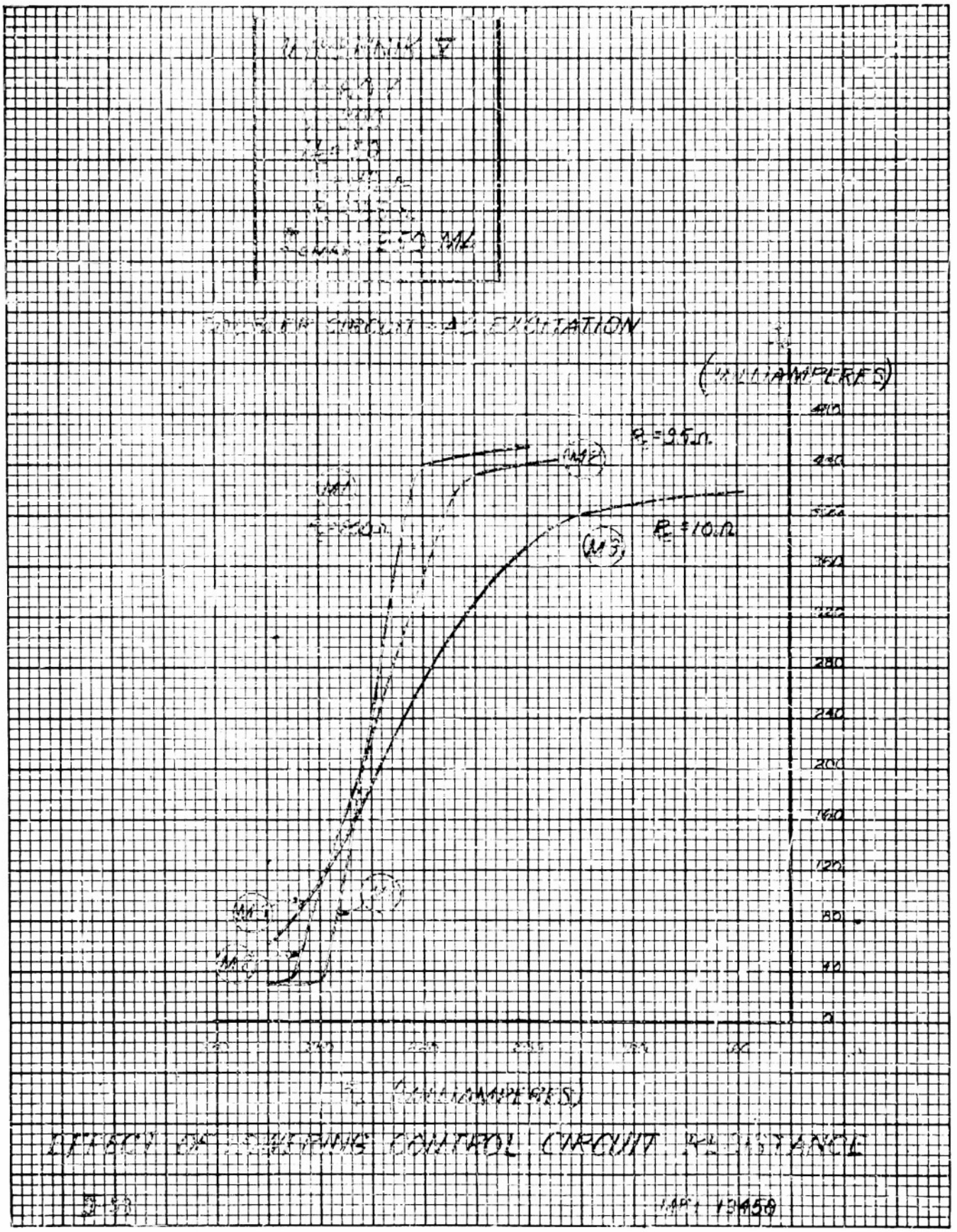
FIELD CIRCUIT
ARMATURE
FIELD CIRCUIT - AMPERE EXCITATION
(MILLIAMPERES)
$R_c = 25\Omega$.
$R_c = 10.\Omega$
400
360
320
280
240
200
160
120
80
40
0
EFFECT OF SHUNTING CONTROL CIRCUIT RESISTANCE
E-53
LAP 19458

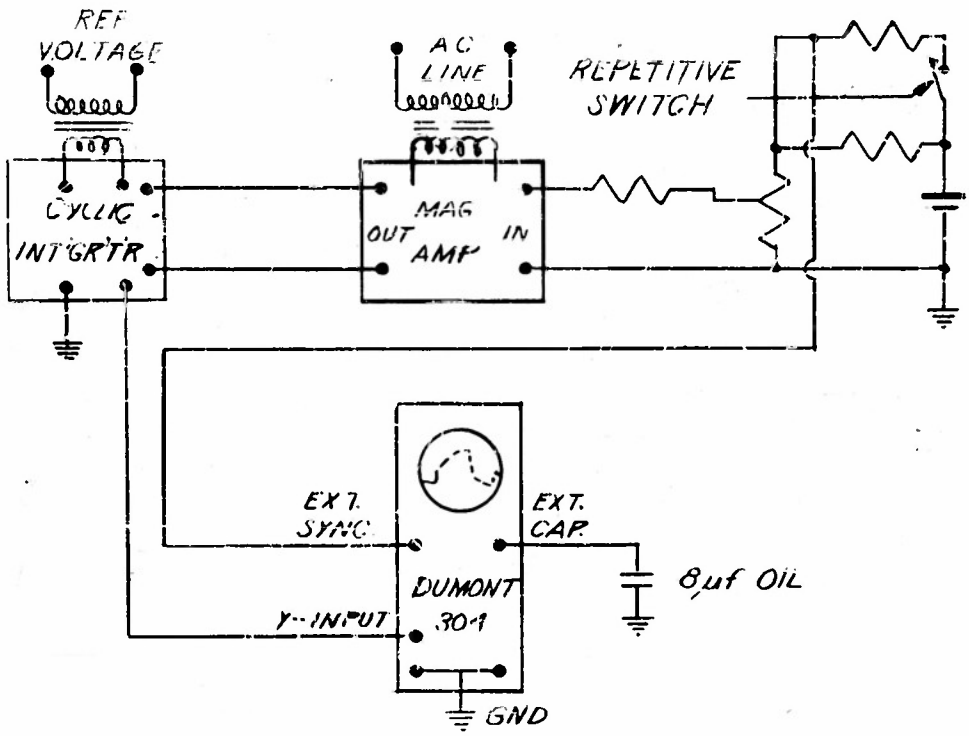

(A)

TEST SET-UP FOR VIEWING TRANSIENT RESPONSE OF MAGNETIC AMPLIFIER ON OSCILLOSCOPE

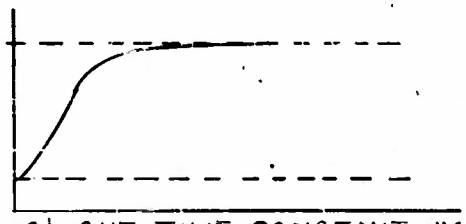

a) ONE TIME CONSTANT SMALL

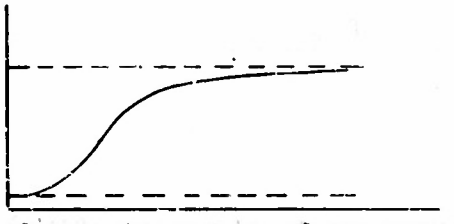

(b) TIME CONSTANTS COMPARABLE

(B)

RESPONSE OF TWO STAGE AMPLIFIER TO STEP INPUT

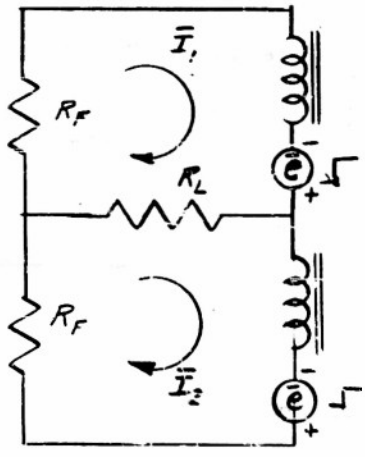

(C)

EQUIVALENT CIRCUIT OF DOUBLER DURING TRANSIENT

(a) Control Windings Shorted

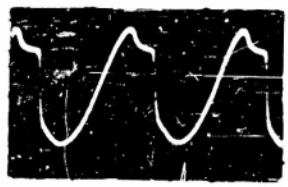

(b) Control Windings In

Control Current with Insufficient Control Circuit Resistance

(c) R_c = 100 Ohms
N = 300
N = 50

(d) R_c = 200 Ohms

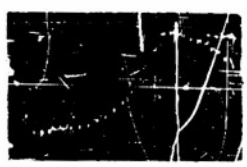

(e) N = 180

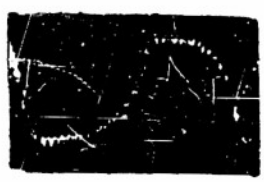

(f) N_c = 20

Transient Response of A. C. Excited Doubler
for Various Parameters

(a) R_L = 50 Ohms
R_F = 7.5 Ohms
T_2 = 4 Cycles

(b) R_L = 100 Ohms
R_F = 7.5 Ohms
T_2 = 7-8 Cycles

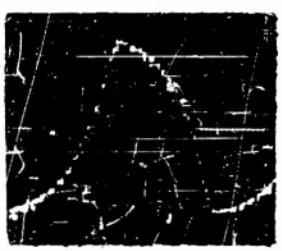

(c) R_L = 200 Ohms
R_F = 7.5 Ohms
T_2 = 12-14 Cycles

(d) R_L = 200 Ohms
R_F = 27.5 Ohms
T_2 = 4 Cycles

(e) R_L = 200 Ohms
R_F = 17.5 Ohms
T_2 = 5-6 Cycles

(f) R_L = 200 Ohms
R_F = 12.5 Ohms
T_2 = 8-9 Cycles

Effect of Load and Foward Mesh Resistances on Transient Response of A.C. Excited Doubler — Hypernik V

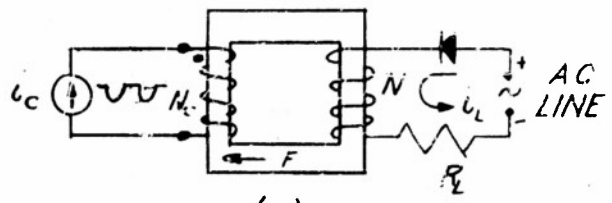

(A)

HALF-WAVE CIRCUITS

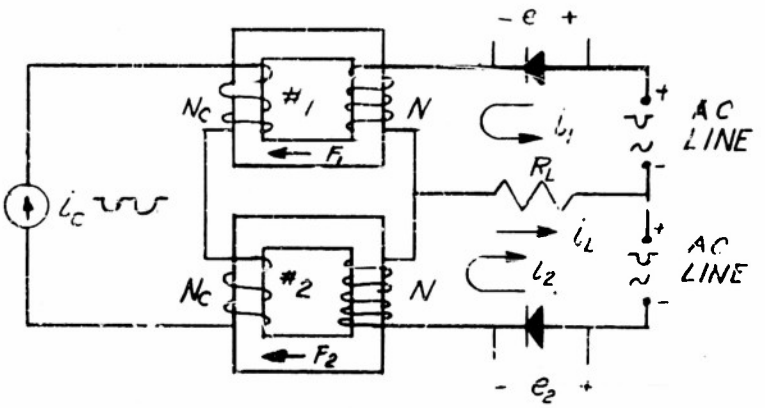

(B)

FULL-WAVE CIRCUIT

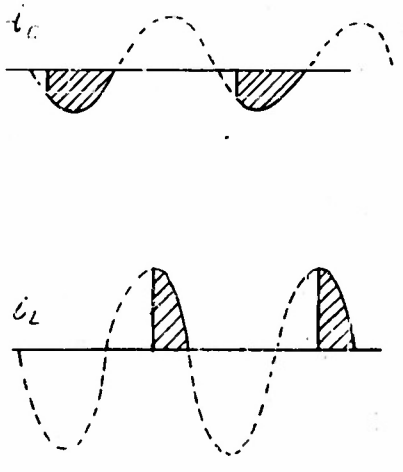

(C)

IDEAL WAVEFORMS
HALF-WAVE CIRCUIT

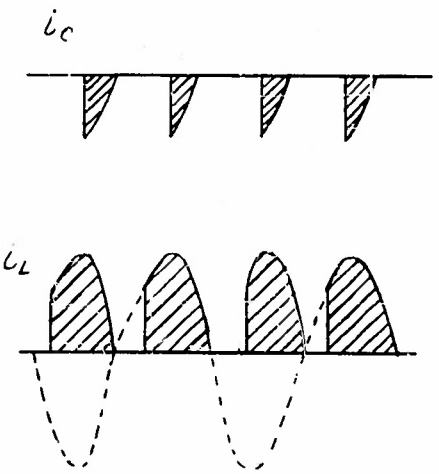

(D)

IDEAL WAVEFORMS
FULL-WAVE CIRCUIT

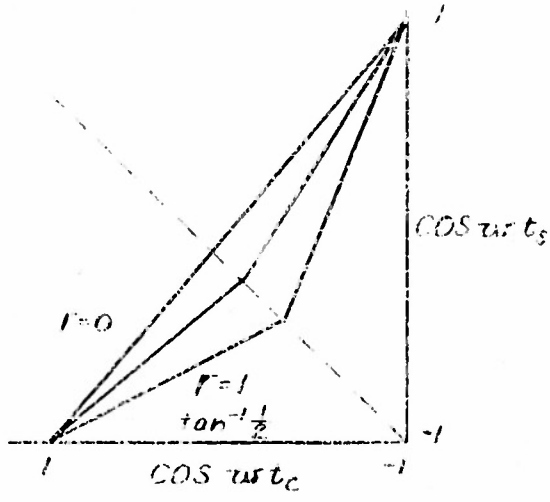

(A)

COSINE RELATIONSHIPS IN HALF-WAVE AND FULL-WAVE CIRCUITS

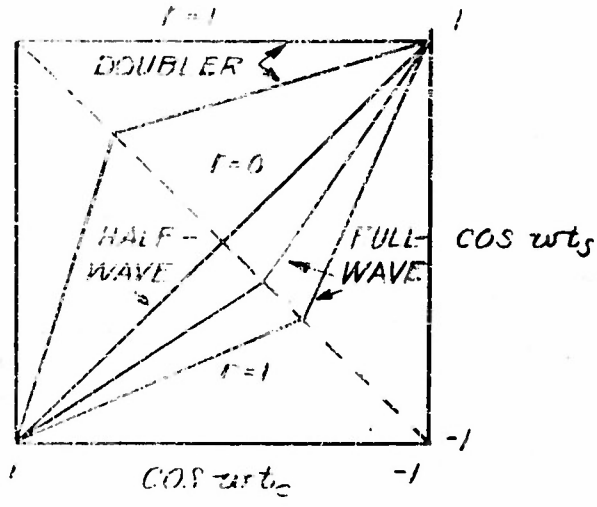

(B)

GENERAL COSINE RELATIONSHIPS

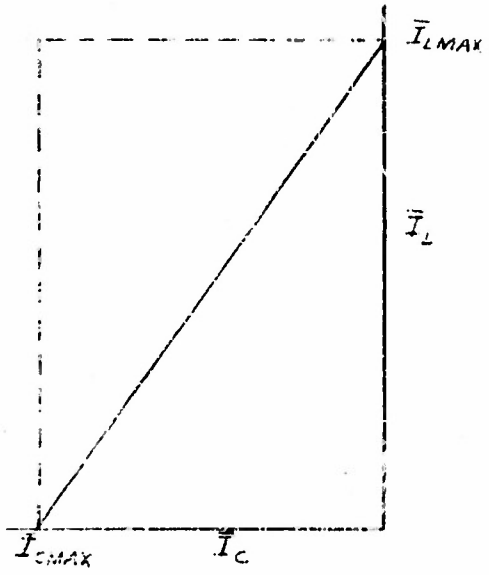

(a) HALF-WAVE

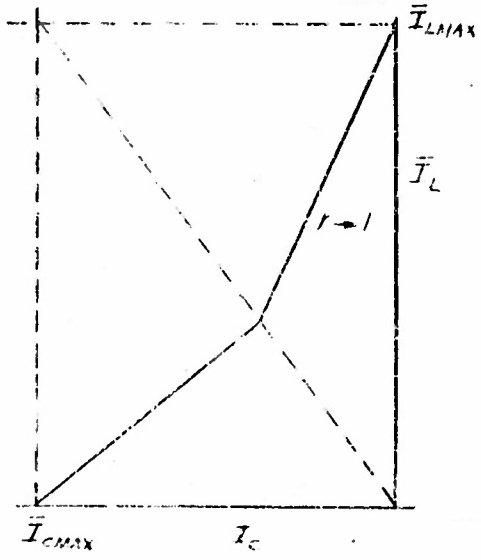

(b) FULL WAVE

(C)

THEORETICAL TRANSFER CHARACTERISTICS

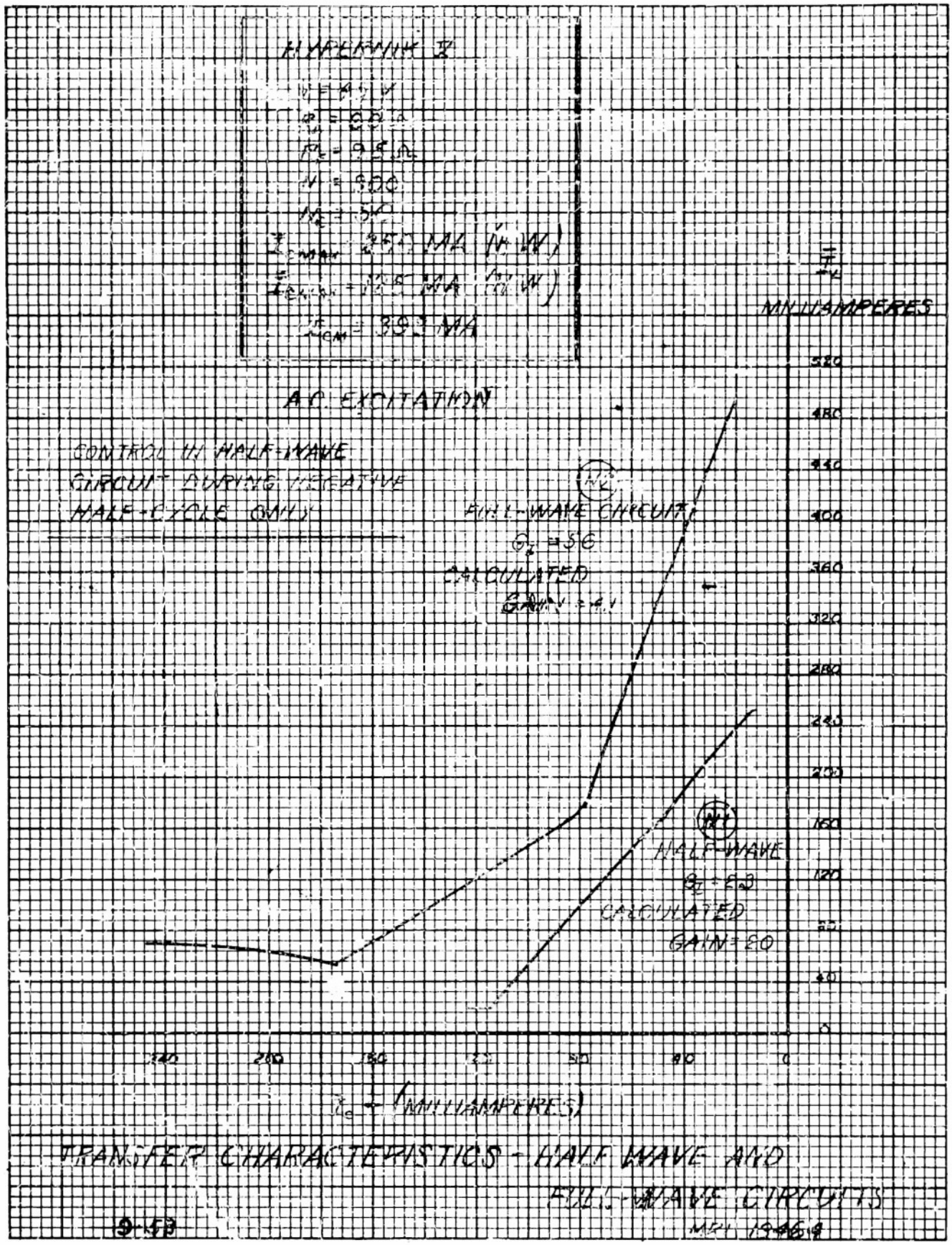

TRANSFER CHARACTERISTICS - HALF WAVE AND FULL-WAVE CIRCUITS

MEH 19466

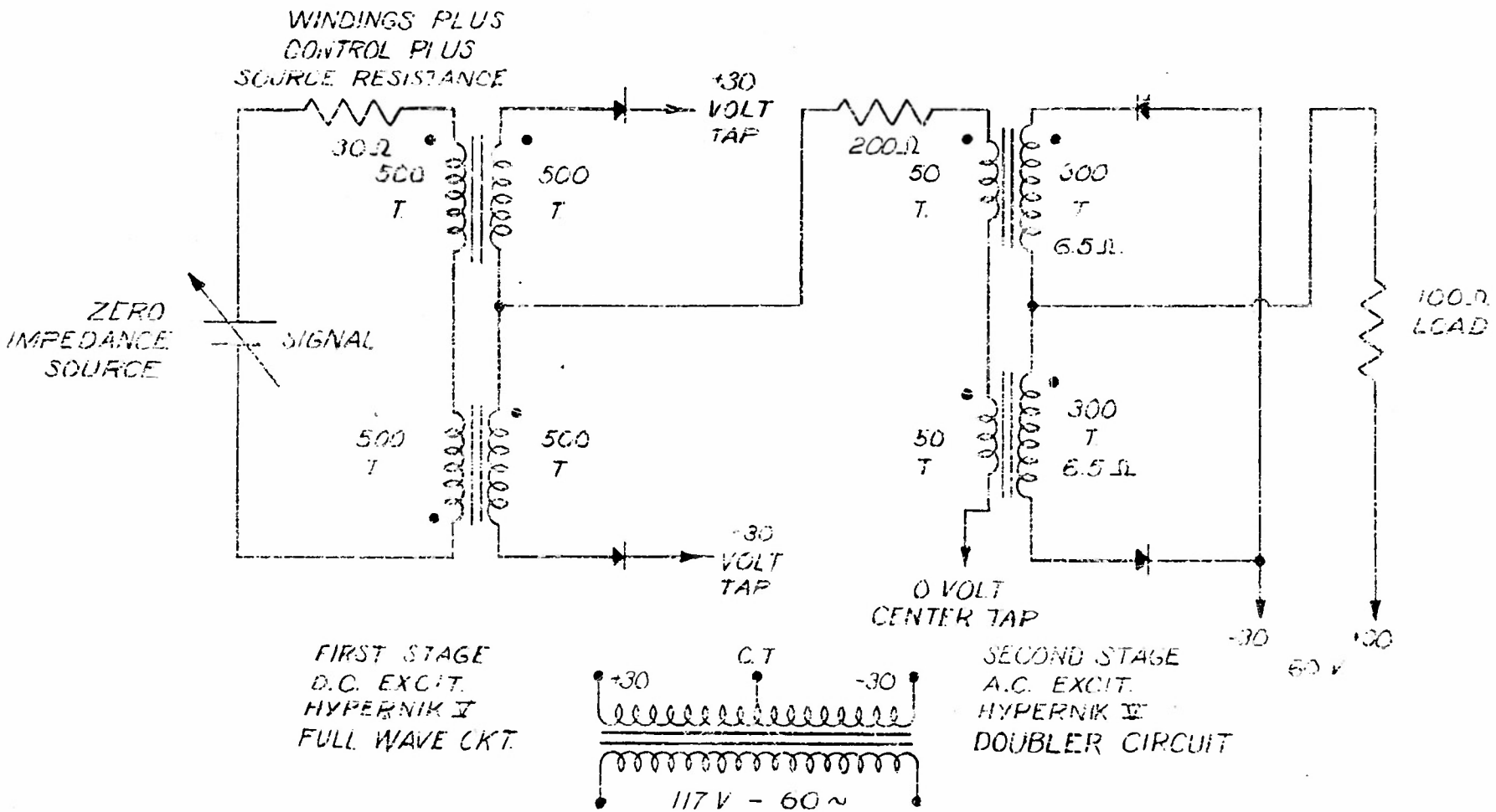

TWO STAGE AMPLIFIER - TEST SET-UP

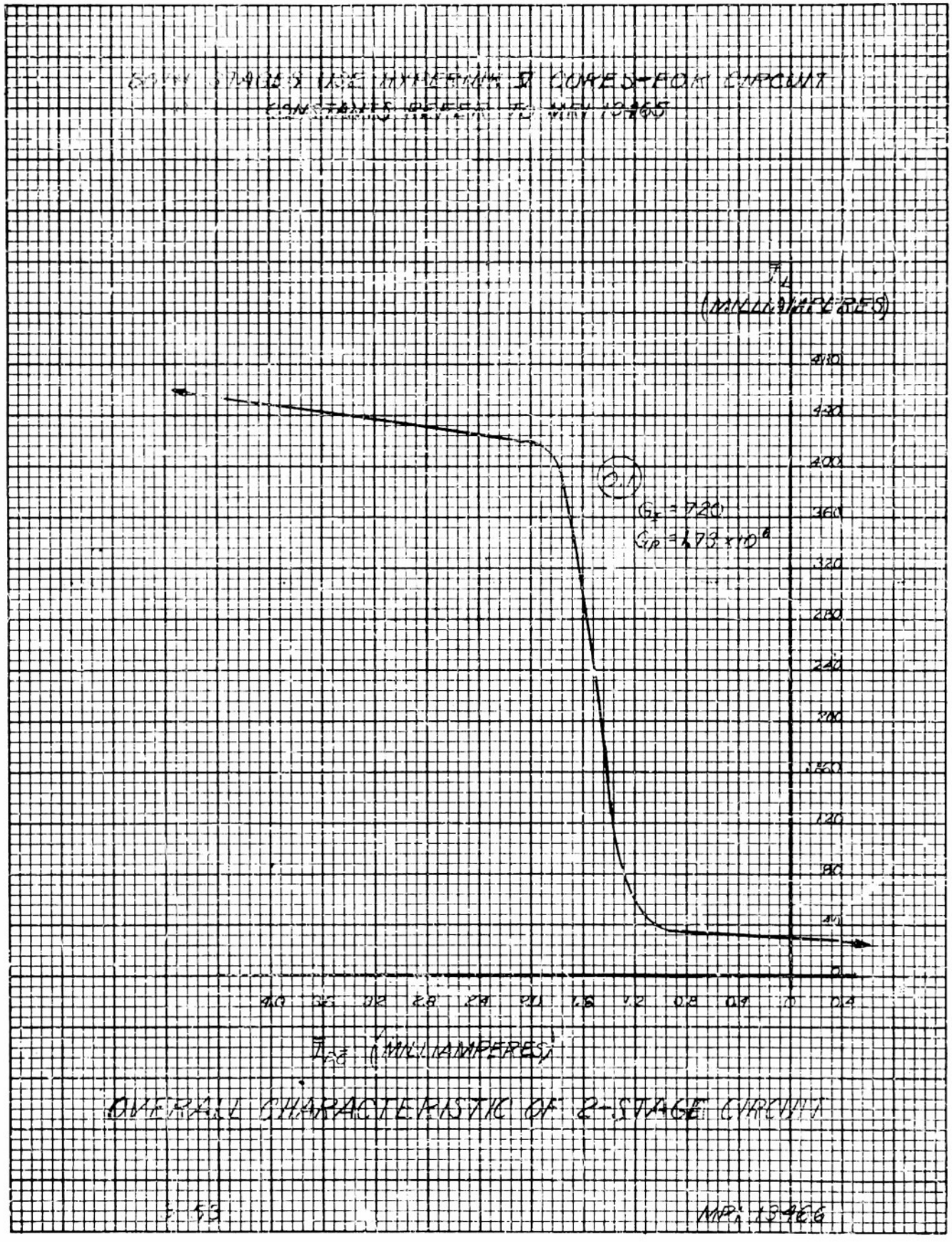

OVERALL CHARACTERISTIC OF 2-STAGE CIRCUIT

MP: 15466

(a)

Typical Response of Half Wave Circuit to Square Wave Input

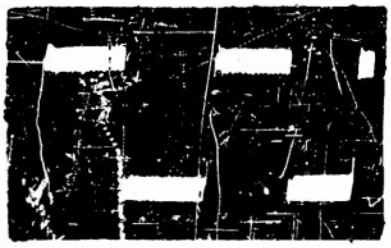

(b)

Typical Response of Full Wave Circuit to Square Wave Input

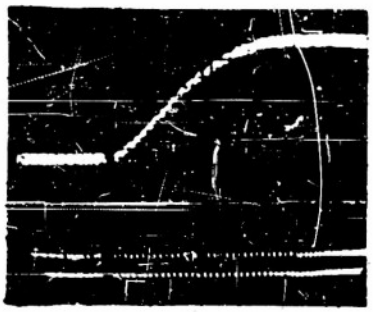

(c)

Response of 2 – Stage Amplifier of MRI 13465 to Step Input

(d)

Output of 3 – Stage Oscillator

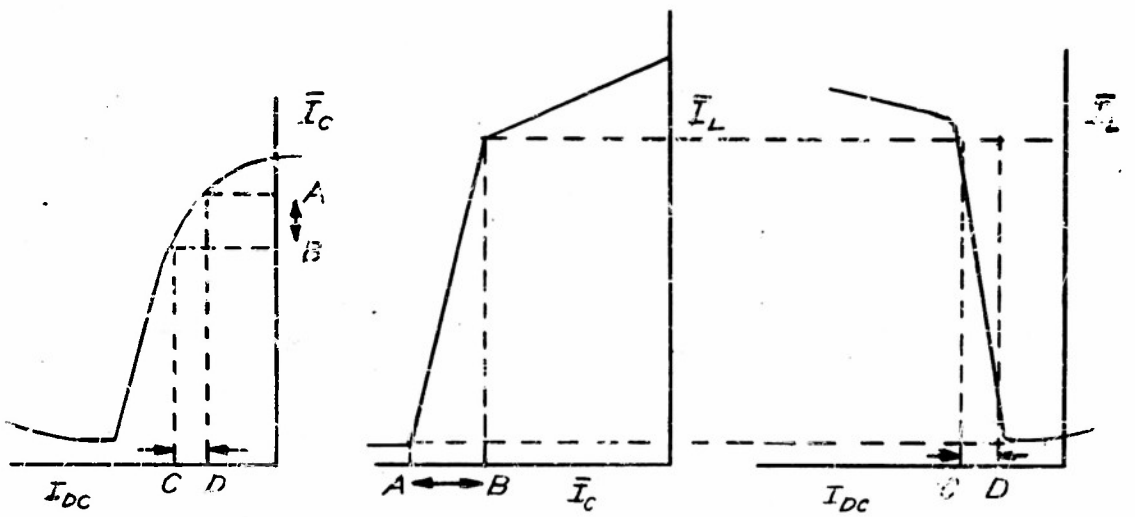

(A)

REGIONS OF OPERATION IN TWO-STAGE AMPLIFIER

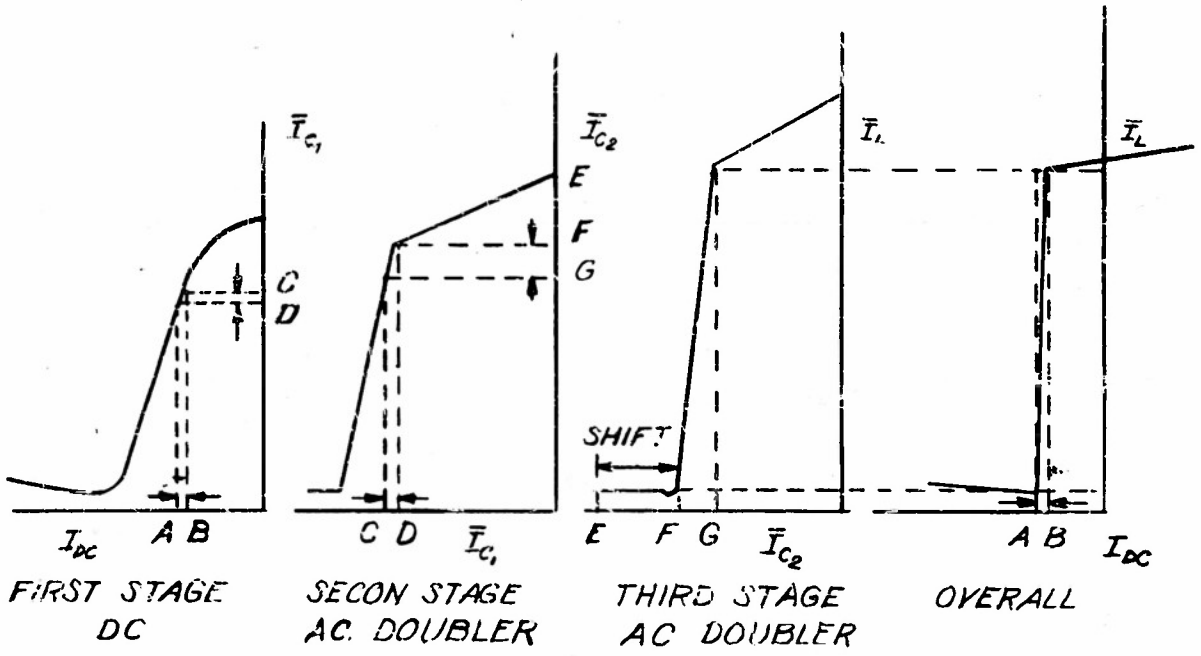

(B)

REGIONS OF OPERATION IN THREE-STAGE AMPLIFIER

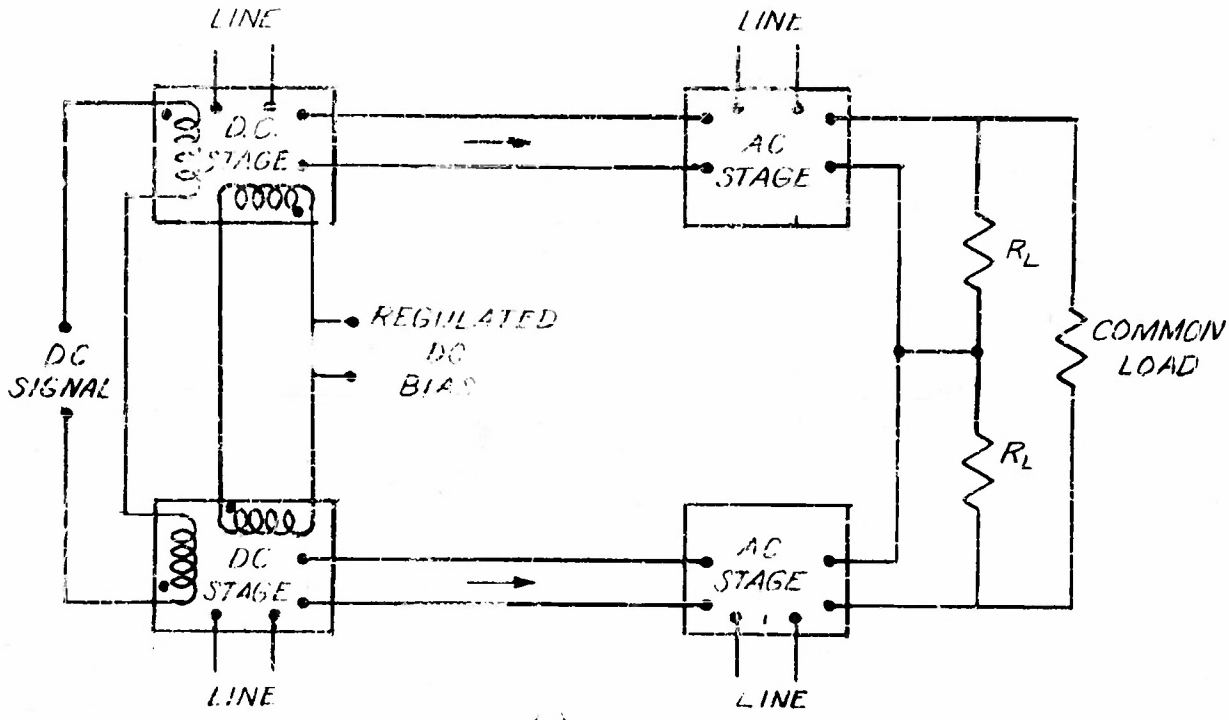

(A)

MULTISTAGE PUSH-PULL SCHEMATIC DIAGRAM

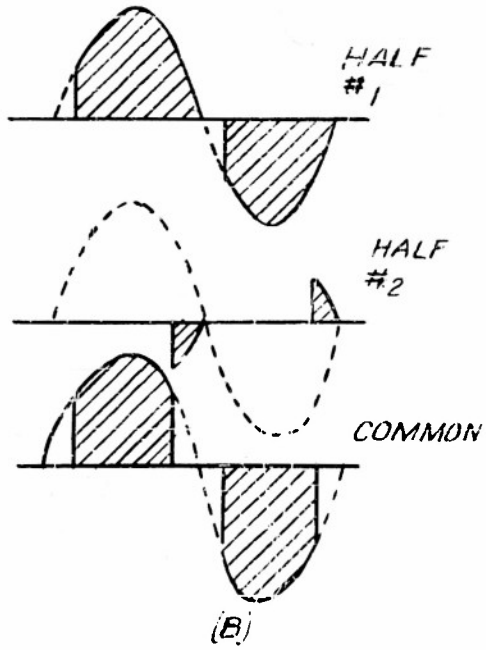

(B)

PUSH-PULL OUTPUT WAVES WITH DOUBLERS AS AC STAGES

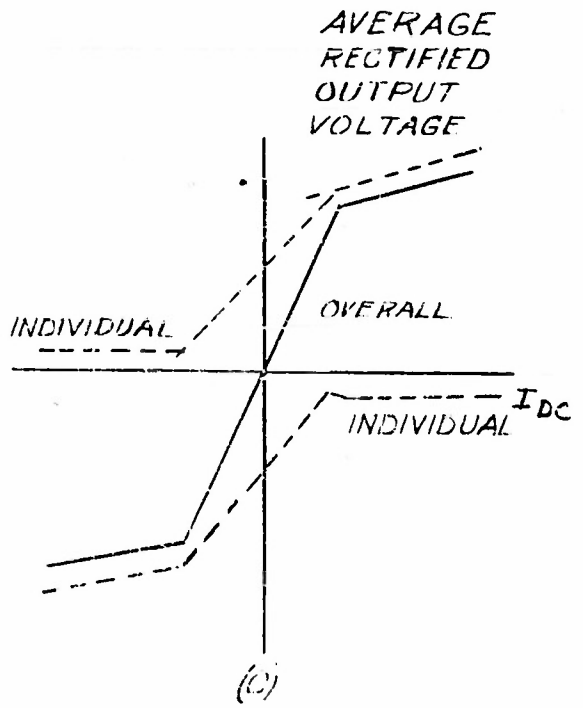

(C)

IDEAL PUSH-PULL CHARACTERISTICS

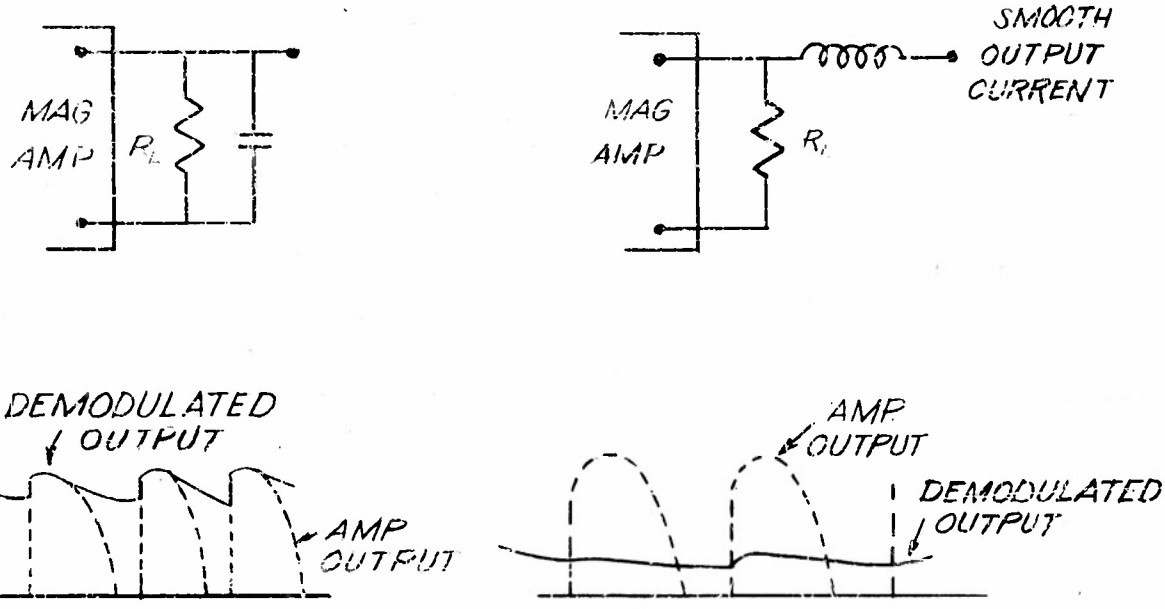

(A)
DEMODULATION CIRCUITS AND WAVEFORMS

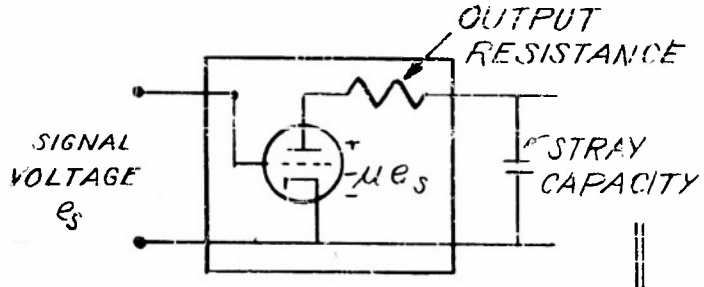

VACUUM TUBE AMPLIFIER

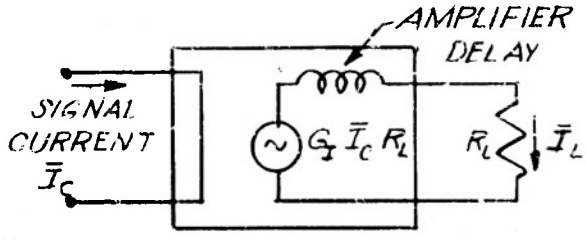

AC MAGNETIC AMPLIFIER

(B)
IDEALIZED LINEAR EQUIVALENT CIRCUITS

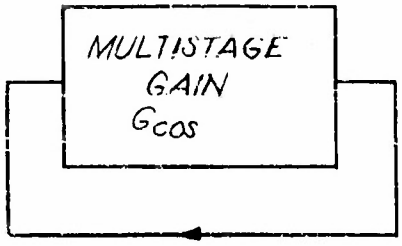

(C)
100% REGENERATIVE FEEDBACK

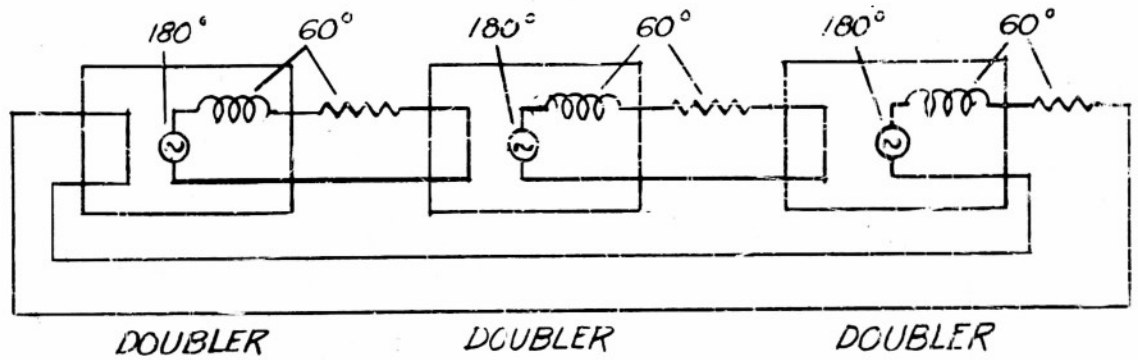

(A) MAGNETIC

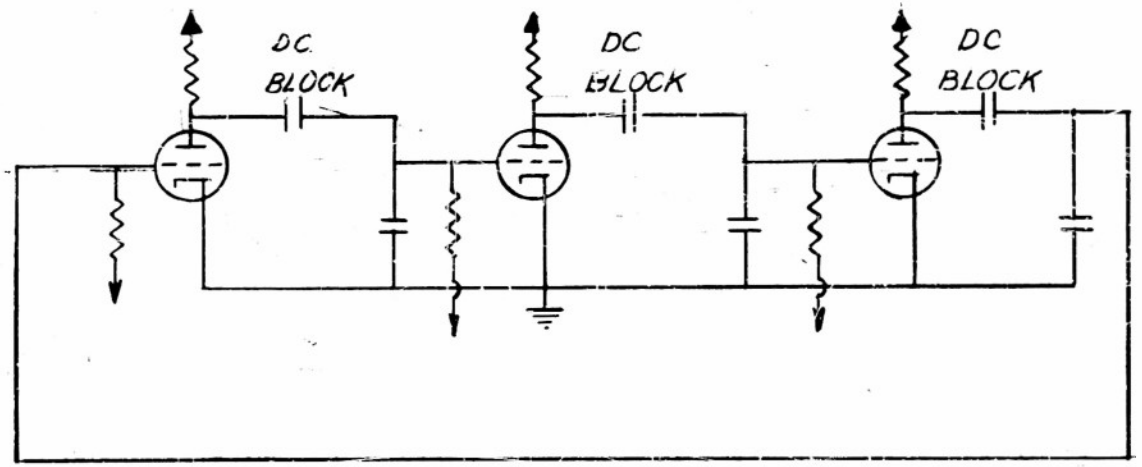

(B) ELECTRONIC

THREE - STAGE OSCILLATORS

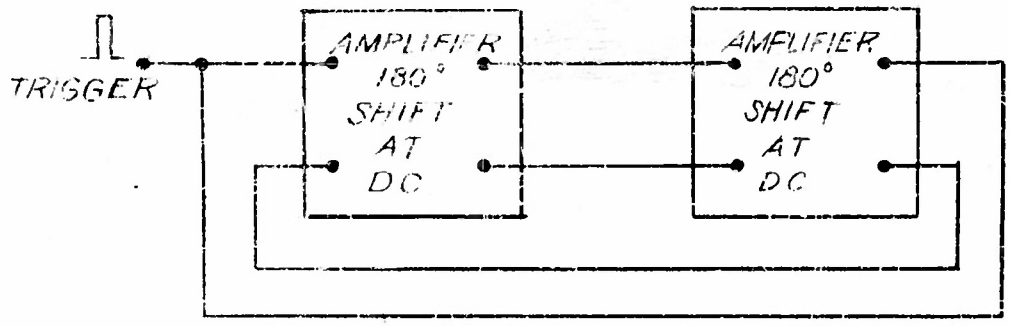

(A) GENERAL

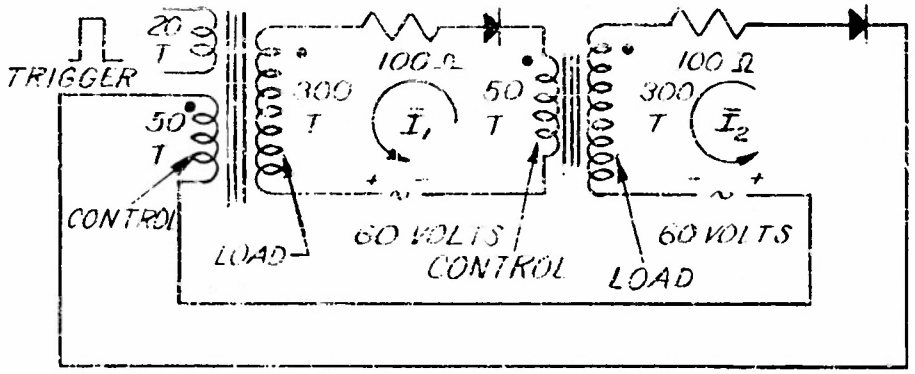

(B) HALF-WAVE FLIP-FLOP
HYPERNIK ℣ CORES

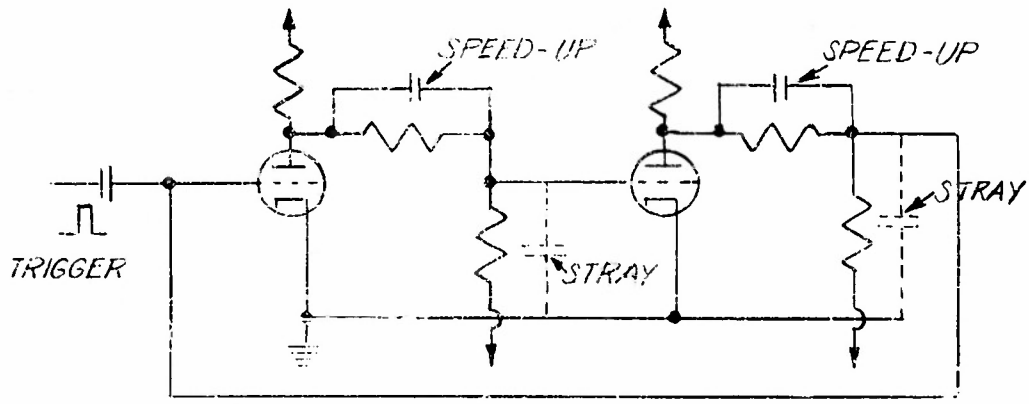

(C) ECCLES-JORDAN TRIGGER CIRCUIT

FLIP-FLOP CIRCUITS

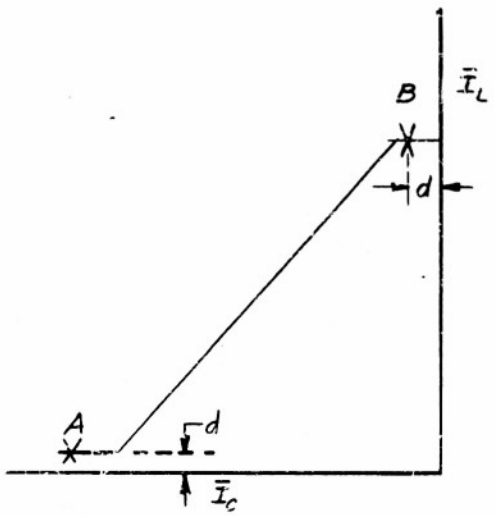

(A)

POINTS OF STABILITY ON TRANSFER CURVES OF HALF-WAVE CIRCUITS WHEN USED AS FLIP-FLOP

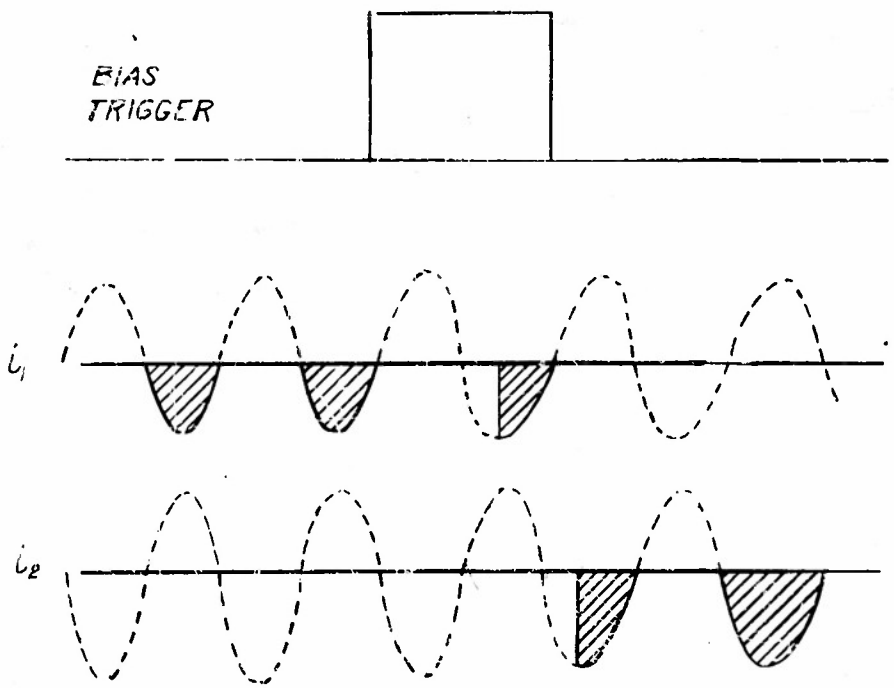

(B)

WAVEFORMS IN FLIP-FLOP CIRCUIT OF MRI 13472 (B)